CZECH TECHNICAL UNIVERSITY IN PRAGUE

FACULTY OF MECHANICAL ENGINEERING

Department of Materials Engineering

&

BANDUNG INSTITUTE OF TECHNOLOGY

FACULTY OF MECHANICAL AND AEROSPACE ENGINEERING

ACCURACY ENHANCEMENT OF THE FUEL LEVEL SENSOR CHECKPOINTS

DIPLOMA THESIS

AUTHOR Bc. Petr Royt

SUPERVISOR – CTU Prof. RNDr. Petr Špatenka, CSc.

SUPERVISOR – ITB Prof. Dr. Ir. Muljo Widodo Kartidjo

PRAGUE 2015

ČESKÉ VYSOKÉ UČENÍ TECHNICKÉ V PRAZE
Fakulta strojní, Ústav materiálového inženýrství
Technická 4, 166 07 Praha 6 Akademický rok: 2014/2015

ZADÁNÍ DIPLOMOVÉ PRÁCE

pro: **Bc. Petra ROYTA**

program: Strojní inženýrství

obor: Výrobní a materiálové inženýrství

název česky: **Návrh zpřesnění výpočtu měřicích bodů hladinového palivoměru osobního automobilu**

název anglicky: Accuracy enhancement of the fuel level sensor check points

Zásady pro vypracování:

Cíl:

Navrhnout opatření pro snížení nepřesnosti indikace palivoměru a zjistit míru vlivu materiálových parametrů plovákové páky.

Postup:

1. Princip plovákového palivoměru a srovnání s ostatním typy palivoměrů.
2. Konstrukce palivoměru a jeho umístění v nádrži, materiály použité na konstrukci komponent palivoměru.
3. Pravidla pro návrh palivoměru.
4. Toleranční řetězec rozměrů sestavy palivoměru a dopad na přesnost indikace.
5. Metody použité v RBCB pro tolerování kontrolních měřicích výšek palivoměru.
6. Sběr dat z výrobních linek, určení jevů a parametrů typických pro palivoměry, které na výstupní kontrole nesplňují toleranci přesnosti indikace.

Praktická část:

7. Návrh opatření vedoucích ke snížení nepřesnosti indikace palivoměru za podmínky nezpřísnění výrobních tolerancí jednotlivých komponent palivoměru.
8. Analýza struktury a mechanických vlastností materiálu drátu plovákové páky a určení vlivu jeho materiálových vlastností na přesnost indikace celé sestavy palivoměru.

Rozsah průvodní zprávy: 40 - 60 stran

Rozsah grafických prací: dle potřeby

SEZNAM DOPORUČENÉ LITERATURY:

[1] Ďaďo, S. a kol.: Měření průtoku a výšky hladiny. Praha: BEN – technická literatura, 2005.
[2] Ashby, M.F.: Material selection in mechanical design. Butterworth-Heinemann, 1999
[3] Macek, K. a kol. Nauka o materiálu cvičení. Praha: Vydavatelství ČVUT v Praze, 2007.
[4] Macek, J., Janovec, J., Jurči, P., Zuna, P.: Kovové materiály, Nakladatelství ČVUT, Praha 2006.
[5] Interní materiály firmy Bosch.

Vedoucí diplomové práce: Prof. RNDr. Petr Špatenka, CSc.

Konzultant diplomové práce: RNDr. Jiří Kalčík, CSc. – R.Bosch -ČB

Datum zadání diplomové práce: 3. října 2014

Datum odevzdání diplomové práce: 18. prosince 2014

Neodevzdá-li student diplomovou práci v určeném termínu, tuto skutečnost předem písemně zdůvodnil a omluva byla děkanem uznána, stanoví děkan studentovi náhradní termín odevzdání diplomové práce. Pokud se však student řádně neomluvil nebo omluva nebyla děkanem uznána, může si student zapsat diplomovou práci podruhé.

Student bere na vědomí, že je povinen vypracovat diplomovou práci samostatně, bez cizí pomoci, s výjimkou poskytnutých konzultací. Seznam použité literatury, jiných pramenů a jmen konzultantů je třeba uvést v diplomové práci.

Zadání diplomové práce převzal dne: 03 -10- 2014 .....
student

ČESKÉ VYSOKÉ UČENÍ TECHNICKÉ V PRAZE Fakulta strojní

.....
Prof. RNDr. Petr Špatenka, CSc.
vedoucí ústavu

.....
Prof. Ing. Michael VALÁŠEK, DrSc.
děkan fakulty

V Praze dne 1. října 2014

DIPLOMA THESIS ASSIGNMENT

(Translation of the Czech version of the Diploma thesis assignment)

For: Bc. Petr Royt

Thesis title: Accuracy enhancement of the fuel level sensor checkpoints

Principles of thesis elaboration:

Objective:

Proposal of measures application of which would lead to reduction of number of fuel level sensors that do not comply with indication accuracy criteria in series production at Robert Bosch Ceske Budejovice GmbH. Analysis of influence of material properties of the wire arm material on increased frequency of fuel level sensors that do not comply with indication accuracy criteria.

Points of elaboration:

1. Working principle of a potentiometric fuel level sensor (FLS) and comparison to other fuel measure systems.
2. Design of FLS, positioning of FLS in a car fuel tank, materials selection for components of FLS.
3. FLS design rules.
4. Tolerance chain of dimensions of FLS and its effect on the FLS indication accuracy.
5. FLS indication accuracy tolerance methods applied at Robert Bosch Ceske Budejovice GmbH.
6. Analysis of data collected from assembly lines, determining of parameters that are typical for FLS which show increased frequency of non-compliance with indication accuracy criteria.

Practical part:

7. Design change proposals application of which would lead to significant reduction of number of FLS that do not comply with indication accuracy criteria.
8. Analysis of material properties of the wire arm of FLS and analysis of correlation between the wire arm material properties and FLS indication accuracy.

DOUBLE DEGREE – MASTER PROGRAM

This diploma thesis was realized in Double Degree - Master Program:

Material Engineering

established between:

Faculty of Mechanical Engineering, Czech Technical University in Prague (FME CTU)
(3 semesters)

and

Faculty of Mechanical and Aerospace Engineering, Bandung Institute of Technology (FMAE ITB)
(2 semesters)

DECLARATION

I declare that I carried out this diploma thesis independently, and only with the cited sources, literature and other professional sources. I assure that the work has not been used, neither completely nor in parts, to pass any previous examination.

Dated: ……

Petr Royt

ACKNOLEDGEMENTS

First of all, I would like to express my sincere gratitude to the supervisor of my thesis Prof. RNDr. Petr Špatenka, CSc. for his valuable advices, kind help and particularly for his patronage of the Double Degree program.

I am deeply grateful to my thesis supervisor Prof. Dr. Ir. Muljo Widodo Kartidjo from the Bandung Institute of Technology for his useful comments and encouragement at the time of the thesis completion.

A special thank goes to my thesis consultant RNDr. Jiří Kalčík, CSc. from Robert Bosch Ceske Budejovice for his valuable help. He never hesitated to give me the right answers to number of my questions.

I am also more than thankful to people from the Department of Materials Engineering at FME, CTU who were always very kind and helpful. A special thank goes to Ing. Jana Sobotová, PhD for her critical scientific discussion and her great dedication to the Double Degree program. To Doc. Ing. Jiří Cejp, CSc. for his gracious help with the tensile testing. To Vlasta Voňková for the skilled help with the metallographic specimen preparation. To Ing. BcA. Jan Podaný, PhD for his highly appreciated consultancy on the interpretation of statistical data.

A special thank goes to Prof. Ing. Ivan Uhlíř, DrSc. without whose dedication the Double Degree program would never have existed.

I also would like to thank to all my colleagues from the ENG4 department in Robert Bosch Ceske Budejovice who have always helped me willingly.

Last but not least my great thanks belong to my family and friends who were immensely supportive.

ABSTRACT

This thesis deals with indication accuracy issues encountered in the series production of potentiometric fuel level sensors in Robert Bosch Ceske Budejovice GmbH. In the first part of the thesis working principle of a potentiometric fuel level sensor (FLS) is described. Then basics of design process of FLS are specified based on the laws of physics and customer specification. The theoretical part also provides brief insight into analysis of tolerance chain of dimensions of FLS components and its impact onto indication accuracy. Methods of tolerance of FLS indication accuracy are described, analysed and compared.

Practical and experimental part is opened with an analysis of data collected from assembly lines. Identification follows of FLS parameters with a particular influence on the rate of FLS non-complying with the indication accuracy criteria at the output control.

Based on the findings an analysis is performed of the wire arm material in order to evaluate the influence of the wire arm material properties on dimensional stability of the wire arm. Tension test and metallographic analysis of the wire arm material are conducted.

Considerable variation of indication accuracy was discovered depending on the wire arm supplier. Tension test of the wire arm material proved variation of mechanical properties among individual wire arm suppliers.

Design change of layout of resistor card of FLS is proposed. Based on tolerance method applied for the tolerance of FLS indication accuracy, widening of checkpoint pads of the resistor card layout is proposed with the consequence of decrease of rate of non-complying FLS that are identified at the output control. The estimation is carried out of a decrease of rate of non-complying FLS that are identified at the output control.

Further design changes are proposed which would eventually lead to a decrease of the rate of beyond specification FLS.

Key words

fuel level sensor, fuel level sender, indication accuracy, materials analysis

TABLE OF CONTENTS

INTRODUCTION

Production of automotive components is characterized by high-volume production batches, high customization for individual customers and the highest demands imposed on the quality and accuracy of products. As regards fuel supply systems those are moreover very complex as they comprise number of subcomponents. These components must be manufactured with the highest possible accuracy so that the whole assembly meets tight specification required by the customer. Any deviation beyond the tolerances identified at the output control of the final assembly poses then a severe issue which disrupts the production fluency and causes idle time which results in an increase of production costs. Figurative phrase “Time is money” is even more appropriate in the case of high volume series production of components with high added value and high production rate.

Objective of the practical part of this thesis is to search for ways and measures application of which would result in increase of the fuel level indication accuracy of a potentiometric fuel level sensor. Basically there is a demand for reduction of number of fuel level sensors which do not comply with indication accuracy criteria at the output control.

Particular attention is given to the analysis of the wire arm of the fuel level sensor as it has the major influence on the fuel level indication accuracy compared to other components. Tension test and metallographic analysis of the stainless steel wire arm are carried out.

1. FUEL LEVEL SENSOR

1.1. Potentiometric fuel level sensor working principle

Potentiometric fuel level sensor (FLS) is a sensor used for measuring of fuel level height inside of a vehicle fuel tank. FLS comprises a floater arm which is firmly attached to a wiper of the actual sensor, which works as a potentiometer. As the floater floats on the fuel level, changing fuel level height H_{fuel} thus moves the floater accordingly. This floater motion is then converted into rotational motion of the wiper of the sensor. Angular position α of the wiper is thus a function of height of the floater (fuel height respectively).

$$\alpha = f(H_{fuel}) \tag{1.1}$$

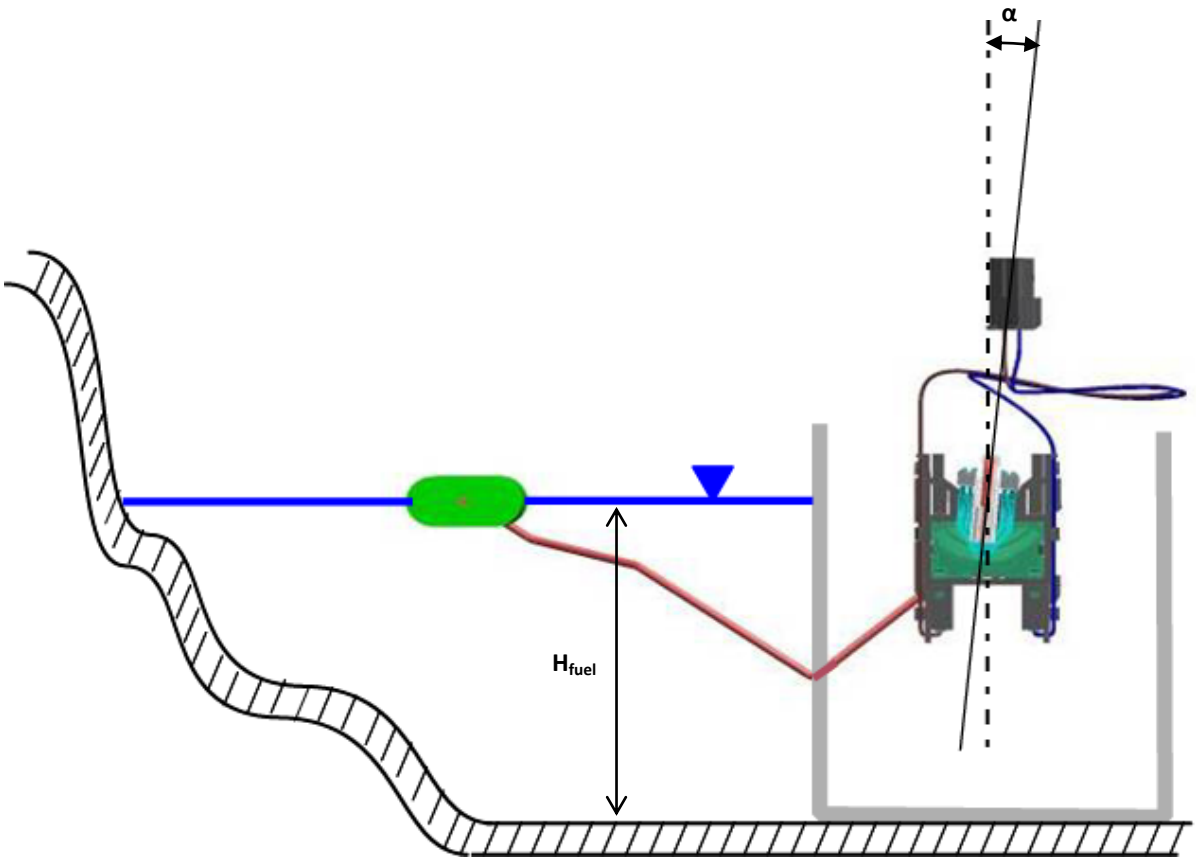

Fig. 1.1 Potentiometric fuel level sensor in car fuel tank.

In the figure 1.2 there is a detail of sensor without floater arm.

Fig. 1.2 Fuel level sensor without floater arm.

Wiper comprises a metal spring which electrically connects two separate electrical tracks on the resistor card. Both tracks consist of pads (also referred to as fingers). The upper track is so called conductive track and it has constant electrical resistance. The lower track is so called resistance track and it has increasing (or decreasing) characteristic of electrical resistance. Thus as the spring creates an electrical circuit at particular angle α, a particular pad of resistance track is engaged in the electrical circuit. Scheme of FLS electrical circuit is in the figure 1.3.

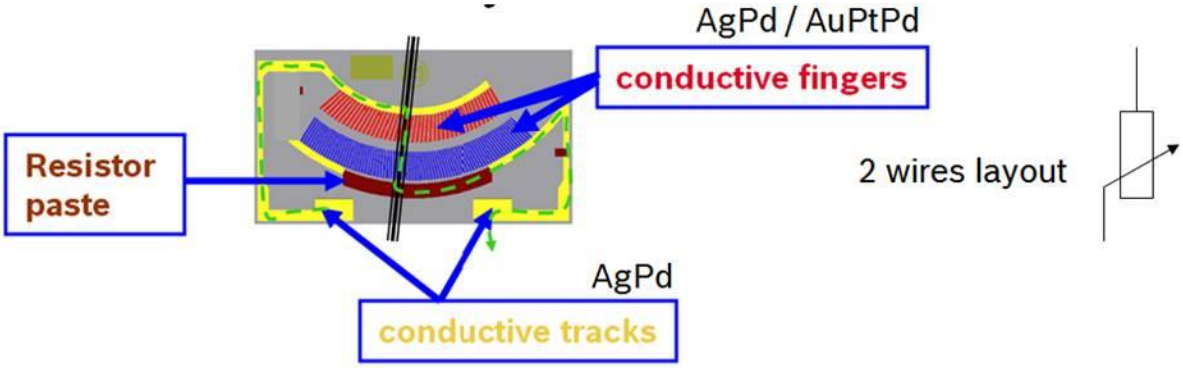

Fig. 1.3 FLS electrical circuit.

The dependence between fuel level height H_{fuel} and resistance value R_{el} indicated by the FLS thus has a discrete, stepped character as resistance increases (or decreases) pad by pad. In the figure 1.4 a decreasing characteristic of FLS is demonstrated.

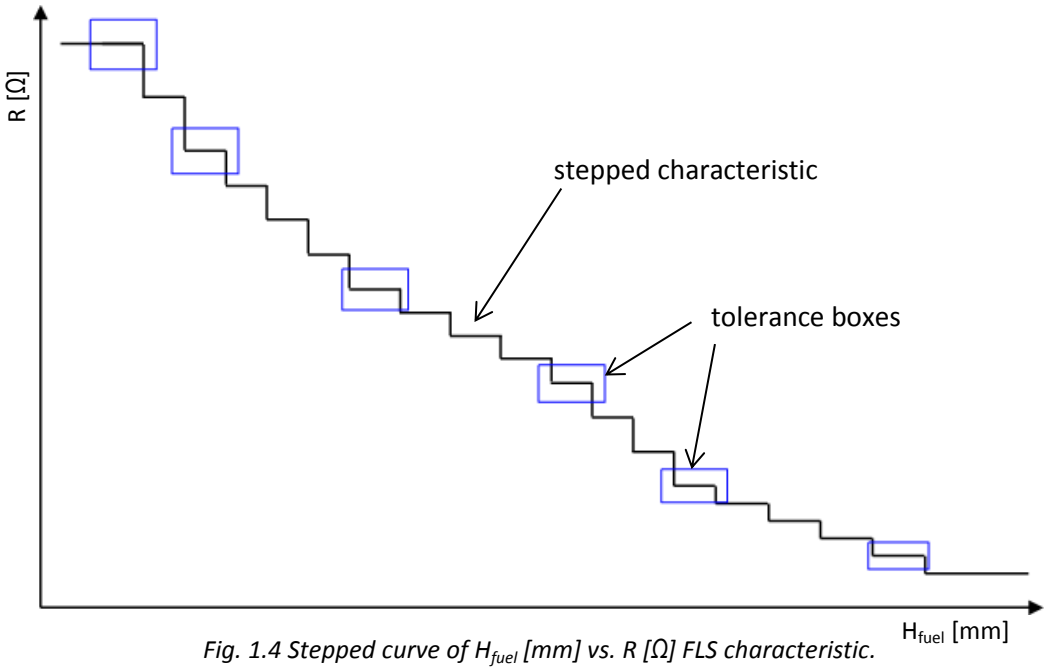

Fig. 1.4 Stepped curve of H_{fuel} [mm] vs. R [Ω] FLS characteristic.

In the picture 1.5 scheme of electrical installation of FLS in a car is depicted. The output voltage U_{FLS} is a function of the angular displacement of floater arm of FLS (fuel level height respectively).

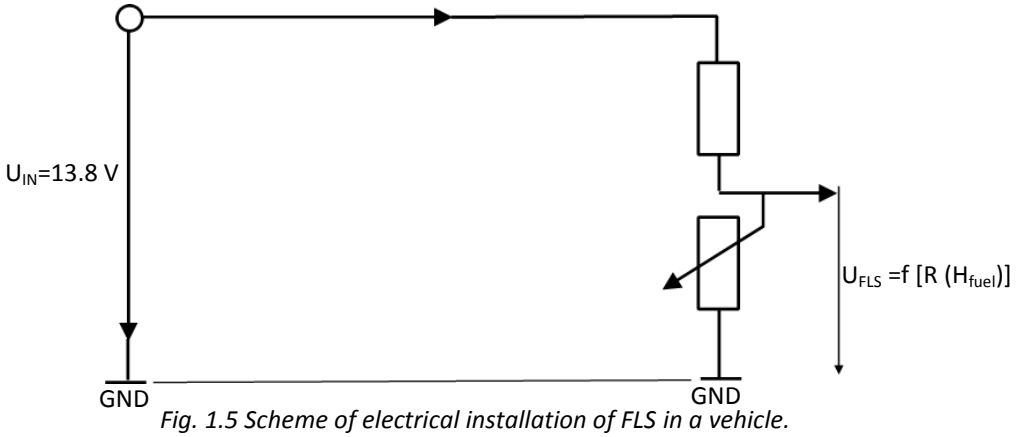

Fig. 1.5 Scheme of electrical installation of FLS in a vehicle.

Output signal of the sensor is then further processed in the vehicle's processing unit and then it is eventually indicated on the dashboard as information on the fuel amount inside the fuel tank.

FLS has following electrical properties:

- FLS works on a potentiometric principle with variable electrical resistance.
- Total resistance of conductive track is approximately 1Ω.
- Resistance range of resistor track is from 7 to 1000 Ω.
- Operating voltage: 5 to 16 V DC, corresponding to the whole vehicle electrical circuit.
- Operating current: 20 to 150 mA.
- Maximum power load is up to 1.5 W.
- Linear resistance characteristic between checkpoints.
- Stepped shape of resistance characteristic.

During the FLS design process many conditions, which are often conflicting, must be taken into consideration so that a reliable product is designed. Out of wide range of conditions FLS must especially meet following requirements:

Robustness against various types of fuel

There is a wide variety of fuels used in cars today and also the standard of fuel quality varies significantly in various car markets in the world. There are also markets where fuel contains high portion of impurities (typical is occurrence of active sulphur) or additives (such as ethanol or methanol). Also content of particles is an issue since it may lead to formation of deposits or intensification of mechanical wear of the contact system.

Fuel is thus an aggressive environment which poses an issue of material degradation and possible malfunction of FLS. In order to ensure robustness in various fuels over the lifetime of FLS, wide range of tests has to be carried out in the development stage before new FLS design can be released.

Functionality and reliability in various conditions and environments

Quality and functionality of FLS must be guaranteed in a wide range of conditions, this functionality is tested in the development stage by various tests such as:

- Durability tests
    - Medium is air or fuel
    - Room temperature or elevated temperature
- Long-term storing in fuel
    - Various temperature settings
    - Evaluation of soaking
- Environment tests
    - Temperature shocks and thermal cycling tests
    - Tests in environments with high humidity
- Vibration tests
    - Impacts, harmonic motion tests, vibrations in random directions etc.
- Robustness in fuel
    - Evaluation of robustness and resistance against fuel additives, impurities (sulphur), particles and various fuel types (ethanol, methanol, diesel, gasoline) etc.

Functionality of FLS must be guaranteed for a wide range of conditions that might occur during lifetime of a vehicle. Typically FLS must withstand and operate flawlessly in:

- wide range of temperatures (from -40°C to +90°C)
- temperature shocks
- vibrations etc.

1.2. ALTERNATIVE FUEL LEVEL SENSOR SYSTEMS

Although the potentiometric floater arm technology for fuel level measurement prevails because of its low cost, high reliability and durability there are also sensors utilising other physical principles under development. Since the potentiometric design main disadvantage is its susceptibility to wear of wiper contact in harsh fuel tank environment the development is aimed at either encapsulation of the contact system or at contactless systems. The ideal design seems then to be such which utilizes physical principles that enable design of FLS without any movable parts.

1.2.1. MAPPS [8]

Sensor that is conceptually the closest to the classical potentiometric design is a contactless system called MAPPS (Magnetic passive position system) shown in figure 1.6. It comprises a small magnet in the wiper body which pulls down flexible contact pads on a contact board producing a characteristic electrical resistance, which is the measurement value. The actual resistor card and layer with flexible contact pads are hermetically sealed and thus not exposed to the fuel environment. There is also no mechanical wear caused by sweeping of a wiper over the resistor card contact surface.

Fig. 1.6 MAPPS (Magnetic passive position system) FLS. [8]

1.2.2. FLS with Hall sensor [7], [9]

A straightforward contactless solution of a fuel level sensor continues to use the same mechanical structure as used in potentiometric FLS and only replaces the resistor card with a contactless magnetic sensor which works on the principle of Hall Effect. In the arrangement depicted in the figure 1.7, the linear Hall sensor is placed in the centre of a diametrally magnetized ring magnet, surrounded by some soft iron ring to guide the magnetic flux.

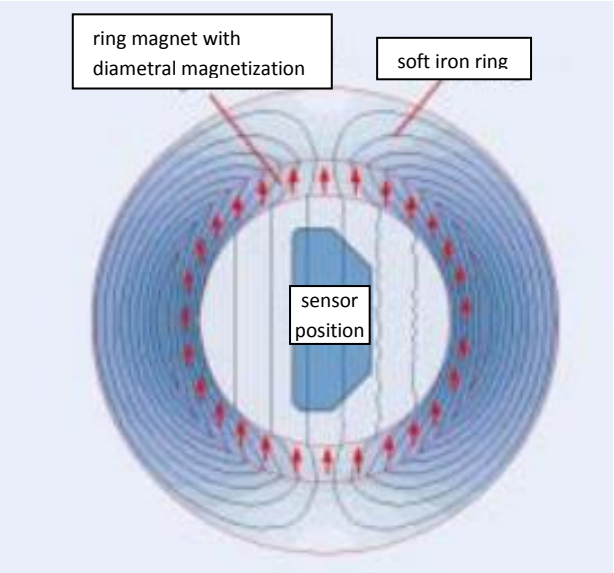

Fig. 1.7 Arrangement of a Hall sensor in FLS. [9]

This implementation has the advantage that the magnetic field *B* inside the ring is sufficiently homogeneous so that a small mechanical misplacement does not lead to big signal deviations. Additionally, the sensor is shielded by the soft iron ring and therefore better protected against external disturbances. Functions such as amplification, temperature compensation, signal conditioning, etc. can be economically added. Hall sensors feature low cost, small size, operation to zero speed, excellent linearity and rotational measurement repeatability in the neighbourhood of 0.05°.

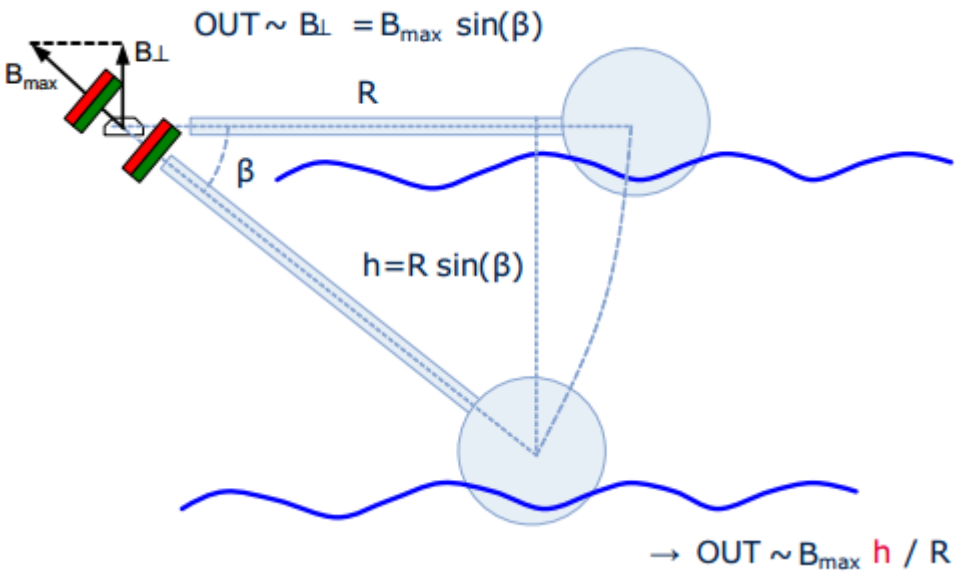

Fig. 1.8 Working principle of FLS with a Hall sensor. [9]

1.2.3. Capacitive FLS [1], [19]

Capacitive FLS usually consists of two concentric vertical cylindrical electrodes capacitance of which varies as the fuel level changes.

$$C = C_0 + C_1 + C_2 = C_0 + \frac{2\pi \cdot \varepsilon_0 \cdot \varepsilon_1}{ln\left(\frac{D}{d}\right)} \cdot h + \frac{2\pi \cdot \varepsilon_0 \cdot \varepsilon_2}{ln\left(\frac{D}{d}\right)} \cdot (H - h) \qquad (1.2)$$

Where:

C_0 is steady capacitance of the terminal

C_1 is capacitance of the immersed portion

C_2 is capacitance of the emerged portion of the electrode

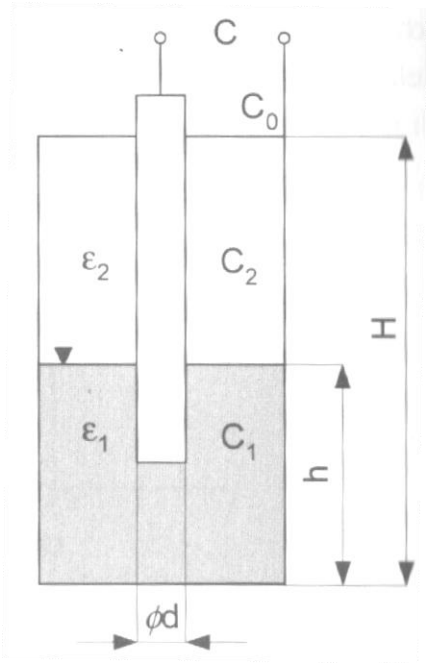

Fig. 1.9 Schematic view of a capacitive FLS. [1]

The capacitive sensor contains no moving parts, is rugged, simple to use, and easy to clean, and can be designed for high temperature and pressure applications. A danger exists from build-up and discharge of a high-voltage static charge that results from the rubbing and movement of low dielectric materials, but this danger can be eliminated with proper design and grounding.

1.2.4. AMR sensors [7], [19]

Anisotropic magnetoresistive FLS is similar to floater level sensors however a permanent magnet pair is sealed inside the float arm pivot. As the floater moves up the motion and location are transmitted as the angular position of the magnetic field. AMR sensors generate changes of resistance as an external magnetic field is rotated with respect to their magnetized thin film (typically consisting of

magnetized NiFe permalloy). The sensor primarily responds to field orientation, rather than field strength. Typically, four AMR sense elements, deposited on a common substrate, are connected in a Wheatstone signal-detection bridge arrangement. AMR sensors are also amenable to fabrication of integrated circuitry directly on the same chip.

The electronic monitoring system does not come in contact with the fluid and is considered intrinsically safe. The sensor similarly features high accuracy down to 0.02 degree of motion, excellent rotational-measurement repeatability, operation to zero speed, rotation-direction sense and maximum operating temperature of 200 °C. Disadvantages include medium size, medium cost, and the active-device bias current requirement.

There is not known any application in automotive fuel level measurement in the series production; however AMR sensors are widely used for fuel indication in aviation or marine applications.

Fig. 1.10 CAD model of FLS based on anisotropic magnetoresistive principle. [20]

1.2.5. Ultrasonic FLS [2], [10]

Ultrasonic FLS is another contactless system that measures the quantity of fuel in the tank by measuring the distance to the fuel level.

Ultrasonic transducers transmit ultrasonic waves then receive those ultrasonic waves reflected from an object. The time delay between transmission and reception of the ultrasonic waves (Time of Flight) is used to detect the position of the object. This technique can be used to determine the height or vertical distance of an object from the ultrasonic sensor. Thus ultrasonic transducers can be used to determine the height or level of fluid in a vehicle fuel tank. There are two different design approaches. Either the ultrasonic level transducer is placed above the fluid (a “face-down” design), so that the acoustic path is in the air or it can be placed below the surface of the liquid (a “face-up design). Figure 1.11 shows the layout used in both cases. Some ultrasound FLS systems also contain special algorithms to compensate for the effects of swashing fuels (slosh). In the case of

complex tank geometries, they also offer the advantage of storing characteristics curves in the sensor module and hence further improving the linearity of the display.

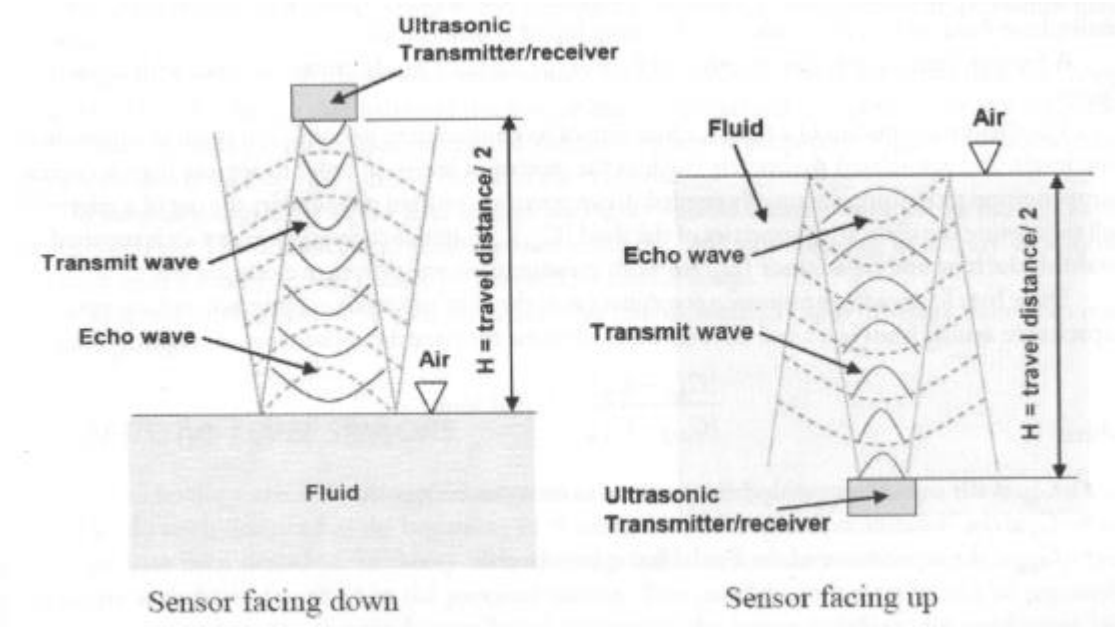

Fig 1.11 Comparison of face-up and face-down layout of the ultrasonic fuel level measurement. [2]

The output of ultrasonic sensors is normally a continuous voltage signal over time. The voltage signal is the representation of the fluid level measured by the sensor. The range, resolution and the linearity of the output signal could be different from one type of ultrasonic sensor to another. The sensor signal representing the fluid level is illustrated in figure 1.12.

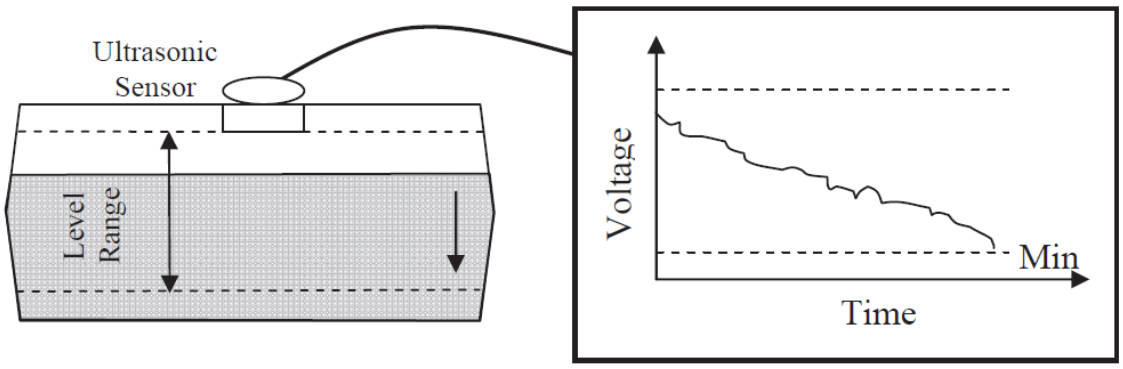

Fig. 1.12 Ultrasonic sensor signal representing fluid level in voltage. [10]

Ultrasonic level sensing has the advantage of no moving parts and hence is very reliable. The resolution is generally adequate for automotive purposes. However, the need for the receiver to be orthogonal to the liquid surface can be a design constraint in some cases. In addition the signal processing requirements, while not particularly complex, can be expensive to implement. Finally, most ultrasound generators are based on the piezoelectric effect and can require high operating voltages. This aspect needs particularly careful handling if ultrasound is to be used close to fuel or other inflammable vapour.

2. FLS DESIGN

2.1. Position of FLS in a fuel tank

Fuel level sensor assembly is mounted in a fuel supply module (FSM) assembly which is mounted inside a fuel tank of a vehicle. The actual FLS is positioned in a FLS pocket (rails positioning FLS housing) of a pot of the FSM which is depicted in figure 2.1.

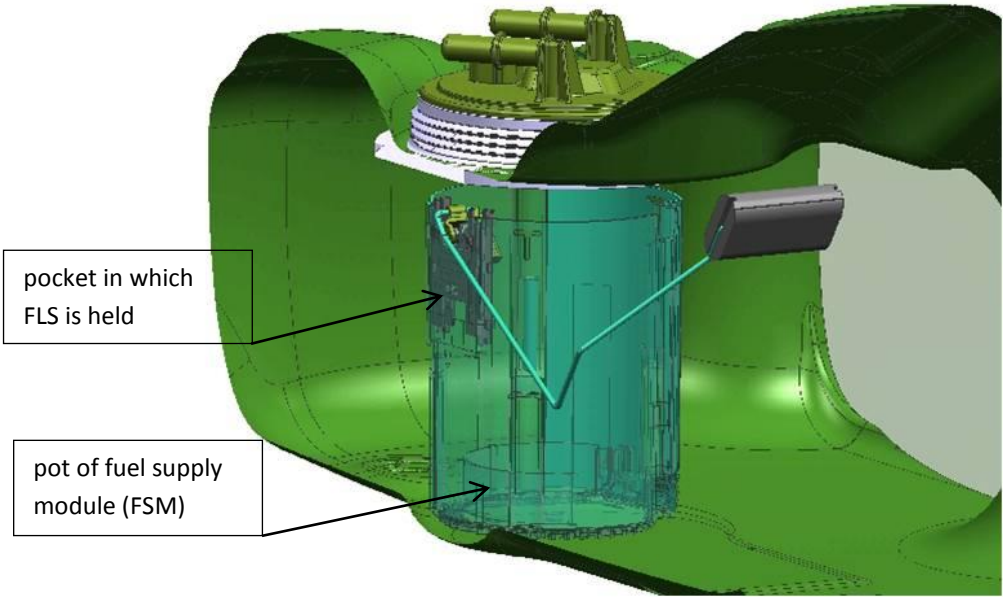

Fig. 2.1 Arrangement of a fuel supply module and FLS inside of a fuel tank.

2.2. FLS components

Fuel level sensor assembly consists of individual components.

Fig. 2.2 CAD model of FLS assembly (without floater arm).

2.2.1. Housing

Housing of FLS is a basic component which holds the whole FLS assembly together. Through its guide rails on the both sides and snap hooks is FLS positioned and fixed in the pocket in FSM pot. Housing also holds resistor card in position. There is a hole in the upper part of the housing which makes a fit for bearing pin. Cable set is also attached to the housing.

FLS housing also defines the angular range α_{max} of the wiper motion, i.e. free space for the wiper rotation between housing mechanical stops.

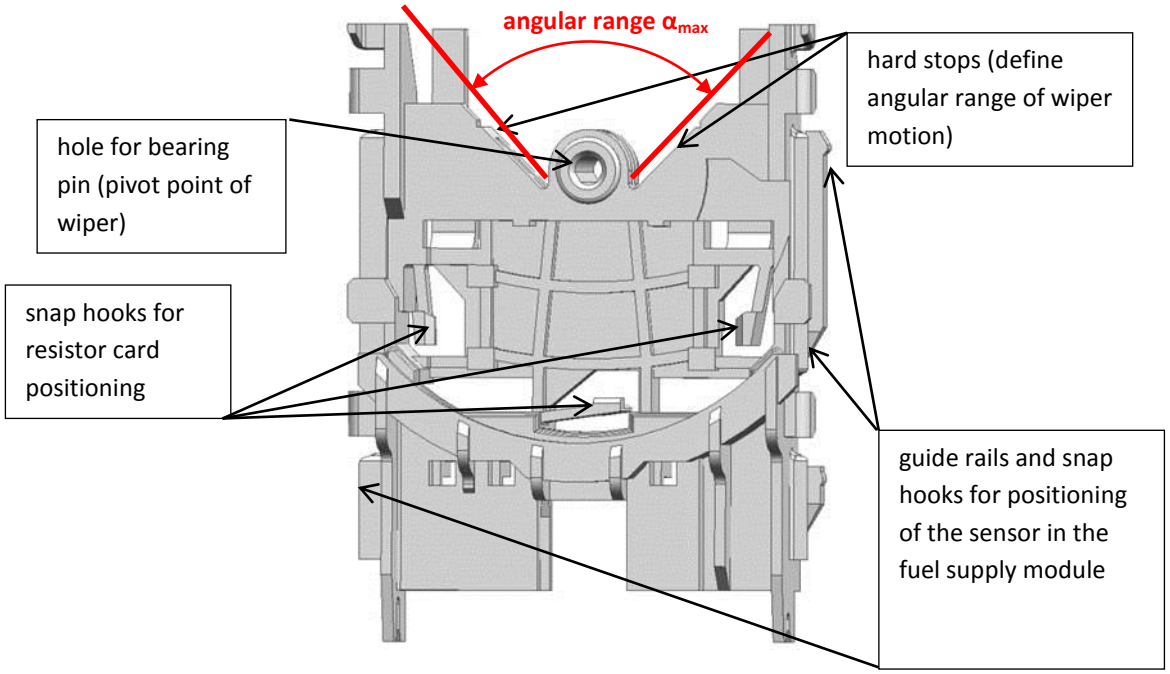

Fig. 2.3 Housing of FLS.

2.2.2. Wiper

Wiper is a connecting component between the floater arm and the resistor card and its function is to convert the vertical motion of the floater into the rotational motion. Wiper rotates around the bearing pin within the angular range given by the housing mechanical stops. Wire of the floater arm is firmly attached to the wiper body by snap hooks.

Wiper is also an electrical component of FLS. Its metal spring is a part of an electrical circuit as it creates an electrical connection between pads of both conductive and resistor track of the resistor card. Thus at a specific angle position of the wiper a particular electrical circuit is created through a particular resistor track pad.

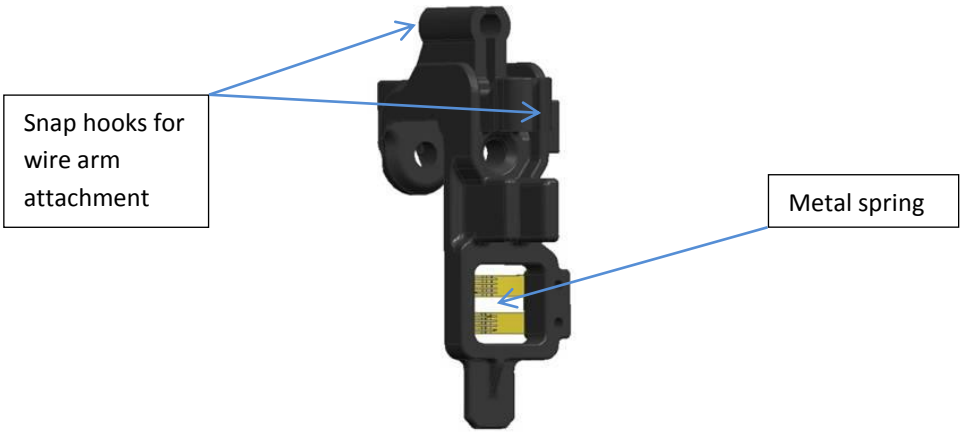

Fig. 2.4 Wiper of FLS.

2.2.3. Resistor card

Resistor card is an electrical component of FLS. There are two separate tracks on the resistor card:

- Resistance track – the lower track consists of pads and resistance track, the electrical resistance increases from minimum to maximum value from one end to the other, the layout design of track can be either:
  - "right" – maximum resistance in the right end of the track, or
  - "left" – maximum resistance in the left end of the track
- Conductive track – the electrical resistance of the conductive track is constant in the whole angular range.

These two tracks are electrically connected by the spring of the wiper. As the wiper sweeps over the resistor card it actually operates as a potentiometer.

Since the electrical resistance increases through the angular range of the resistor track, the resistance values measured on pads of the resistor track have discrete, stepped character as can be seen in the height-resistance characteristic.

In the resistor track there are particular pads the positions of which come from the actual checkpoints fuel level heights required by the customer. Between these checkpoint pads the resistance characteristic is linear.

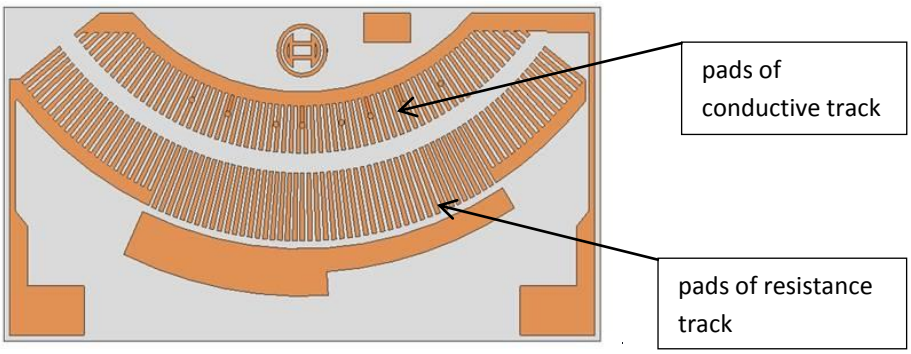

Fig. 2.5 Resistor card.

2.2.4. Bearing pin

Bearing pin is pressed in the hole of the housing. Bearing pin works as a pivot point for the wiper (floater arm) motion.

Fig. 2.6 Bearing pin.

2.2.5. Floater arm

Floater arm is a subassembly (wire arm, floater and washer) that converts the vertical changes of the fuel level height into the angular positioning of the wiper on the resistor card. It is enabled by a connection of the floater (which floats on the fuel level) and the wiper by a wire arm. The wire arm is at one end firmly attached to the wiper body by snap hooks, at the other wire end the floater is put on and secured by a washer. The axis of the wire arm rotation and the longitudinal axis of the floater are always parallel.

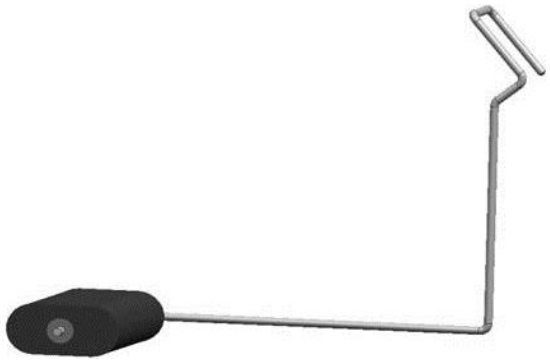

Fig. 2.7 Floater arm

Wire arm

Design of the wire arm varies for each FLS design because it has to enable reaching of required fuel levels in the fuel tank. The shape of the wire arm is thus defined by the free space in the tank. Wire arm has straight segments between bends; the wire is 2.5 mm thick.

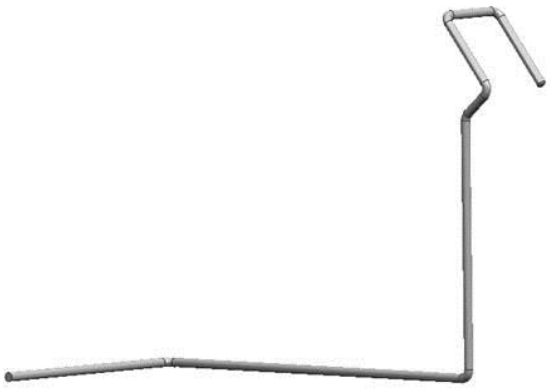

Fig. 2.8 Wire arm.

Floater

Floater is vitally important component for the FLS function. Each floater has to be designed in such a way that it provides sufficient buoyant force to develop moment to overcome both gravity of the floater arm and internal friction in the FLS contact system. It has to enable reaching fuel levels through the entire designed angular range of the housing. There are two major floater designs:

- **Rotational floater**

  The fit of a rotational floater on the wire enables the floater to rotate freely around its axis. This means the floater keeps its orientation parallel to the fuel level through the whole travel range.

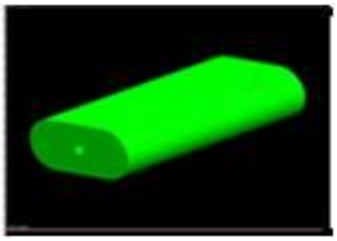

Fig. 2.9 Rotational floater.

- **Fixed floater**

  There is a groove in the fixed floater body through which it is kept in a fixed position to the wire. Fixed floater cannot rotate and thus its position relative to the fuel level is variable.

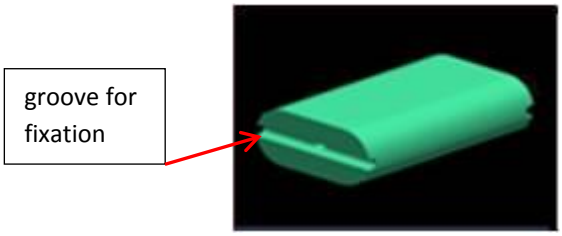

Fig. 2.10 Fixed floater.

2.3. Material application in FLS design

FLS assembly is completely immersed in fuel or in fuel vapours for the entire lifetime of a vehicle. In order to guarantee flawless functionality of FLS in such aggressive environment FLS components have to be made of materials highly resistant against fuel attack.

- **POM** [6]

Housing and wiper body are made from polyoxymethylene (POM), also known as acetal, polyacetal or polyformaldehyde, is an engineering thermoplastic used in precision parts requiring high stiffness,

low coefficient of friction and excellent dimensional stability. Because POM exhibits very low levels of cold flow, it is extremely creep resistant over a wide range of loads, times and temperatures. Its excellent resistance against swelling in liquid fuel environment is the main characteristic for which it is preferred over other polymer materials for application in fuel handling systems. It also performs high abrasion and heat resistance. POM is characterized by its high strength, hardness and rigidity to −40 °C. POM is intrinsically opaque white, due to its high crystalline composition, but it is available in all colours. POM has a density of 1420 $kg.m^{-3}$. POM homopolymer is a semi-crystalline polymer (75–85% crystalline) with a melting point of 175 °C.

- **Nitrophyl** [11]

Floater of FLS is made of Nitrophyl. Nitrophyl is a trademark for elastomer material used for floaters for liquid level sensing in fuel tanks. It is impervious to gasoline and fuel additives. It has very low density between 160 and 190 $kg.m^{-3}$ combined with resistance against swelling. Nitrophyl can operate in temperature range from -57°C to 104°C.

- **Stainless steel** [12]

The wire of the floater arm is made of X10CrNi18-8 stainless steel (also referred to as EN 10270-3-1.4310-NS-2.5). The wire material is a chromium-nickel austenitic stainless steel. The wire is cold worked and bent into the designed shape. Austenitic steels are typical for its excellent ability to strengthening when cold worked compared to the ferrite or ferrite-pearlite steels.

- **Brass**

Bearing pin is made of brass. Its surface has relatively low coefficient of friction and it also withstands aggressive fuel environment.

- **Aluminium oxide**

Alumina (Al_2O_3) is used as the substrate material of the printed circuit board of the actual potentiometer – resistor card. Alumina ceramics is inert and therefore is highly resistant to chemical attack. The corrosion resistance of alumina ceramics is generally far superior to metals. For the fuel level sensor application its high wear resistance is also advantageous.

- **Noble metals and their alloys** [4], [5]

Since the electrical circuit of the potentiometer is directly immersed in the fuel it must be made of highly corrosion resistant material. Yet both layout tracks on the resistor card and contact spring of the wiper have to be also wear resistant and have low coefficient of friction. Moreover it must have high electric conductivity. This combination of conflicting requirements can be met only by narrow group of metal alloys.

Resistor card layout materials

For the layout of the resistor card alloys of noble metals are used:

Ag + Pd

Liquid and solid silver and palladium are completely soluble in one another. Electrical contacts made of high palladium alloys provide surety of contact due to the absence of tarnish film. Silver-palladium alloys have very good corrosion and wear resistance.

Au + Pt

Gold-platinum alloys are used on resistor card layout for their excellent corrosion resistance. Gold-platinum also perform increased wear resistance. They have even better properties compared to silver-palladium alloys.

Materials for the wiper contact

Wiper designs of various FLS platforms employ various metals or their combinations. Precious metals are well known for their excellent resistance to corrosion in ordinary environments, but they are finding increasing application also in the construction for handling highly corrosive environment. Noble metals and their alloys are used such as:

Gold

Gold is used for its excellent electrical conductivity and corrosion resistance.

Silver

Silver is used as a cheaper alternative for gold spring.

Inconel + Nickel + Gold plating

Inconel is applied as a carrier for gold plated nickel nuggets which create the actual contact with the layout of the resistor card.

3. FLS COMPONENTS DESIGN RULES

Designing of every new FLS is a process in which customer's requirements are transformed into a new FLS design. Physical, geometrical, technological, economical and further aspects have to be taken into consideration during the design process.

3.1. Boundary conditions in FLS design

When each new FLS design starts it is already restricted by following specifications:

3.1.1. Fuel tank and FSM design

Shall the FLS designer start with a new FLS design he/she is always provided with a CAD model of a fuel tank in which fuel supply module (FSM) is already positioned. This can be considered as a customer specification since it is a result of the previous design stage. Basically it restricts design process in these ways:

- The actual position of FSM inside the fuel tank determines the position of FLS housing inside the fuel tank. The FLS housing is mounted in a pocket in the wall of the FSM pot.
- Fuel tank shape is another constriction that limits the designing of FLS. The floater arm shall not collide with the fuel tank wall in any position of the floater arm within its entire trajectory.

3.1.2. Fuel specification

Another part of customer's specification is what fuel is supposed to be used in the car. Fuel specification is vitally important for the design process because the FLS components have to be chosen and designed accordingly so that they are robust enough in contact with aggressive fuels. Moreover, robustness against fuel has to be considered in wide range of long-time operating conditions - mainly wide temperature range.

3.2. Physical principles in FLS design

From the point of view of mechanics, lever fuel level sensor operates on principles of fluid mechanics, to be specific on principles of hydrostatics.

Floater attached to the wire arm floats on a free fuel surface. The volume of floater immersion is given by the Archimedes' principle, i.e. the buoyant force F_{LIFT} acting on the floater is calculated as:

$$\boldsymbol{F}_{LIFT} = m\boldsymbol{g} = \rho_l V \boldsymbol{g} \qquad (3.1)$$

Where:

ρ_l is density of the liquid

V is volume of the liquid displaced by the floater (i.e. floater immersion)

g is the gravitational acceleration

Working principle of the lever FLS says that the transverse motion of the fuel level is converted into the rotational motion of the wire arm. In both cases of increasing and decreasing fuel level certain requirements must be met.

3.2.1. Increasing fuel level

In case of increasing fuel level the floater arm is moving upwards as the fuel tank is filled up from empty to full (so called E-F motion). It must be ensured that the floater provides sufficient buoyant force through complete floater arm travel range. This is ensured by the maximum floater immersion criterion. There are basically two phases of this motion.

- First phase starts with completely empty tank when fuel starts to fill up the tank. The fuel level height changes from 0 mm up to a certain level when the floater is submerged to such an extent ($H_{fuel} = h_1$) when the moment of the buoyant force $\vec{M}_{BF}$ reaches the static equilibrium to the sum of both moment of gravitational force of the floater arm $\vec{M}_{GR}$ and the moment of the frictional resistance of the FLS $\vec{M}_{FR}$.

$$\vec{M}_{BF} < \vec{M}_{GR} + \vec{M}_{FR} \qquad (3.2)$$

In this phase when fuel level height is below h_1 there is no motion of the floater arm, which means there is a certain narrow region of the fuel level height close to empty tank in which fuel level changes are not detectable.

- Shall the fuel level increase further, wire arm begins to rotate around its pivot point - bearing pin as an effect of the buoyant force acting on the floater. Wiper moves over the resistor card and the FLS indicates according to the actual fuel level. Rotational motion of the floater arm is possible until the hard stop of the housing is reached ($H_{fuel} = h_2$).

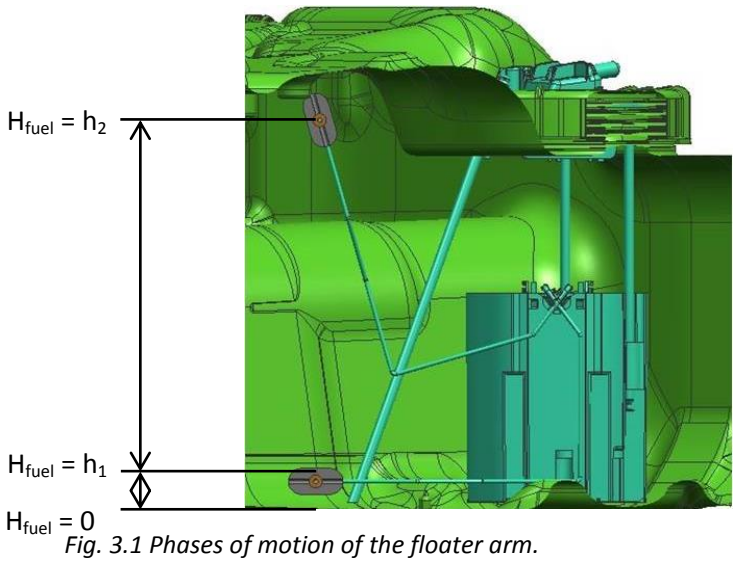

Fig. 3.1 Phases of motion of the floater arm.

Floater arm can be lifted only if sufficient buoyant force is developed by the floater. The moment from the buoyant force of the floater $\vec{M}_{BF\_incr}$ has to act against sum of both:

- moment of the gravitational force of the floater arm $\vec{M}_{GR}$
- moment of frictional resistance in the contact system of FLS $\vec{M}_{FR}$

$$\vec{M}_{BF\_incr} = \vec{M}_{GR} + \vec{M}_{FR} \tag{3.3}$$

Frictional component of the buoyant force

Moment of the frictional resistance in the FLS contact system $\vec{M}_{FR}$ is considered to be constant in the entire floater arm travel range:

$$\vec{M}_{FR} = const. \tag{3.4}$$

$$\vec{M}_{FR} = \vec{F}_{FR} \cdot R_{FA} \tag{3.5}$$

Where:

R_{FA} is radius of the floater arm

$\vec{F}_{FR}$ is force respective to the moment of frictional resistance $\vec{M}_{FR}$ and radius R_{FA}

In order to lift the floater arm frictional resistance of FLS has to be counteracted. Thus floater has to be large enough so that sufficient moment $\vec{M}_{LIFT\_FR}$ is developed from the buoyant force $\vec{F}_{LIFT\_FR}$:

$$\vec{M}_{LIFT\_FR} = \vec{F}_{LIFT\_FR} \cdot cos\gamma \cdot R \tag{3.6}$$

Where:

$$\vec{F}_{LIFT\_FR} \cdot cos\gamma = \vec{F}_{FR} \tag{3.7}$$

Thus $\vec{F}_{LIFT\_FR}$ needed to counteract the frictional resistance in contact system of FLS is calculated:

$$\vec{F}_{LIFT\_FR} = \frac{\vec{M}_{FR}}{cos\gamma \cdot R} \tag{3.8}$$

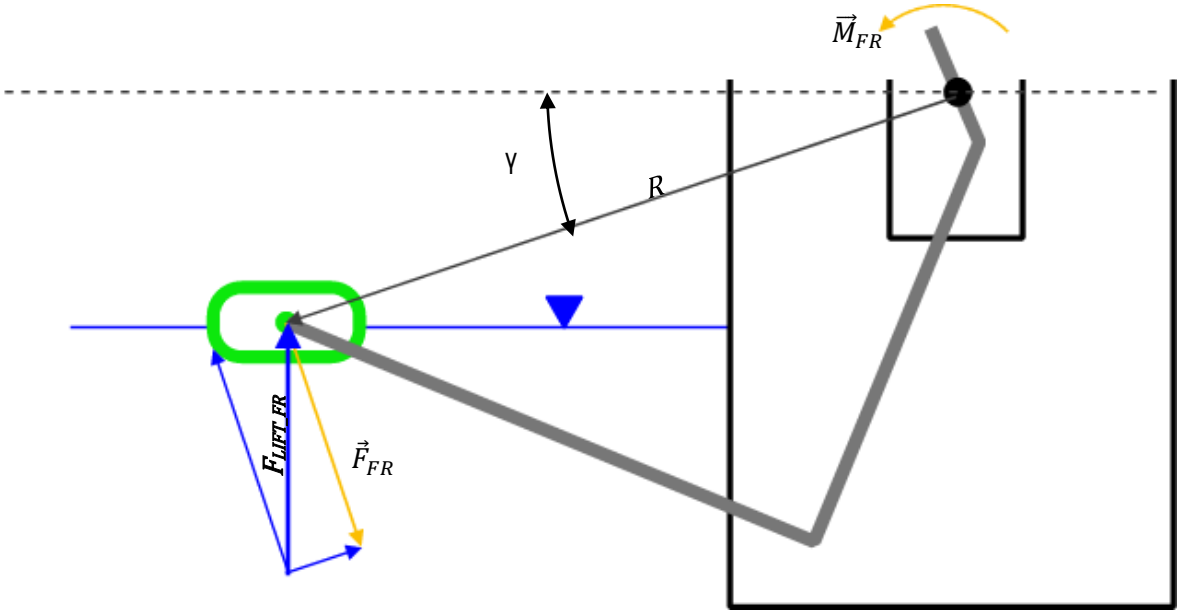

Fig. 3.2 Scheme of static equilibrium of the buoyant force F_{lift_FR} acting on the floater arm against the frictional resistance M_{FR} in the FLS contact system.

Gravitational component of the buoyant force

Moment of the gravitational force $\vec{M}_{GR}$ of the floater arm is variable according to the angle γ_{CG}:

$$\vec{M}_{GR} = \vec{G}_{FA\_tang} \cdot L_{CG} \tag{3.9}$$

Where:

$\vec{G}_{FA\_tang}$ is the tangential component of the gravitational force which has the rotational effect on the floater arm

$$\vec{G}_{FA\_tang} = \vec{G}_{FA} \cdot cos\gamma_{CG} \tag{3.10}$$

Where:

$$\vec{G}_{FA} = m_{FA} \cdot \vec{g} = const. \tag{3.11}$$

Where:

m_{FA} is mass of the floater arm,

$\vec{g}$ is gravitational acceleration,

L_{CG} is a distance of the floater arm centre of gravity from the pivot point

In order to lift the floater arm gravity of the floater arm has to be counteracted. Thus floater has to be large enough so that sufficient moment $\vec{M}_{LIFT\_GR}$ is developed from the buoyant force $\vec{F}_{LIFT\_GR}$:

$$\vec{M}_{LIFT\_GR} = \vec{F}_{LIFT\_GR} \cdot cos\gamma \cdot R \tag{3.12}$$

Moment from the gravitational force of floater arm $\vec{M}_{GR}$ is function of the angle γ. Component of the lifting force to counteract the gravitational force $\vec{F}_{LIFT\_GR}$ can be expressed from the lever equation:

$$\vec{F}_{LIFT\_GR} \cdot cos\gamma \cdot R = \vec{G}_{FA} \cdot cos\gamma_{CG} \cdot L_{CG} \tag{3.13}$$

Thus $\vec{F}_{LIFT\_GR}$ needed to counteract gravity of floater arm is calculated:

$$\boldsymbol{\vec{F}_{LIFT\_GR} = \frac{\vec{G}_{FA} \cdot cos\gamma_{CG} \cdot L_{CG}}{cos\gamma \cdot R}} \tag{3.14}$$

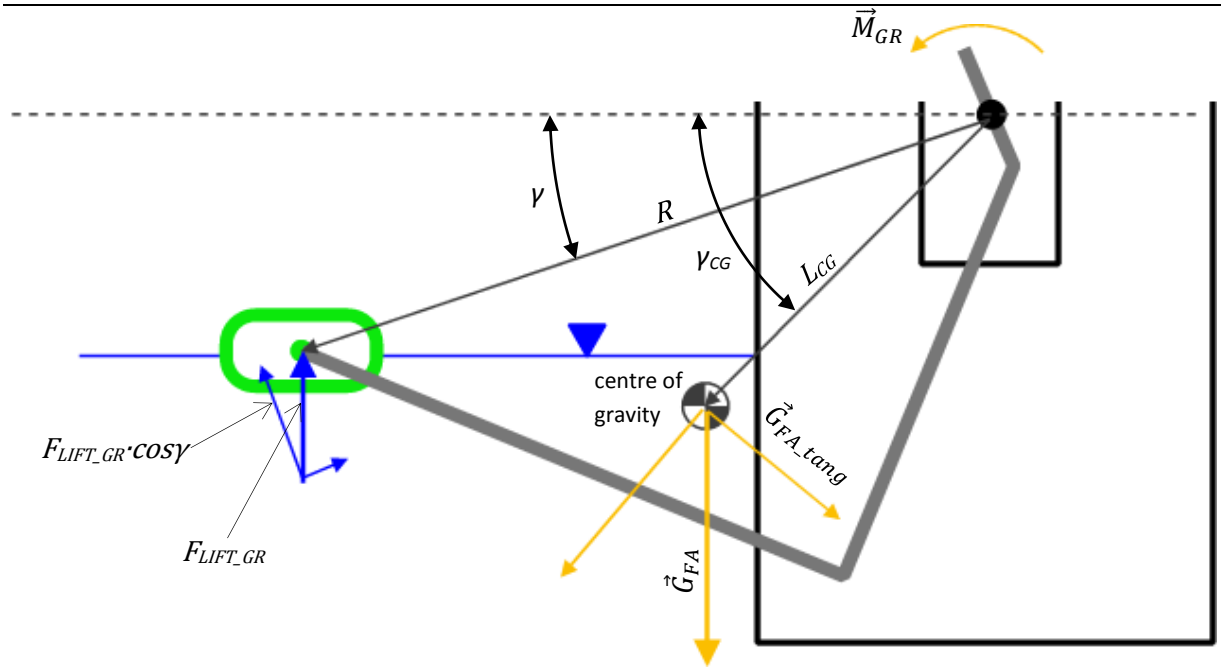

Fig. 3.3 Scheme of static equilibrium of the buoyant force acting on the floater arm against the gravity of the floater arm.

The buoyant force to develop the moment to ensure buoyancy and functionality of FLS is than simply a sum of both frictional and gravitational components:

$$\vec{F}_{LIFT\_INCR} = \vec{F}_{LIFT\_GR} + \vec{F}_{LIFT\_FR} \tag{3.15}$$

$$\vec{F}_{LIFT\_INCR} = \frac{\vec{G}_{FA} \cdot cos\gamma_{CG} \cdot L_{CG}}{cos\gamma \cdot R} + \frac{\vec{M}_{FR}}{cos\gamma \cdot R} \tag{3.16}$$

$$\boldsymbol{\vec{F}_{LIFT\_INCR} = \frac{\vec{G}_{FA} \cdot cos\gamma_{CG} \cdot L_{CG} + \vec{M}_{FR}}{cos\gamma \cdot R}} \tag{3.17}$$

In order to quantify the portion of the immersed floater volume the equation (3.17) is put in (3.1):

$$\frac{\vec{M}_{FR} + \vec{G}_{FA} \cdot cos\gamma_{CG} \cdot L_{CG}}{cos\gamma \cdot R} = \rho_{l.} \cdot V \cdot g \tag{3.18}$$

$$\boldsymbol{V = \frac{\vec{M}_{FR} + \vec{G}_{FA} \cdot cos\gamma_{CG} \cdot L_{CG}}{cos\gamma \cdot R \cdot \rho_l \cdot g}} \tag{3.19}$$

The buoyant force is function of the angle γ. High values of the angle γ correspond to the lowest – empty position of the floater arm. Thus it is important to always check whether the floater can develop sufficient buoyant force to lift the floater arm from the empty position.

3.2.2. Decreasing fuel level

It must be ensured that the floater arm has mass that provides sufficient gravitational force to counteract internal friction of FLS contact system through the complete wire arm travel range. This is ensured by the minimum floater immersion criterion.

Floater arm is lifted in the upper position given by the hard stop of the housing. Shall the fuel level start decreasing (F-E motion) the motion of the floater arm can be divided in following phases.

- Fuel level starts decreasing however the floater arm stays still in the full hard stop position until the moment of the buoyant force $\vec{M}_{BF}$ is in static equilibrium to the moment of the gravimetric force of the wire arm minus the moment of frictional resistance of the FLS.

$$\vec{M}_{BF\_decr} = \vec{M}_{GR} - \vec{M}_{FR} \tag{3.20}$$

- Shall the fuel level decrease further the floater arm begins to rotate around its pivot point (bearing pin) as an effect of the gravimetric force. Wiper moves over the resistor card and the FLS indicates according to the actual fuel level. Rotational motion of the floater arm is possible until the hard stop of the housing is reached. Any further fuel level decrement below the hard stop is not detectable by FLS.

Buoyant force developed from fuel on the floater when the wire arm decreases is calculated similarly as in case of the increasing level. However in the case of decreasing level the buoyant force is lower because the frictional resistance acts in the opposite direction.

$$\vec{F}_{LIFT\_DECR} = \vec{F}_{LIFT\_GR} - \vec{F}_{LIFT\_FR} \tag{3.21}$$

$$\vec{F}_{LIFT\_DECR} = \frac{\vec{G}_{WA} \cdot cos\gamma_{CG} \cdot L_{CG}}{cos\gamma \cdot R} - \frac{\vec{M}_{FR}}{cos\gamma \cdot R} \tag{3.22}$$

$$\boldsymbol{\vec{F}_{LIFT\_DECR} = \frac{\vec{G}_{WA} \cdot cos\gamma_{CG} \cdot L_{CG} - \vec{M}_{FR}}{cos\gamma \cdot R}} \tag{3.23}$$

In order to quantify the portion of the immersed floater volume equation (3.23) is put in (3.1):

$$\frac{\vec{G}_{WA} \cdot cos\gamma_{CG} \cdot L_{CG} - \vec{M}_{FR}}{cos\gamma \cdot R} = \rho_{l.} \cdot V \cdot g \tag{3.24}$$

$$\boldsymbol{V = \frac{\vec{G}_{WA} \cdot cos\gamma_{CG} \cdot L_{CG} - \vec{M}_{FR}}{cos\gamma \cdot R \cdot \rho_l \cdot g}} \tag{3.25}$$

3.2.3. Hysteresis

Hysteresis is the dependence of the output of a system not only on its current input, but also on its history of past inputs. The dependence arises because the history affects the value of an internal state. To predict its future outputs, either its internal state or its history must be known.

In the figure 3.4 the difference of the buoyant force between increasing and decreasing fuel level is depicted.

The diagram also shows the difference of floater immersion since the decreasing fuel level has lower floater immersion compared to the increasing fuel level. This phenomenon is the cause of higher hysteresis of FLS assembly when measured in fuel (immersion of floater is variable with respect to the floater arm position) compared to dry measurements (floater lies on solid lifting rod, thus the height position between floater and lifting rod is constant).

Simply by supplying from equation (3.17) and equation (3.23) difference between $\vec{F}_{LIFT\_INCR}$ and $\vec{F}_{LIFT\_DECR}$ can be calculated.

$$\Delta F = F_{LIFT\_INCR} - F_{LIFT\_DECR} = 2 * \frac{M_{FR}}{cos\gamma \cdot R} = 2 * F_{FR} \qquad (3.26)$$

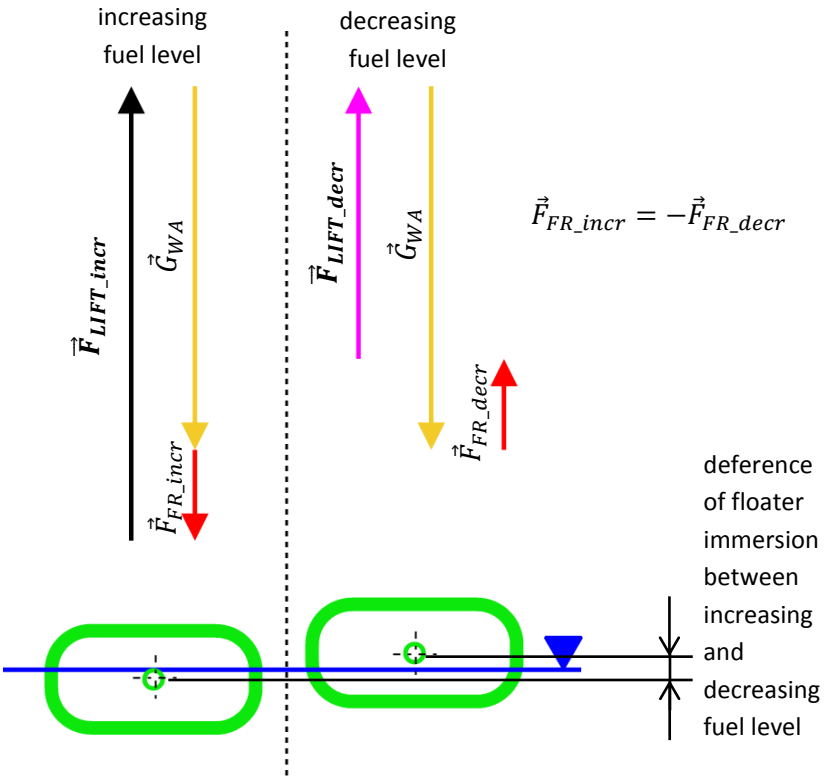

Fig. 3.4 Schematic comparison of the buoyant force acting on the floater arm (increasing and decreasing fuel level situations are compared).

In the FLS construction hysteresis is observed due to its mechanical properties:

- **Free play between movable parts with a clearance fit**

  There is a free play fit between the wiper hole and the bearing pin. This free play fit causes a slightly shifted mutual position of the wiper on bearing pin when the floater arm is lifted up compared to the position when the floater arm goes down.

- **Elastic deformation of the FLS**

  Components of FLS do not have absolute stiffness and under load they deform elastically to certain extent. Wire arm was found to contribute predominantly to this hysteretic behaviour.

- **Variable floater immersion**

  Concerning the hysteresis projecting in the FLS height-resistance characteristic a significant difference can be observed between measurement using a lifting rod for floater lifting (so called dry heights measurement) and measurement in liquid (fuel) when floater is lifted by the buoyant force of the fuel (so called wet heights measurement).

  In case of the measurement in fuel the portion of the floater immersed in fuel is variable with respect to the angular position of the floater arm described by the angle γ (see equations 3.19 and 3.25). Therefore in case of dry measurement, FLS characteristic shows reduced hysteresis behaviour compared to the measurement in fuel because in the dry measurement occurs no immersion.

Due to the hysteresis in FLS it is obvious that the height vs. resistance characteristic of increasing fuel level is not precisely overlapping characteristic of the decreasing fuel level. These two characteristics have identical profile shapes however there is a slight shift between them in the height direction as it is shown in the figure 3.5.

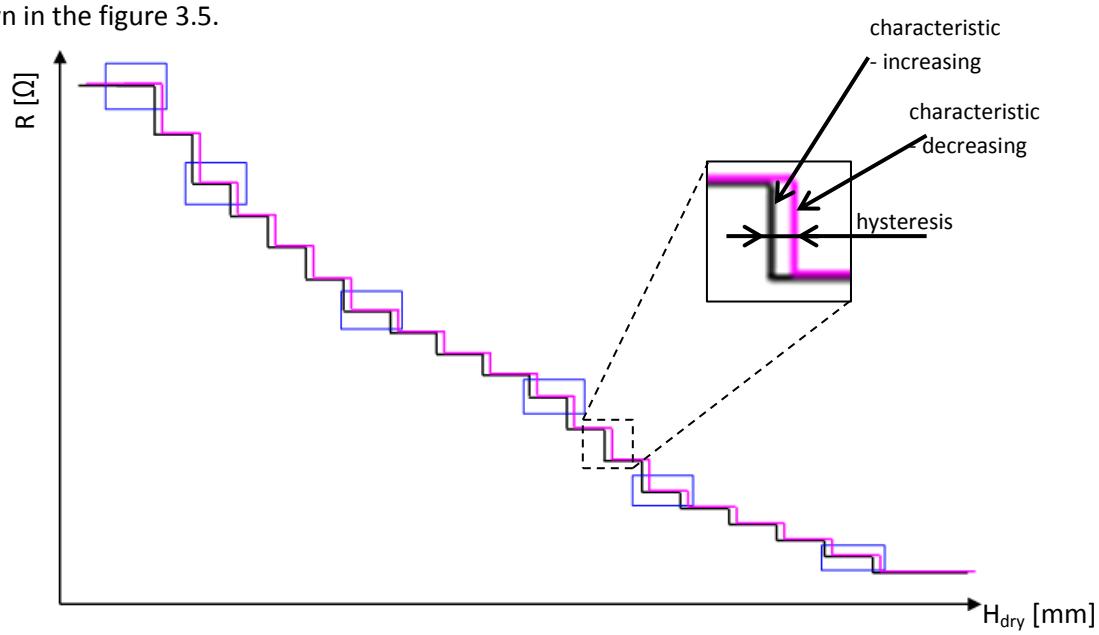

Fig. 3.5 Mutual shift between FLS characteristics for increasing and decreasing fuel level.

3.3. Customer-specific parameters

There is a set of parameters in the FLS design which are specified by the customer. Normally these parameters are:

3.3.1. Set of fuel level height values – checkpoints

The basic input data which is always provided by the customer is what the actual fuel level heights are at which the indication must be guaranteed with certain accuracy. These heights are called checkpoints and they represent fuel level heights measured from the bottom of the fuel tank. Usually there is between 4 and 12 checkpoint for the FLS design. This means the designer is provided with a set of fuel height vs. resistance values from the customer such as in the table 3.1.

Tab. 3.1 Representative set of fuel level heights H_{fuel} and electrical resistance values R_{el}.

fuel level height – H_{fuel} (nominal)	resistance – R_{el} (nominal)
[mm]	[Ω]
3.38	290.0
24.52	248.2
55.02	179.1
103.47	120.8
156.65	72.3
203.17	10.8

The designer is also provided with the CAD model of the fuel tank. Since the fuel tanks of modern cars have very complex irregular shapes also the dependence between fuel level height and actual volume of fuel in the tank is non-linear, i.e. fuel level height vs. electrical resistance has also non-linear characteristic. Nevertheless the characteristic is linearized between the actual checkpoints.

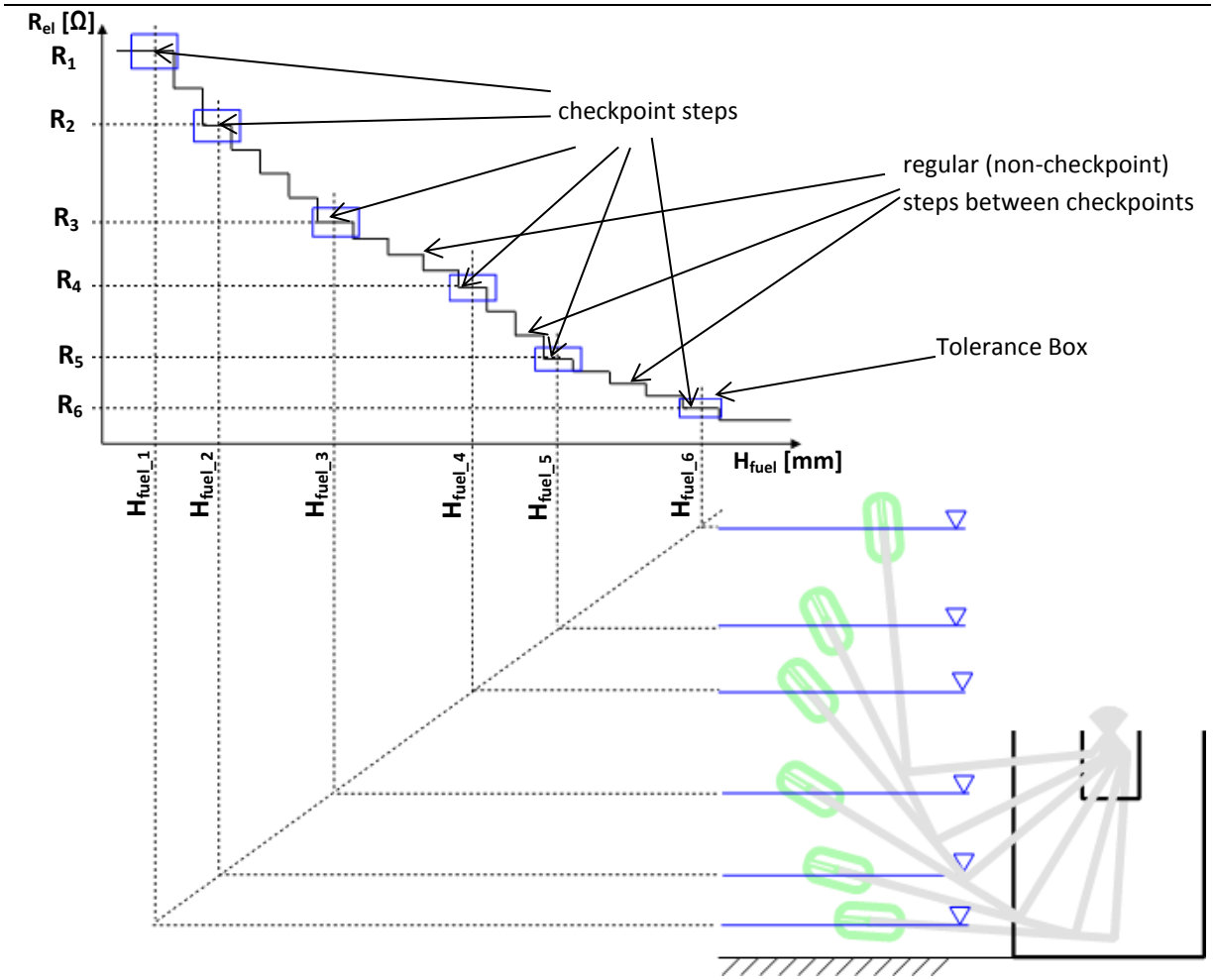

Fig. 3.6 Relation between floater position (given by checkpoint fuel level height H_{fuel}) and the resistance value R_{el} measured at given height.

3.3.2. Clearance between the floater arm and the tank wall

One of the main safety aspects that must be maintained is that the floater arm can move freely in the whole travel range, without any possibility of getting blocked by the tank wall or any other component. This is always checked in the design phase as an envelope is simulated around the whole floater arm trajectory (figure 3.7). There is always an additional safety distance between the envelope and the floater arm trajectory which ensures, that even in the worst case components alignment there will always be clearance between the floater and the tank wall. The envelope thus shall not collide with the tank wall. The clearance value between the envelope and the wire arm is specified either by the customer or by an internal design rule.

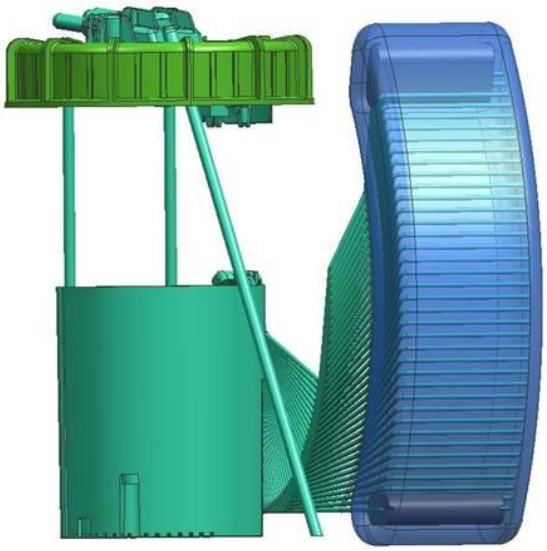

Fig. 3.7 Envelope simulated around the floater trajectory.

3.4. Individual design parameters

When all previous design stages were considered after that the actual individual designing process comes and eventually results in a new FLS design. The FLS components which vary design from design are: housing angular range, wire geometry of the floater arm, resistor card.

Given the tank shape and the exact position of the FLS pocket of FSM in the tank, designer's task is to design the wire arm and the angular range accordingly. It must cover complete fuel level range as it is specified by the customer; however the floater arm shall not collide with the tank wall at any floater arm position. This requires a skilled designer who designs both the housing angular range and the wire arm design simultaneously so that requirements are met. After this stage, when the wire arm design is finished, it comes to the designing of the resistor card layout.

3.4.1. TSG Wizard

TSG Wizard is a single-purpose software developed for purposes of the FLS design process. TSG Wizard is a CAD module incorporated in NX Unigraphics 3D CAD software which makes FLS designing very intuitive and user friendly.

Free 3D design within the actual free space in the fuel tank CAD model enables easy modelling and verification of various floater arm designs (various wire lengths, various wire bending designs, various floater designs). The floater arm is designed according to the free space in fuel tank and fuel level heights range. It is necessary to consider both the housing angular range and the floater arm radius at the same time since these parameters are closely related.

After the floater arm is designed the verification of buoyancy is checked by the TSG Wizard software based on relevant input data (fuel density, floater material density, moment of frictional resistance in FLS contact system) and data calculated from the actual floater arm and housing designs (3D coordinates of the centre of gravity of the floater arm, mass of the floater arm etc.).

The verification at this stage is very important since it tells the designer whether the floater can provide sufficient moment of the buoyant force so that the floater arm will not get stuck at any point through the floater arm travel when fuel level increases. And the other way around it verifies if the floater arm can provide sufficient moment of the gravimetric force so that it will not get stuck due to the friction in the FLS contact system when going down. If this is not met the design of the floater arm has to be modified, basically it can be done by:

- selection of a bigger floater (provides increased lifting force, thus increased moment)
- designing of a longer wire arm – floater is more distant from the pivot point, thus also moment from the buoyant force is higher

When the design is verified the dry heights H_{dry} are calculated relative to the checkpoints fuel level heights H_{fuel} provided by the customer. Dry height H_{dry} is a parameter which stands for the vertical distance between bottom of the fuel tank and the lower surface of the floater.
According to the design of the wire arm also the height coordinates have to be transformed into angular coordinates α on the resistor card (figure 3.8). These parameters are also calculated by TSG Wizard.

Subsequently the resistor card layout is designed by TSG Wizard which is determined by:

- housing angular range
- angular position of checkpoints calculated in the previous stage

The layout of the resistor card is designed in such a way that when the wiper connects checkpoint pads at the angular positions calculated in previous stage the resistance value specified by the customer will be indicated.
The regular (non-checkpoint) pads between checkpoint pads are designed in such a way that linearized characteristic between the checkpoint pads is achieved.

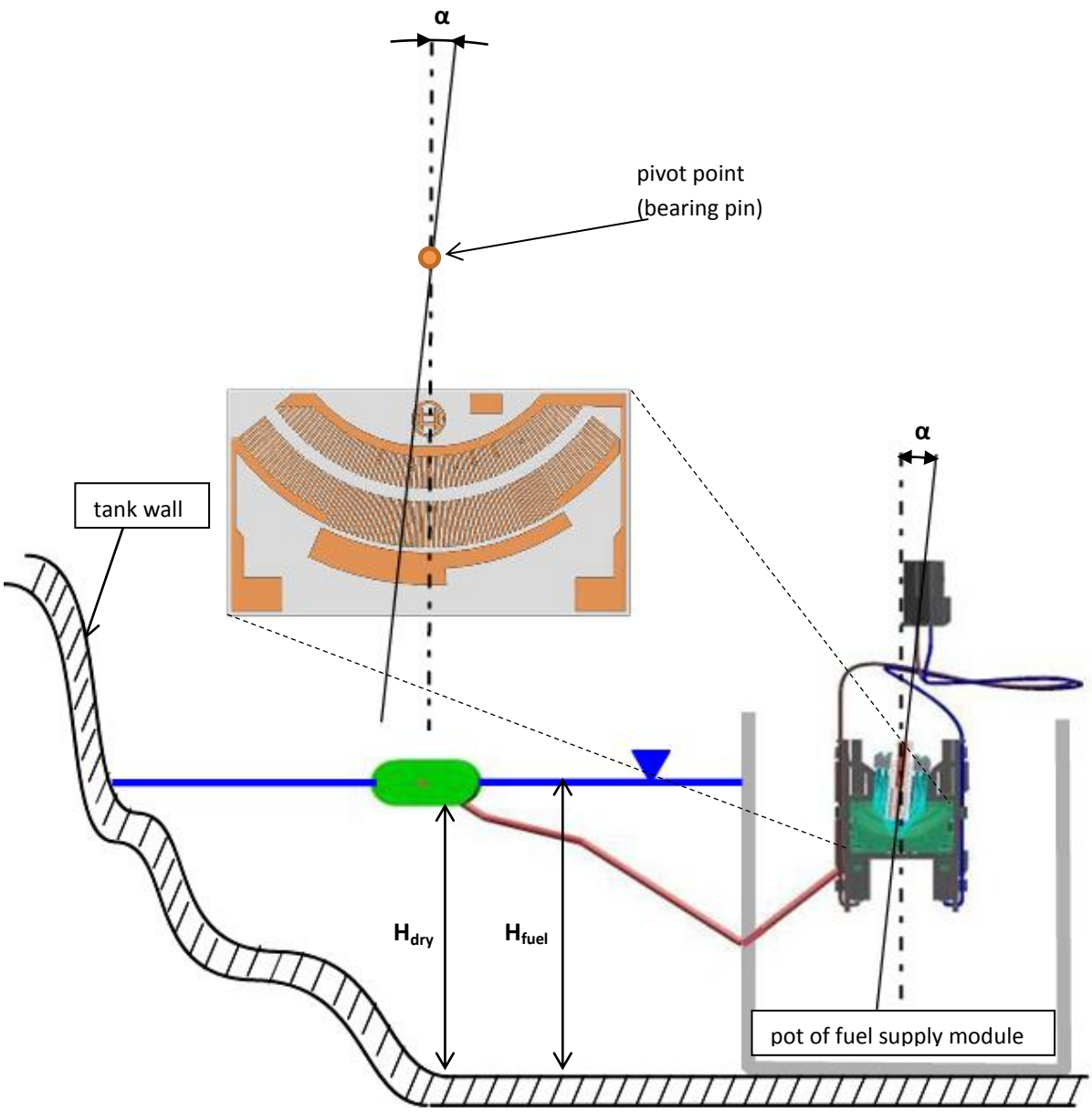

Fig. 3.8 Relationship between the floater position (H_{dry} or H_{fuel} parameter) and the angular displacement of the wiper on the resistor card (α).

As the original input data at the beginning of the design process is the fuel level height vs. resistance characteristic (H_{fuel} vs. R_{el}), the outcome of the design process is a transformation of those into the dry height vs. resistance characteristic (H_{dry} vs. R_{el}).

The dry height vs. resistance characteristic (H_{dry} vs. R_{el}) is further the only FLS characteristic which is measured and evaluated in the series production.

In the figure 3.9 the scheme is depicted of the transformation of input parameters into outputs. The transformation takes place during the design process of a new FLS.

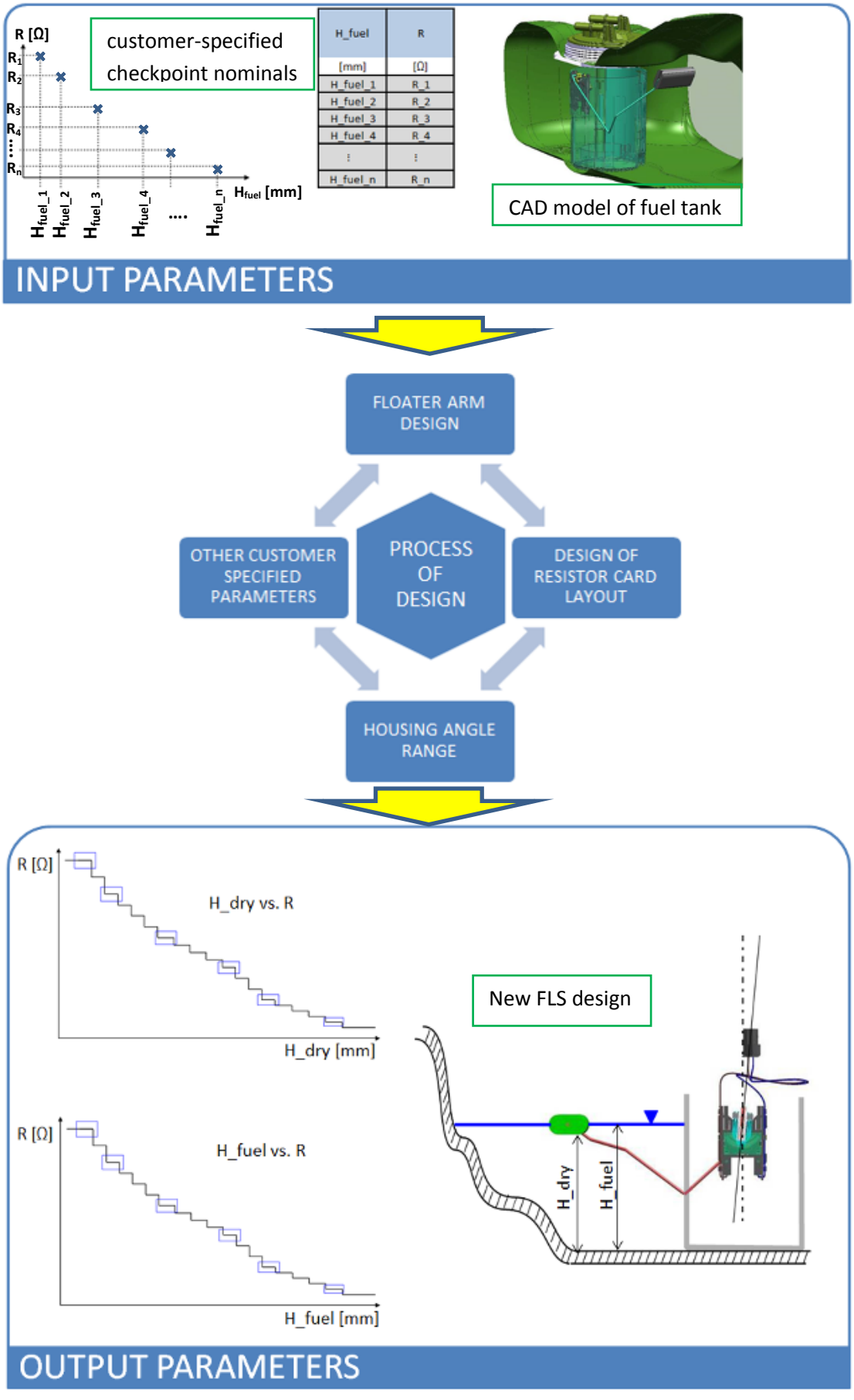

Fig. 3.9 Diagram of the transformation of customer-specified parameters into a new FLS design.

3.4.2. Design rules and recommendations in the FLS components design

wire arm design – radius

- Short wire arm benefits because it projects less the FLS angular inaccuracy compared to the long wire arms.
- On the other hand long wire arm has the same tolerance of end segment position deviation (+/- 1 mm) as the short wire arm.
- FLS with a short wire arm is easier for assembly into a fuel tank.
- Short wire arm allows application of a wider housing angular range and thus increases the indication resolution (more pads can be printed onto resistor card).
- Long wire arm increases moment developed by the floater (floater on a very short wire arm may not develop sufficient moment to float on the fuel level).
- Very long wire arm has higher mass and thus needs a bigger floater.
- Very long wire arm may cause high inaccuracy of FLS indication.

floater design

- rotational floater
    - It has reduced hysteresis.
    - Lower space demands in full position means it can detect higher maximum fuel level compared to fixed floater.
- fixed floater
    - More robust design (wears less than revolving floater).
- floater hole manufacturing technology
    - Moulded hole is preferred over drilled hole because of better wear properties.

housing design

- Housing design is mainly determined by the angular range which comes as a result of the FLS designing process.
- Wider angular range requires a wider layout on the resistor card thus it may lead to a higher cost.
- On the other hand wider angular range enables design with more pads, which implies higher resolution of indication.

resistor card design

- resistor card layout is determined by:
    - housing angular range
    - number and angular position of checkpoints
    - "left" or "right" layout orientation, i.e. angle vs. resistance characteristic of the resistor card can be either increasing or decreasing
- resistor card layout design rules:
    - angular position of checkpoint pads in resistor card layout is calculated and modelled in TSG Wizard based on:
        - checkpoint fuel level heights given by customer's specification
        - geometry of the actual FLS design which comes from the previous design stage
    - first and last checkpoint pads shall not be closer than 1,5° to the housing mechanical stop
    - total number of checkpoint pads is from 4 to 12 (based on the customer's specification)
    - the FLS characteristic is linearized in between individual checkpoints

4. TOLERANCE ANALYSIS OF FLS

In order to find out the tolerance range in which the fuel height indication of complete FLS assembly (FLS + floater arm) can range due to the variation of dimensions of individual subcomponents, all relevant dimensions of individual subcomponents and tolerances of these dimensions have to be taken into account so that a tolerance chain is calculated.

Two cases – positive and negative deviation from the ideal nominal floater height position are calculated as a combination of worst case in-tolerance dimensions of the subcomponents. By combination of these it is calculated what is the maximum possible inaccuracy of indication of complete FLS assembly when the "worst case" in-tolerance subcomponents get assembled.

In the picture 4.1 all relevant dimensions of FLS components are marked out.

4.1. Tolerance analysis of FLS assembly with a rotational floater

$$\boldsymbol{H_{dry+}} = A_+ + p_+ + N_+ \cdot \sin(90 - \alpha_{max} + \alpha) + \frac{M + M_+}{2} - \frac{L + L_-}{2} + x_+ + J + J_- - \frac{H + H_+}{2} + K_+ + dh\alpha_+ \quad (4.1)$$

$$\boldsymbol{H_{dry-}} = A_- + p_- + N_- \cdot \sin(90 - \alpha_{max} + \alpha) + \frac{M + M_-}{2} - \frac{L + L_+}{2} + x_- + J + J_+ - \frac{H + H_-}{2} + K_- + dh\alpha_- \quad (4.2)$$

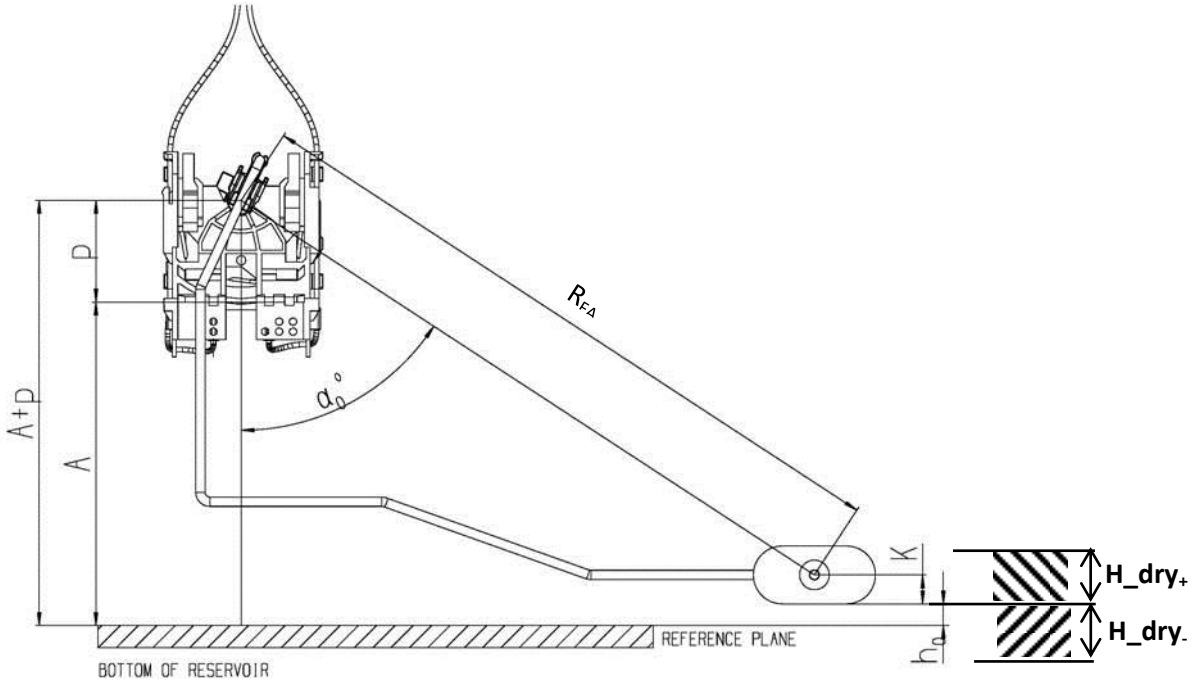

Fig. 4.1 Basic dimensions of FLS assembly with the floater arm in the empty hard stop position.

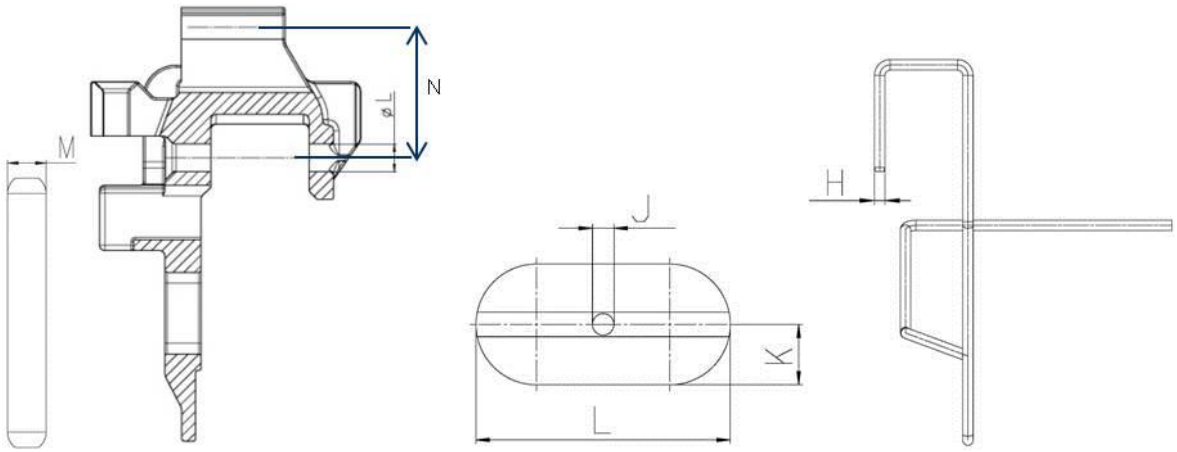

Fig. 4.2 Dimensions of FLS components relevant for the tolerance analysis.

Where:

$$dh\alpha_+ = A + p - R_{FA} \cdot \cos(\alpha_0 + \alpha + \alpha_+) - H_{dry} \quad (4.3)$$

$$dh\alpha_- = A + p - R_{FA} \cdot \cos(\alpha_0 + \alpha + \alpha_-) - H_{dry} \quad (4.4)$$

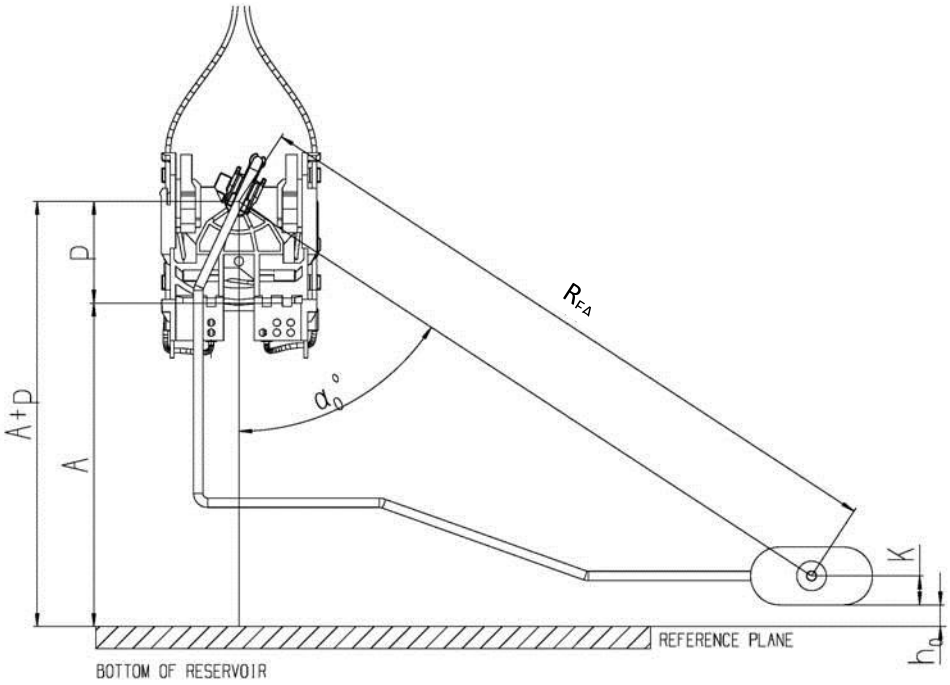

Fig. 4.3 Dimensions of FLS assembly relevant for the dry height (H_{dry}) calculation.

Where:

$$H_{dry} = A + p - R_{FA} \cdot \cos(\alpha_0 + \alpha) - K \tag{4.5}$$

When $\alpha = 0°$ then $H_{dry} = h_0$

Where:

$$R_{FA} = \sqrt{x^2 + (y_{(drw)} - N)^2} \tag{4.6}$$

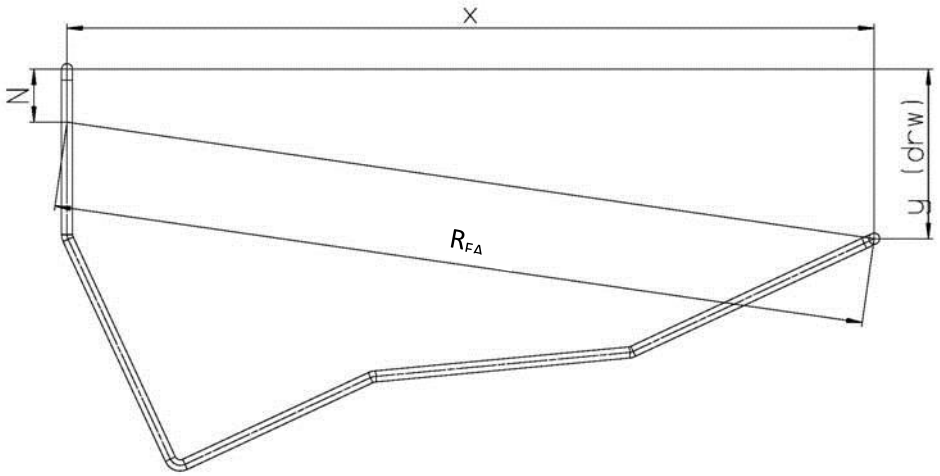

Fig. 4.4 Dimensions of a wire arm.

$$\alpha_0 = arccos \frac{A + p - h_0 - K}{R_{FA}} \tag{4.7}$$

Tab. 4.1 Dimensions of components relevant for tolerance analysis.

nominal	tol+	tol-	unit	
A	A+	A-	[mm]	distance between housing vertical position hard stop and bottom of fuel tank
p	p+	p-	[mm]	distance between housing vertical position hard stop and pivot point
N	N+	N-	[mm]	distance between pivot point and snap hook (for wire fixation) of wiper
α_max	/	/	[deg]	full angular range of the housing between hard stops
α	α+	α-	[deg]	wire arm angular position (from empty hard stop of housing)
α_0	/	/	[deg]	angle between vertical axis and connecting line between pivot point and end segment of the wire in the floater arm empty position
M	M+	M-	[mm]	bearing pin diameter
L	L+	L-	[mm]	diameter of the wiper hole for the bearing pin fit
x	x+	x-	[mm]	horizontal dimension of the wire arm (from wire drawing)
y (drw)	y+	y-	[mm]	vertical dimension of the wire arm (from wire drawing)
J	J+	J-	[mm]	diameter of the floater hole
H	H+	H-	[mm]	wire thickness
K	K+	K-	[mm]	half of the floater thickness
R_{FA}	R+	R-	[mm]	wire arm radius
H_dry	H_dry+	H_dry-	[mm]	dry height (H_dry)
h_0	h_0+	h_0-	[mm]	value of H_dry for α=0° (floater arm in the empty position)
/	dhα+	dhα-	[mm]	dry height deviation due to angular deviation (α+, α-) of FLS

In table 4.2 there are representative examples of worst case tolerance values that are calculated for a complete FLS assembly for three various wire arm radii (design with rotational floater is considered).

Tab. 4.2 Representative example of worst case deviation from the nominal dry height; three different floater arm radii are considered.

Floater arm radius **R = 120mm**		
nominal dry height (H_{dry})	+ tol (H_{dry+})	- tol (H_{dry-})
[mm]	[mm]	[mm]
1,16	2,96	-2,60
4,48	3,17	-2,76
9,38	3,45	-2,98
13,82	3,68	-3,17
23,64	4,13	-3,56
36,30	4,63	-4,03
50,68	5,10	-4,50
66,94	5,53	-4,94
85,74	5,88	-5,34
100,70	6,05	-5,56
121,53	**6,14**	**-5,73**
141,86	6,05	-5,71

Floater arm radius **R = 170mm**		
nominal dry height (H_{dry})	+ tol (H_{dry+})	- tol (H_{dry-})
[mm]	[mm]	[mm]
3,38	4,64	-3,57
12,43	4,94	-3,84
24,52	5,31	-4,19
34,61	5,60	-4,48
55,02	6,13	-5,02
78,79	6,64	-5,59
103,47	7,04	-6,08
129,19	7,30	-6,46
156,65	**7,38**	**-6,68**
176,97	7,28	-6,69
203,17	6,92	-6,49
226,40	6,33	-6,05

Floater arm radius **R = 220mm**		
nominal dry height (H_{dry})	+ tol (H_{dry+})	- tol (H_{dry-})
[mm]	[mm]	[mm]
4,99	5,86	-4,27
18,17	6,21	-4,62
35,47	6,66	-5,07
49,64	6,99	-5,43
77,70	7,58	-6,08
109,51	8,10	-6,72
141,63	8,45	-7,23
174,20	**8,59**	**-7,55**
207,91	8,46	-7,64
232,11	8,16	-7,51
262,20	7,48	-7,05
287,51	6,53	-6,30

4.2. Tolerance analysis conclusions

Following conclusions can be drawn from FLS tolerance analysis if the worst case tolerance chain is considered:

- The longer is the floater arm radius the higher is the possible deviation of indication of FLS.
- If the worst case criterion is applied the deviation can theoretically reach above 8 mm from nominal.
- The plus and minus deviation values are not symmetrical around the nominal value, this occurs since a shift within free play of both wiper on bearing pin and floater on wire are considered.
- There occurs a slightly higher deviation on a fixed floater than on a rotational floater; however the difference is rather negligible.

5. CHECKPOINT TOLERANCE METHODS

Each fuel level sensor that leaves the assembly line must meet certain accuracy of fuel level indication. There is always a set of checkpoint fuel level heights (checkpoints) at which certain accuracy of indication is guaranteed for the customer. This requires some methods of accuracy tolerance which can simply and quickly evaluate whether each assembled FLS complies or not with the checkpoint height tolerances.
Each FLS has its electrical characteristic, so called dry height vs. resistance characteristic. The position and shape of the curve of this characteristic thus can be used for the accuracy assessment and thus for identification and separation of FLS which do not comply with the accuracy criteria.

There are two different methods applied for the checkpoint tolerance – Tolerance Box evaluation method and Nominal Height evaluation method.

5.1. Tolerance Box evaluation method

The so called Tolerance Box method evaluates height and electrical resistance tolerance separately. This method evaluates the FLS characteristic by defining rectangular shaped (“box” shaped) areas placed onto the FLS characteristic. The position of these boxes corresponds to the nominal position of the checkpoint values. The dimension of the boxes is then what defines the tolerance for the shape of the FLS characteristic, i.e. FLS indication accuracy.

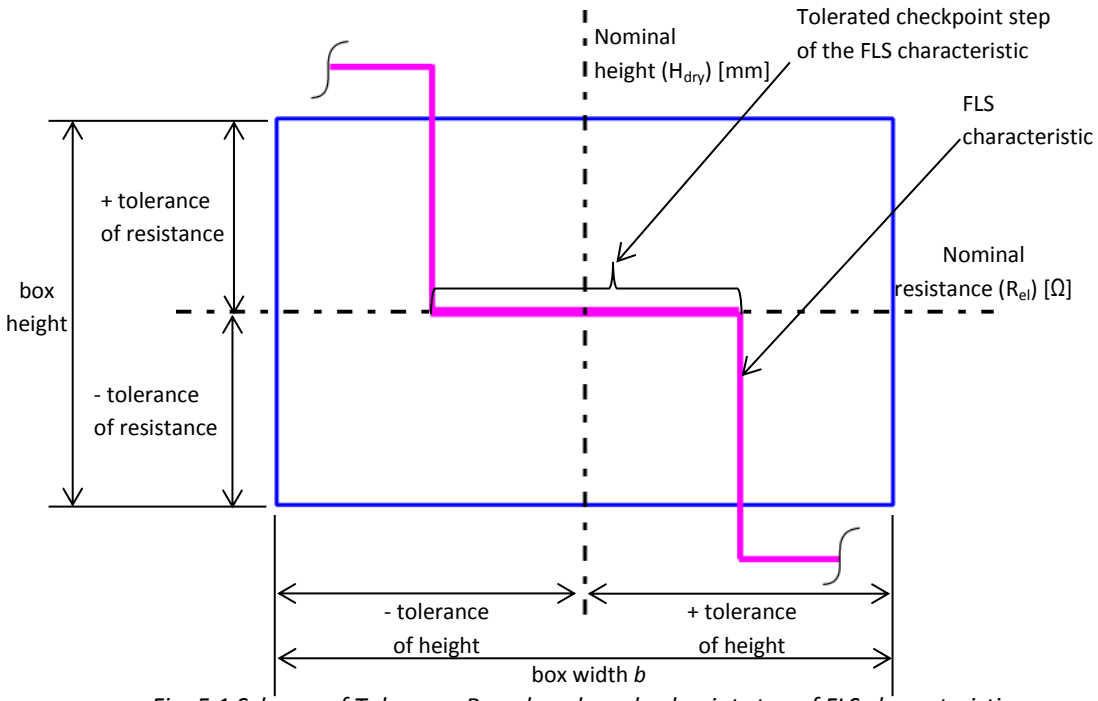

Fig. 5.1 Scheme of Tolerance Box placed on checkpoint step of FLS characteristic.

The common rules for dimensions of the tolerance box:

- The height of the box is defined by tolerance of electric resistance value. Generally, higher nominal resistance values have wider resistance tolerance.
- The width of the box *b* is then given as the +/- height tolerance value which comes from the customer specification (majority of FLS have box width *b* = 4 mm, i.e. ±2 mm from nominal).

Accuracy acceptance criteria (Tolerance Box method)

The tolerance criterion is that the checkpoint step must be placed inside of the area defined by the tolerance box in such a way, that the step overlaps at least 5% of the box width. If it does not, the FLS is evaluated as not complying with the acceptance criteria (NOK).

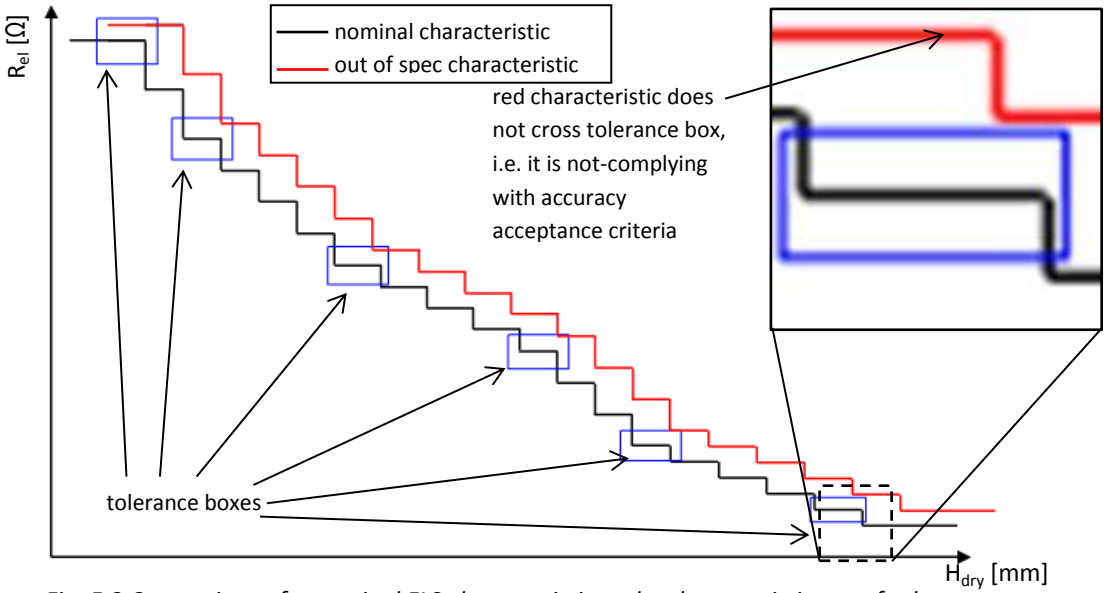

Fig. 5.2 Comparison of a nominal FLS characteristic and a characteristic out of tolerance.

Note:

Generally, FLS characteristic might be shifted in both electrical resistance values (y axis) and in height values (x axis). Since the point of this thesis is analysis of indication accuracy, and there are no issues registered due to the electrical resistance inaccuracy, only deviation in height values (x axis direction) will be considered in the following analysis, i.e. shift in the electrical resistance values will be neglected.

An example of this tolerance method is in the picture 5.3. There are two characteristics compared to the nominal characteristic. Both of them are shifted in the height direction (x axis) towards the border of the tolerance box, either in a positive height direction or in a negative height direction. In both cases the checkpoint step overlaps the minimal limit of 5% of tolerance box width thus they both meet the acceptance criteria.

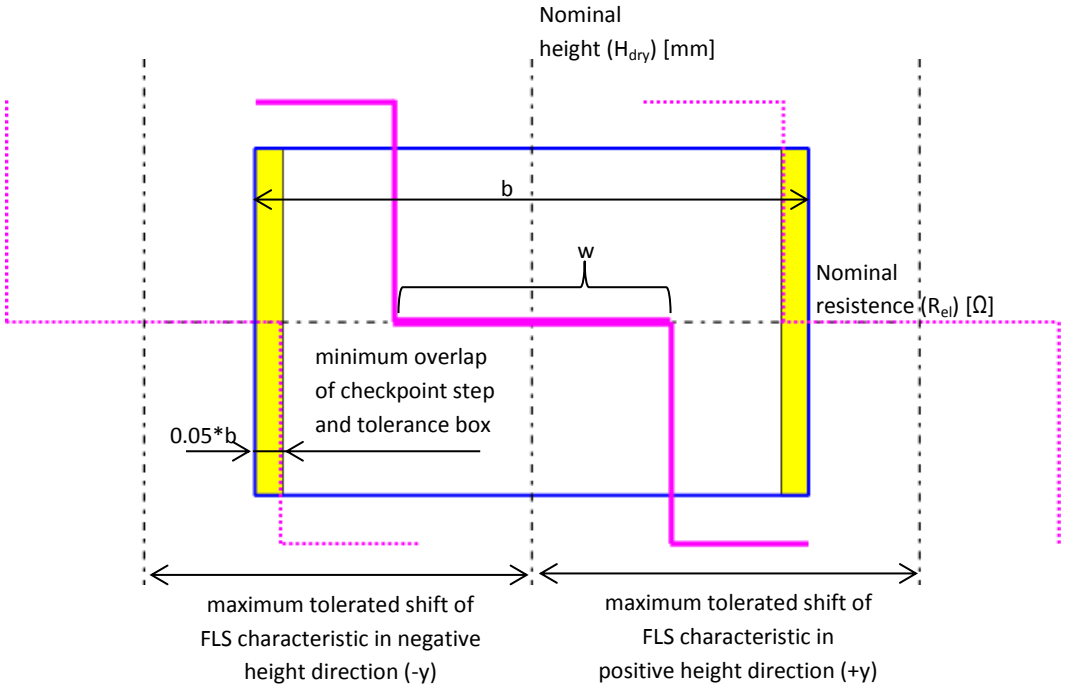

Fig. 5.3 Comparison of FLS characteristic in nominal position and characteristics shifted towards tolerance borders given by the width of tolerance box.

Based on the fact that the checkpoint step must intersect the tolerance box a formula can be derived for the calculation of a maximum tolerated shift of the characteristic from the nominal position.

$$\pm y_{tol\_box} = \frac{b}{2} - 0.05 \cdot b + \frac{w}{2} \qquad (5.1)$$

Where following parameters directly affect the actual FLS height tolerance:

5.1.1. Width of tolerance box (*b*)

The width of the tolerance box is the first parameter to adjust in order to increase the FLS height tolerance. The wider is the box the larger is the tolerance range for the accuracy of FLS height indication. Obviously wider box means potentially lower accuracy of the FLS for the customer.

5.1.2. Width of checkpoint step (*w*)

The width of the checkpoint step is another parameter which significantly affects the height tolerance range of the FLS. Basically, wider step ($w_2 > w_1$) enables that the characteristic can be shifted more from its nominal position in the height direction ($y_2 > y_1$), while still complying with the 5% overlap condition.

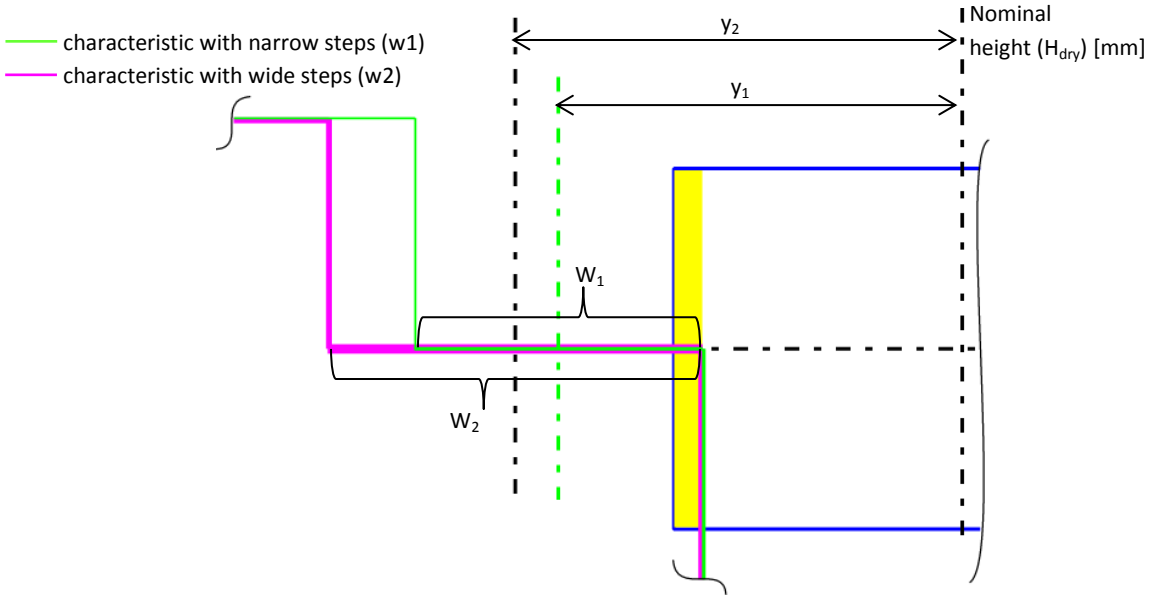

Fig. 5.4 Comparison of maximum tolerated shift of FLS characteristic from the nominal position (characteristic with narrow steps is compared to the characteristic with wide steps).

The width of each step of FLS characteristic is determined by:

- dimensions of the resistor card layout.
- floater arm radius

The width of the step is actually combination of both widths of pad and space on the resistor card layout as it is shown in the figure 5.5.

The picture also shows the relationship between wiper contact position and the actual indicated electric resistance value. When the contact is in the position 1 there is a switch in the resistance value (from R_{el_1} to R_{el_2}), value R_{el_2} is than indicated until the contact reaches the position 2 on the resistor card when the resistance switches from R_{el_2} to R_{el_3} and so on.

Finally the picture also shows the influence of the floater arm radius R_{WA} and the angular position γ of the floater arm on the step width w in the dry height versus resistance (H_{dry} vs. R_{el}) characteristic.

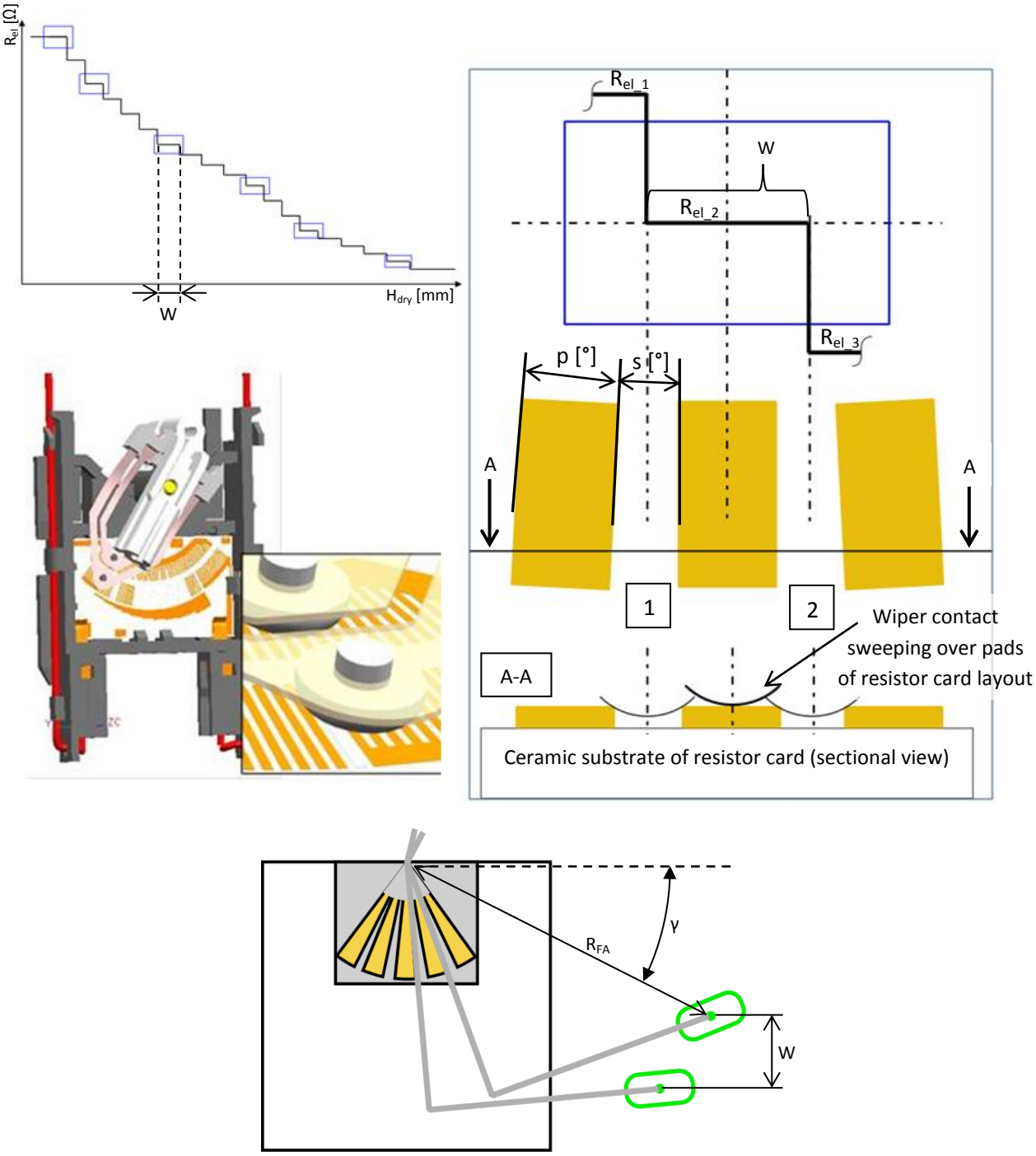

Fig. 5.5 Influence of the pad width (p) and the space width (s) of the resistor card layout and the influence of the floater arm radius (R_{FA}) on the width (w) of a step of FLS characteristic.

This means that in order to change the size of the step of the FLS characteristic, either the dimension of the pads *p* and spaces *s* on the resistor card layout or the floater arm radius R_{FA} have to be modified. Wider pads logically result in wider steps of the FLS characteristic. On the plus side wider pads provide increased tolerance of the deviation from H_{dry} nominal value. On the contrary the indication resolution around the checkpoint value is reduced.

$$w = \frac{2\pi R_{FA}}{360}(p + s) \cdot cos\gamma \tag{5.2}$$

If the equation (5.2) is put into the equation (5.1) the tolerance of deviation from H_{dry} nominal provided by the Tolerance Box method is calculated:

$$\pm y_{tol\_box} = \frac{b}{2} - 0.05 \cdot b + \frac{\frac{2\pi R_{FA}}{360}(p+s)\cdot cos\gamma}{2} \qquad (5.3)$$

5.1.3. Wire arm radius (R_{FA})

The wire arm radius has a significant effect on the FLS height tolerance. However its influence shall be divided in two opposing effects:

Positive effect:

Wire arm with a longer radius results in wider steps of the FLS characteristic as the floater on a longer wire arm has longer travel. Characteristic with wider steps then can be shifted more from its nominal height position as it shows figure 5.6.

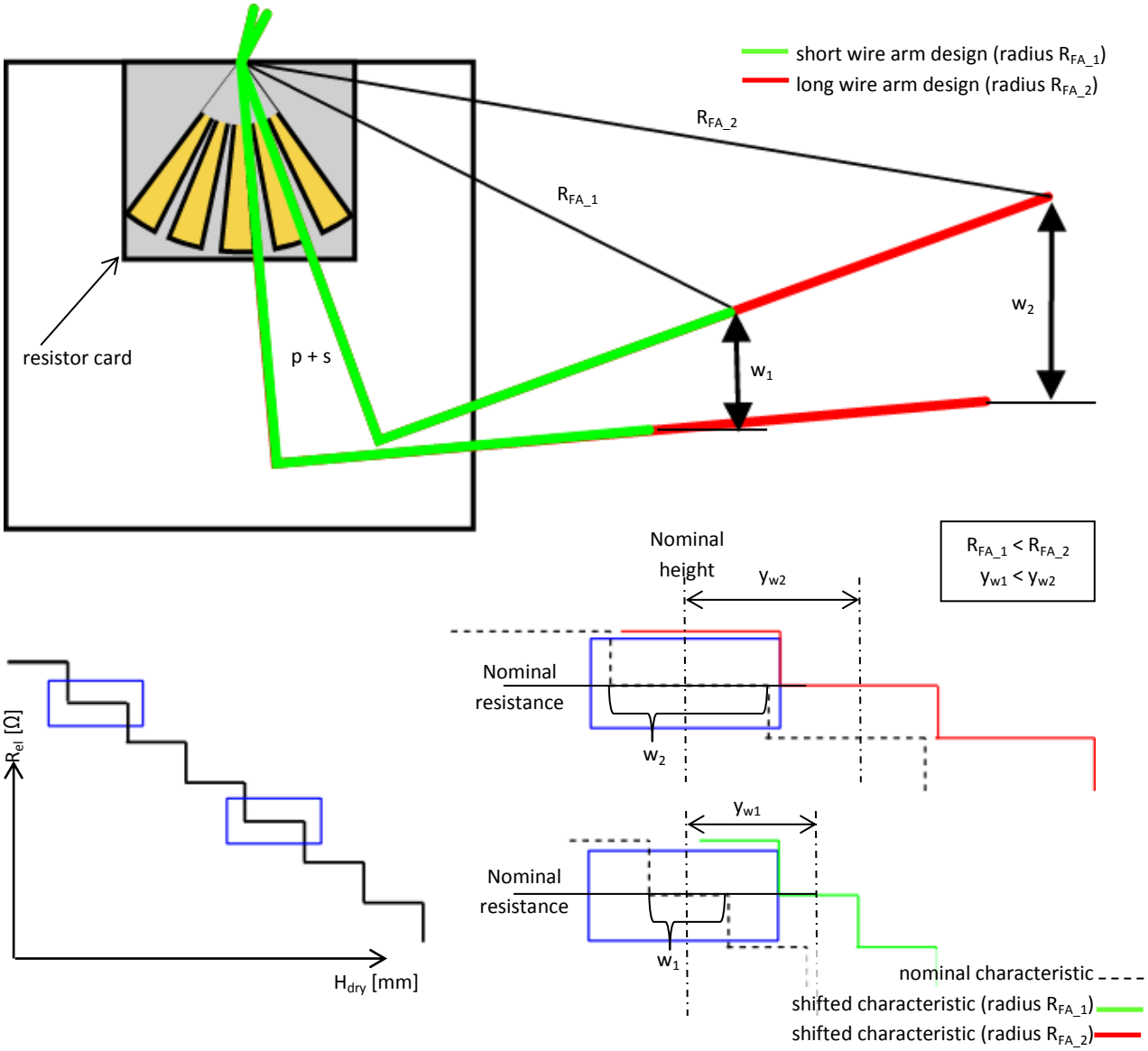

Fig. 5.6 Influence of the floater arm radius on the tolerance of deviation from the nominal dry height.

Negative effect:

On the other hand, there is a significant negative influence of the long wire arm since it projects more the FLS angular deviation α_{dev} as it shows figure 5.7. The picture shows that if there is a big angular deviation of the actual FLS (due to e.g. imprecisely manufactured resistor card or housing or other FLS components) by application of a wire arm with long radius the characteristic might not cross the tolerance box. In other words there is a certain value of angular inaccuracy of FLS above which the negative effect of the long wire arm radius prevails over the positive effect of wider steps of the characteristic mentioned above.

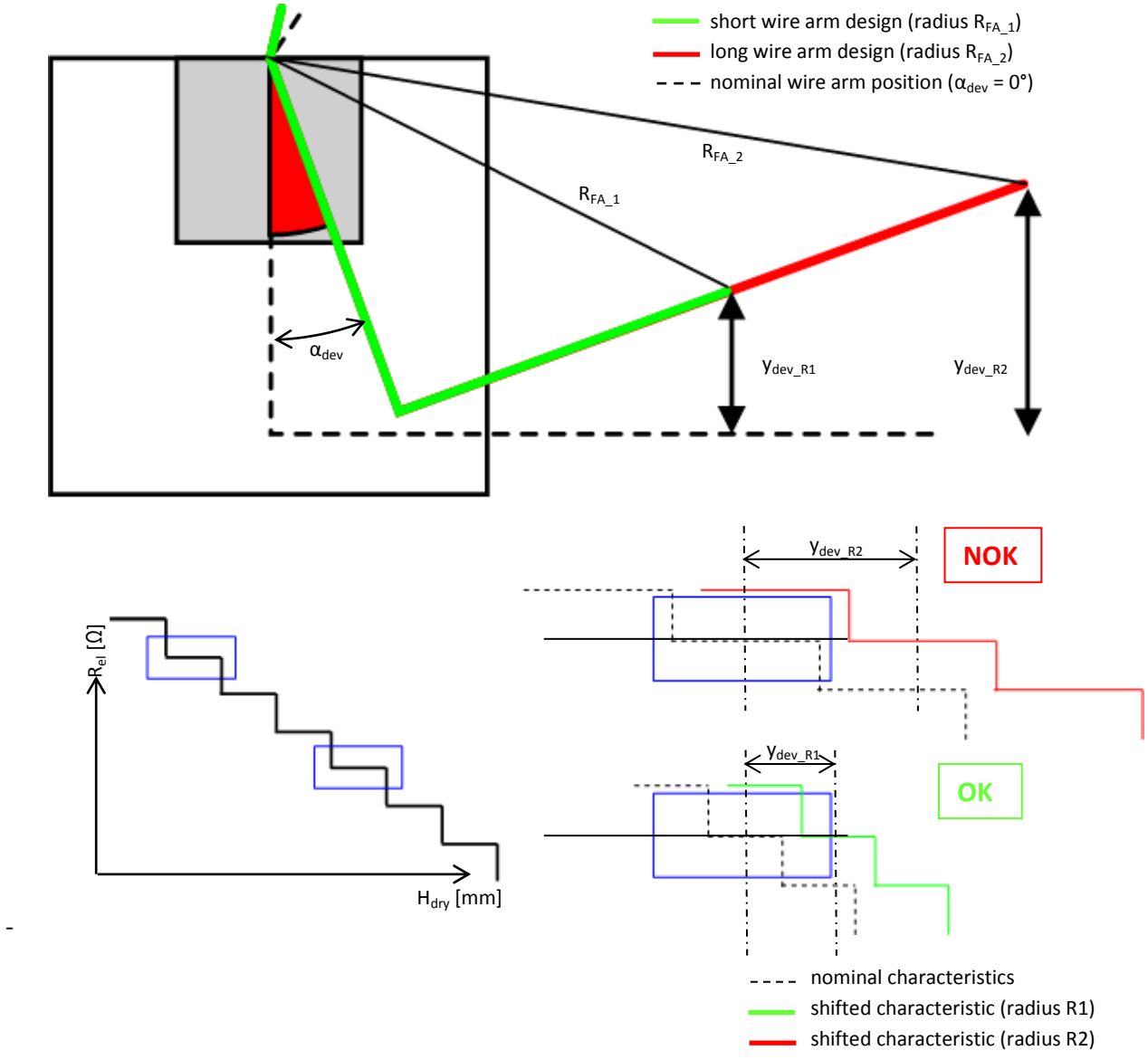

Fig. 5.7 Influence of floater arm radius on tolerance of deviation from nominal dry height (case of angular deviation of FLS).

There are also other parameters that may have influence on the FLS accuracy when evaluating by the Tolerance Box method is applied. They have only minor influence in the majority of designs but it

is important to be aware of their effect since in specific designs they might also play role in FLS indication tolerance.

- Height of the tolerance box (resistance tolerance value)
- Resistance resolution (ohm per segment parameter)
    - Ohm per segment parameter defines the resistance value difference between two neighbouring pads on resistor card, from the resistor card design rules minimum ohm per segment ΔR_{el} = 1,5 Ω

Theoretically, in specific applications resistance tolerance value could be higher than ohm per segment value. It would result in a situation in the picture 5.8 when FLS characteristic could be shifted in the height direction by one more step in both plus and minus direction.

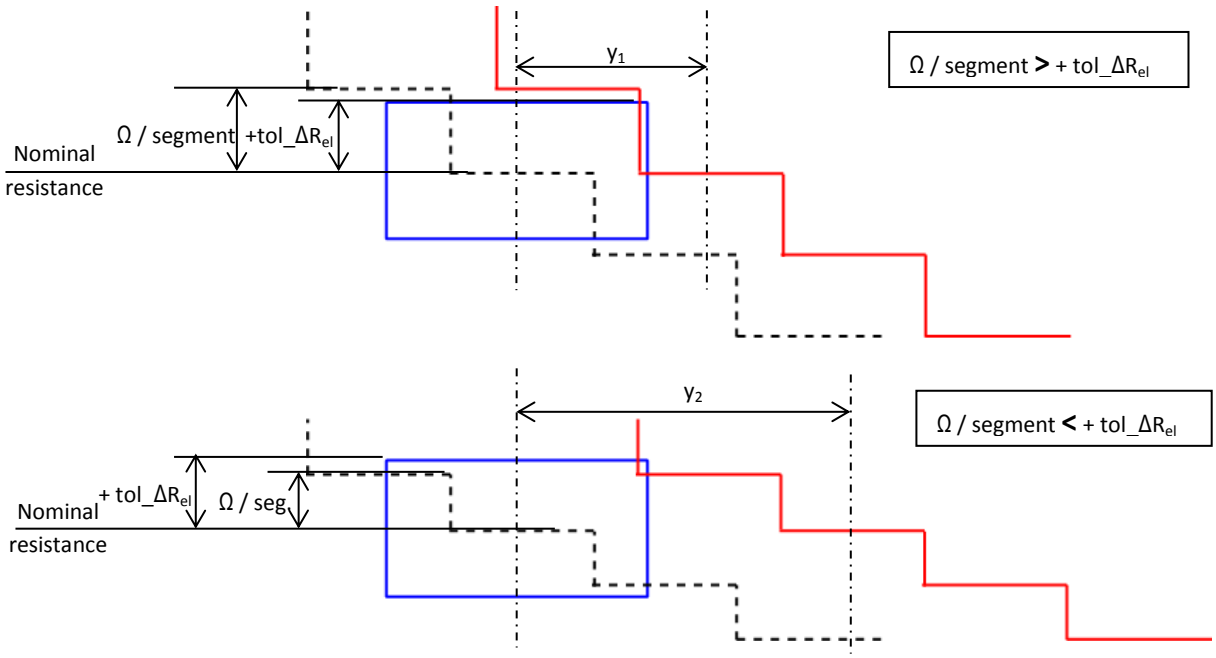

Fig. 5.8 Influence of Ohm per segment parameter on tolerance of deviation from nominal dry height.

FLS characteristic in such position would still pass the Tolerance Box method acceptance criterion however the actual deviation from the nominal would be very high ($y_2 > y_1$). This situation might arise only in a specific application which would typically combine:

- high resolution (high number of pads on resistor card – more than 80 pads)
- wide angular range (+/- 45°, i.e. 90°)
- low total resistance range (maximum resistance value <160 Ω)

This combination of parameters would result in a low value of ohm per segment parameter and thus risk of ohm per segment value being lower than resistance tolerance value.

To prevent this possible issue, designs with high number of pads should follow:

$$\frac{R_{el\_max} - R_{el\_min}}{number\ of\ pads} > tol\_\Delta R_{el} \qquad (5.4)$$

5.2. Nominal Height evaluation method

The Nominal Height evaluation method; which is sometimes also referred to as "Plus/minus" Pad evaluation method; is an alternative way of FLS electrical characteristic evaluation. In essence this method, unlike the Tolerance Box method, considers only the resistance tolerance as there is no explicit height tolerance. In this method resistance values on the nominal checkpoint heights are measured.

Nominal height tolerances are calculated in following way:

- Height tolerance is converted into the angle tolerance (i.e. height tolerance provided by the width *b* of tolerance box in Tolerance Box evaluation method is converted into relevant angular position *α* on the resistor card layout).
- It is checked which pad of the resistor card is reached at that angle and the calculated angle tolerances are compared with the angle values of pads neighbouring the nominal angle pad value.
- The resistance value difference between nominal pad and neighbouring pad (which covers the angular tolerance) is calculated.
- The calculated resistance value is then added up with the additional checkpoint tolerance value (1,2 Ω) and with the linearity tolerance value of the neighbouring pad (0,8 Ω).

Accuracy acceptance criteria (Nominal Height method)

Resistance measured at the nominal height H_{dry} must be within the calculated interval of the resistance tolerance.

Example

In this example principle of nominal height tolerances is described for a particular nominal height H_{dry}:

1. Nominal dry height:

$$H_{dry} = 70.4\ mm \tag{5.5}$$

2. Tolerances of the nominal dry height by the tolerance box width ±2 mm:

$$H_{dry\_min} = 68.4\ mm \tag{5.6}$$

$$H_{dry\_max} = 72.4\ mm \tag{5.7}$$

3. For these heights are calculated relevant angles on the resistor card layout:

Tab. 5.1 Angular position on the resistor card corresponding to dry heights.

DRY HEIGHT [mm]	ANGLE [°]
68.4	-4.02
70.4	-3.20
72.4	-2.41

4. Angles -4.02° and -2.41° are compared with the angles around the nominal value (-3.20° to which correspond R_{el} = 90 Ω):

Tab. 5.2 Pad number vs. pad angular position vs. pad resistance value.

PAD NUMBER	ANGLE [°]	RESISTANCE [Ω]
26	-5.34	96.67
27	-4.27	93.33
28	-3.20	90
29	-2.05	86.4
30	-0.90	82.8

5. Angle tolerance is ±1 pad, which corresponds to resistance difference ΔR_{el} = 3.6 Ω.
6. There is an additional tolerance ±1.2 Ω which is always applied for the checkpoint pad.
7. There is an additional linearity tolerance ±0.8 Ω for the resistance pads neighbouring the checkpoint pad; total tolerance for resistance value measured at nominal height 70.4 mm is:

$$+tol_{nomH} = 3.6 + 1.2 + 0.8 = +5.6\Omega \quad (5.8)$$

$$-tol_{nomH} = -3.6 - 1.2 - 0.8 = -5.6\Omega \quad (5.9)$$

$$R_{el\_nom\_H} = 90 \pm 5.6\Omega \quad (5.10)$$

In the picture 5.9 there is the maximum upper and lower resistance value which shall be measured at the nominal height (H_{dry} = 70.4 mm). The FLS characteristic meets the acceptance criteria only if either the nominal checkpoint pad or one of its neighbouring pads is contacted when floater is on the checkpoint nominal height position. The height tolerance then can be derived from that by shifting the characteristics in the height (x axis) direction. Logically it can be shifted only to such an extent that the one neighbouring step is still intersected by the nominal height value.

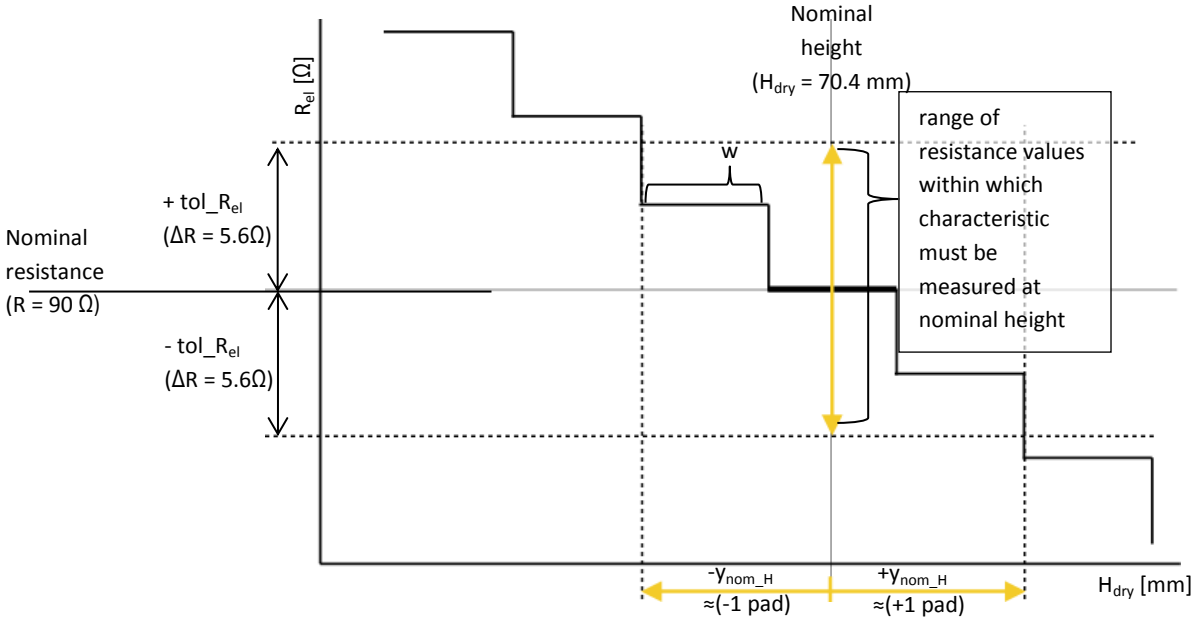

Fig. 5.9 Range of resistance values to be measured at the nominal height according to the Nominal Height evaluation method; relevant tolerance of a shift of the FLS characteristic from the nominal height $\pm y_{nom\_H}$.

Tolerance of thedeviation from H_{dry} nominal provided by the Nominal Height method is then calculated:

$$\pm y_{nom\_H} = 1.5 \cdot w \tag{5.11}$$

$$\pm y_{nom\_H} = 1.5 \cdot \left(\frac{2\pi R_{FA}}{360}(p+s) \cdot cos\gamma\right) \tag{5.12}$$

In the example the angle tolerance covers ±1 neighbouring pad, however in specific cases (such as for combination of very low ohm per segment values, high number of pads and short floater arm radius) the angle tolerance according to the Nominal Height tolerance method might cover up to ±2 neighbouring pads.

From the point of view of height tolerance this would allow considerably higher shift by which the characteristic can be moved as it can be seen in the picture 5.10.

$$\pm y_{nom\_H} = 2.5 \cdot w \tag{5.13}$$

Nevertheless this is rather a theoretical issue related to a specific and unusual combination of design parameters as it can similarly arise in case of the Tolerance Box assessment method described in the chapter 5.1.

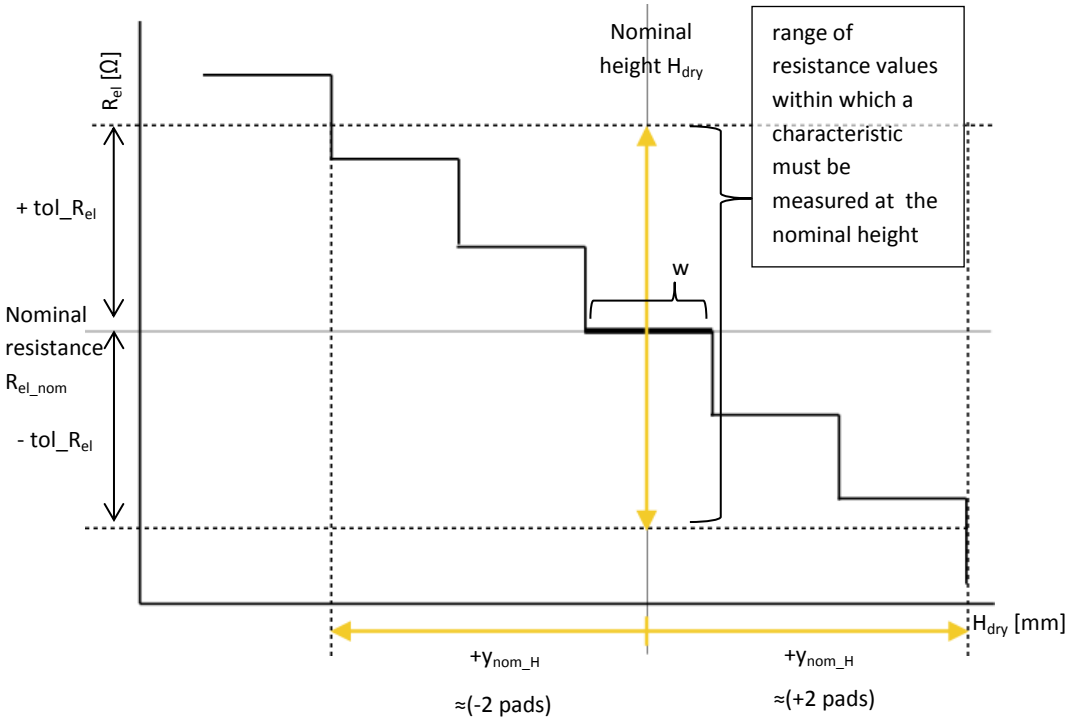

Fig. 5.10 Worst case range of resistance values to be measured at the nominal height according to the Nominal Height evaluation method; relevant tolerance of a shift of the FLS characteristic from the nominal height.

5.3. Comparison of Tolerance Box and Nominal Height evaluation methods

In the figure 5.11 there is a representative example of comparison of both Tolerance Box and Nominal Height methods. The blue dotted line is the characteristic in the maximum tolerated height deviation position if evaluated by the Tolerance Box method. The red dotted line is then analogically evaluated by the Nominal Height method.

As the diagram shows, permissible shift of the characteristic in the height direction is comparable for both methods; however the Tolerance Box method is always slightly stricter (for any combination of the resistor card layout design and floater arm radius) since it provides a more tight tolerance of accuracy of the fuel level height indication.

$$\pm y_{tol\_box} < \pm y_{nom\_H} \tag{5.14}$$

$$1.5 \cdot w < \frac{b}{2} - 0.05 \cdot b + \frac{w}{2} \tag{5.15}$$

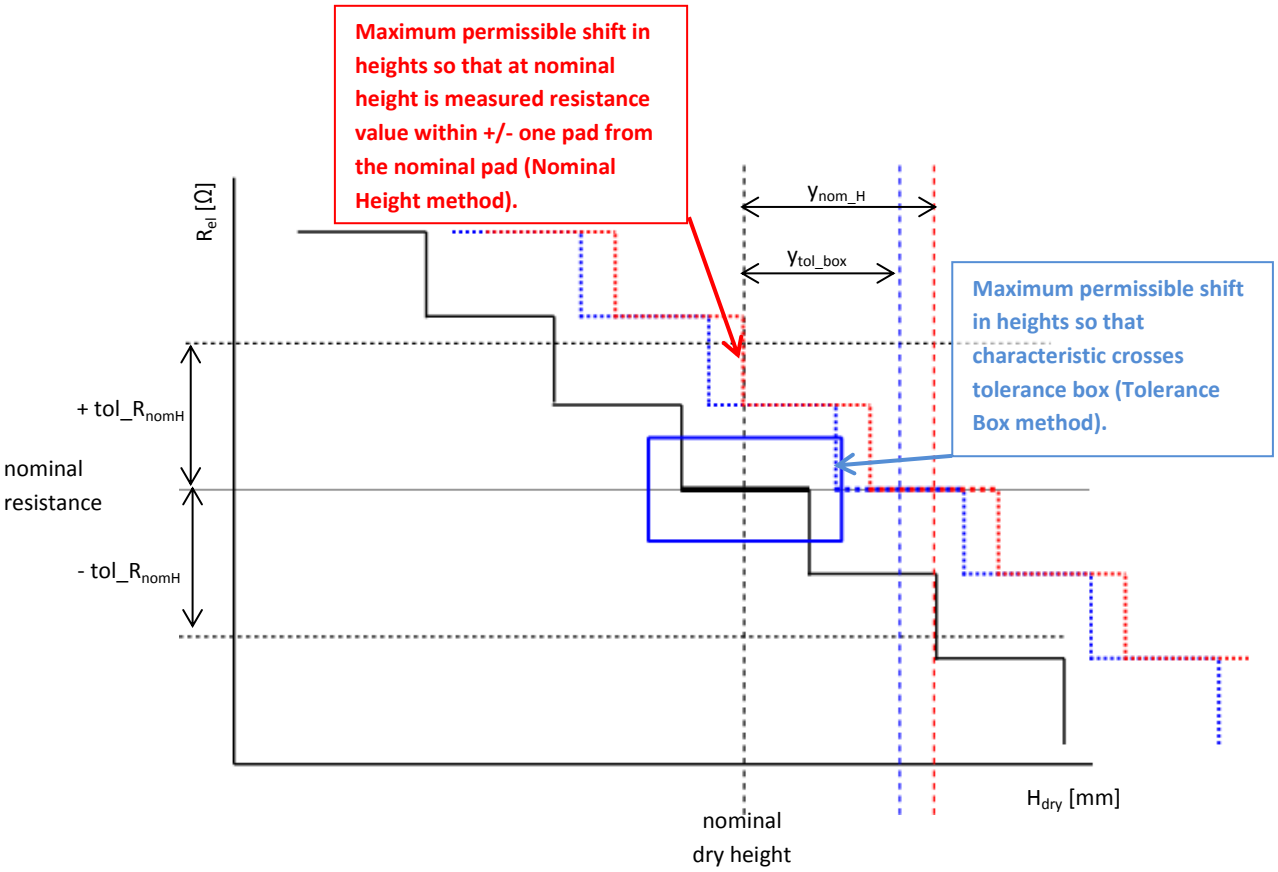

Fig. 5.11 Comparison of tolerance of deviation from nominal dry height (Tolerance Box vs. Nominal Height evaluation method).

Tolerance Box method advantages:

- Higher FLS indication accuracy.

Tolerance Box method disadvantages:

- Higher probability of FLS out of tolerance.

Nominal Height method advantages:

- Provides wider tolerance range (i.e. lower probability of FLS out of tolerance).
- Simpler evaluation at output control, it is only checked whether the resistance value is in the tolerance at each H_{dry} nominal check height.

Nominal Height method disadvantages:

- Lower indication accuracy can be guaranteed compared to the Tolerance Box method.
- Each particular FLS design needs individual calculation of tolerances.

Both methods can fail in such designs when the ohm per segment value is very low (typically below 2 Ohms as for the Nominal Height method or below resistance tolerance provided by the size of tolerance box as for the Tolerance Box method). Effects of very low ohm per segment value are shown in figures 5.8 and 5.10.

The Tolerance Box evaluation method is currently preferred and this method is applied in the series production on all assembly lines for the FLS characteristic evaluation.

6. MEASUREMENT OF FLS CHARACTERISTIC AT THE OUTPUT CONTROL OF ASSEMBLY LINE

After the assembly process of each fuel supply module (FSM) a functional test of FLS is performed. This measurement is performed with FLS assembly mounted in FSM.

6.1. Inline measurement of FLS characteristic

Measuring bench (figure 6.1) measures the FLS characteristic (H_{dry} vs. R_{el} characteristic) with 2 kHz sampling rate. The floater height H_{dry} measurement is done by incremental rotational sensor which is connected with a ball screw for the vertical adjustment of the position of the lifting rod that lifts the floater.

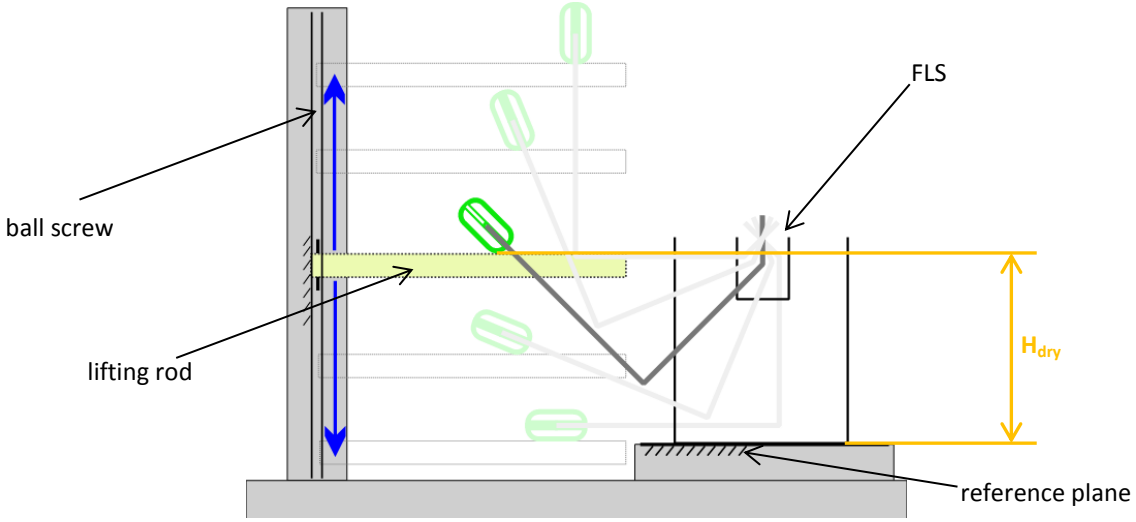

Fig. 6.1 Scheme of the kinematics of FLS measurement on the bench at output control.

6.1.1. Electrical resistance (R_{el}) measurement

In the picture 6.2 there is a scheme of the electrical connection for the FLS measurement at the output control of assembly line.

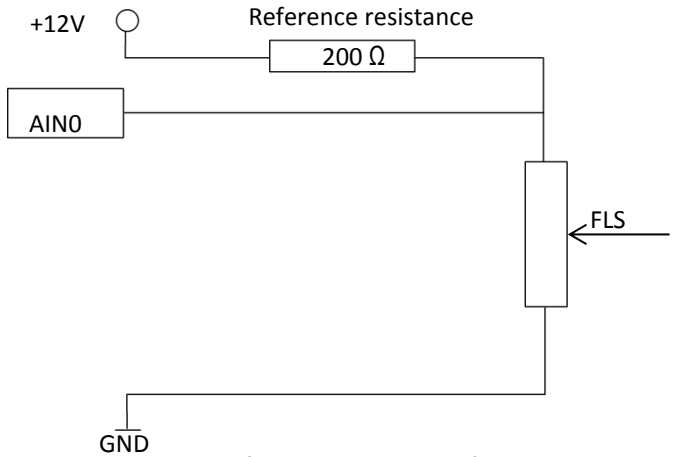

Fig. 6.2 Scheme of the measurement of FLS.

FLS is powered by 12 V voltage through reference 200 Ω resistance. Current streaming through the sensor can be simply calculated from equation:

$$I_{FLS} = \frac{12}{R_{FLS}} \tag{6.1}$$

For the average FLS resistance $R_{FLS} = 300\ \Omega$, the current is approximately 40 mA. Voltage at the FLS output is then calculated:

$$U_{FLS} = \frac{12 \cdot R_{FLS}}{R_{FLS} + 200} \tag{6.2}$$

For the average FLS resistance $R_{FLS} = 300\ \Omega$ voltage is approximately 7.2 V.

Such a measurement configuration has a variable accuracy. With increasing resistance values accuracy decreases, for resistance values above 1000 Ω accuracy decreases more rapidly, in that region measurements can only be taken as informative.

6.1.2. Dry heights (H_{dry}) measurement

Resolution capability for dry heights measurement depends on the sampling rate and speed of the motion of the lifting rod which lifts the floater arm. The sampling rate is 2 kHz and normal speed of the lifting rod motion is 150 mm.s^{-1}. The accuracy of the dry heights measurement is then simply calculated:

$$\frac{150}{2000} = \pm 0.075\ mm \tag{6.3}$$

Cycle of FLS measurement:

- Lifting rod slides to the lowest position, where automatic calibration of the electrical circuits is performed.
- Lifting rod travels up and lifts the floater through the entire travel range of the floater arm to the highest position, during the upward motion checkpoint tolerance boxes are calculated.
- Lifting rod travels down with the floater to the lowest position, the FLS characteristic is measured and its relative position to the position of the checkpoint tolerance boxes is evaluated.

For the evaluation of the accuracy compliance the Tolerance Box method described in detail in chapter 5.1 is used. Basically, FLS characteristic must cross all tolerance boxes (figure 6.3), if one or more tolerance boxes are not crossed FLS is evaluated as NOK (not OK), i.e. not complying with the accuracy criteria.

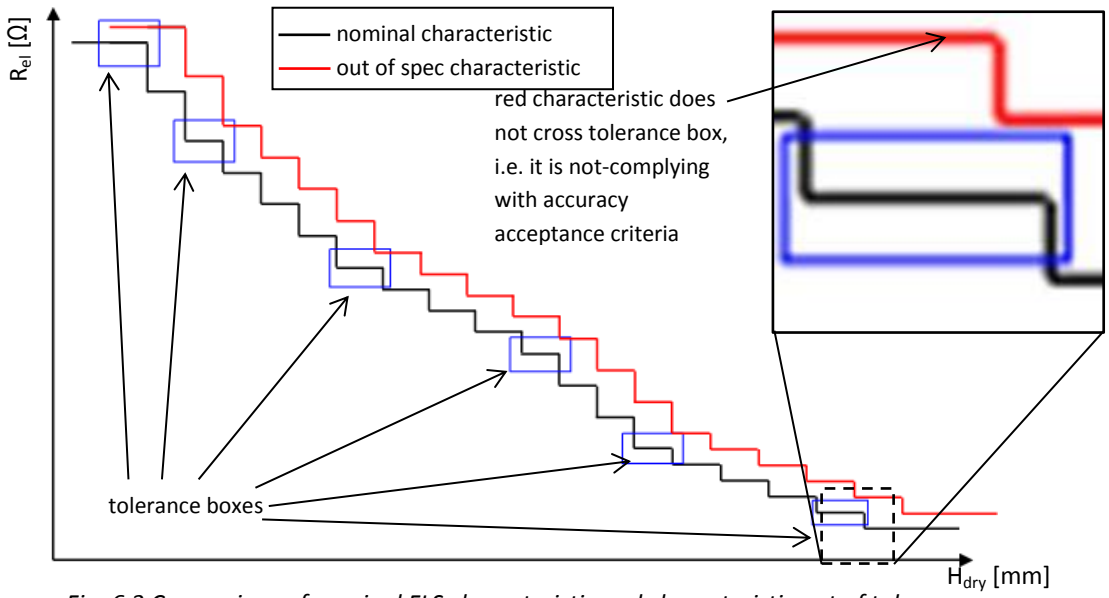

Fig. 6.3 Comparison of nominal FLS characteristic and characteristic out of tolerance.

6.2. Correction by manual bending of wire arm

If FLS does not meet the accuracy acceptance criteria, which means FLS characteristic does not cross all tolerance boxes; wire of the floater arm of FLS is manually bent by the operator at the assembly line.

By the bending of the wire of the floater arm the FLS characteristic (floater position respectively) is shifted in the correct position within the accuracy compliance. After the wire bending the FLS measurement is performed again to verify if the correction was achieved.

Manual bending can be done twice. If the measurement after the second wire arm bending still proves non-complying FLS, it is scrapped.

Correction of a non-complying FLS by manual bending of wire arm is logically time consuming and therefore uneconomical and costly. Thus there is a desire to find out ways how to increase FLS indication accuracy so that scrapping is eliminated or at least reduced substantially.

PRACTICAL PART

In the previous pages it was described which factors come into play from the point of view of accuracy of FLS indication. Since there is a certain percentage of FLS which do not comply with the accuracy acceptance criteria when checked at the output control of the series production assembly line, it is required to find out measures how to decrease the number of these not complying FLS.

Aims of the practical part:

- Analysis of data collected from assembly lines and identification of parameters typical for FLS that exhibit high rate of non-compliance with accuracy criteria; this is covered in chapter 7.
- Materials analysis of the wire arm, evaluation of mechanical properties of the wire arm supplied from various manufacturers, which is explained in chapter 8.
- Proposal of correction in design process and proposal of design change of layout of resistor card that are described in chapters 9 and 10.

7. ANALYSIS OF DATA FROM ASSEMBLY LINES

7.1. Motivation

There is a certain fraction of FLS production which do not comply with the accuracy acceptance criteria and so they have to be manually bent by an operating person at the assembly line, which is both time consuming and costly. In order to decide on the root causes collection of data from assembly lines and its analysis was made.

7.2. Methodology of collecting of data

- Data were collected for nine months period from November 2013 to July 2014 from six assembly lines.
- A total number of 128 various projects were analysed.
- A total number of 2 643 957 fuel supply modules (FSM) were produced in this period on these lines.
- A total number of 129 561 FSMs out of all produced FSMs had FLS assembly which did not comply with the accuracy criteria when measured at the output control which is **4.9%**; wire arm of these non-complying FLS had to be corrected by manual bending of the wire and then measured again.

The data were sorted out and classified from various criteria, to identify which criteria possibly have the major influence on the rate of the accuracy failure. Rate of the accuracy non-compliance was classified from following criteria:

- Wire arm radius
- Assembly line
- Floater design (rotational vs. fixed)
- FLS platform
- Wire arm manufacturer

7.3. Collected data

In the table 7.1 complete productions are sorted according to five chosen criteria.

Tab. 7.1 Rate of FLS non-compliance.

Wire arm radius		Total production	Bent (NOK) modules	Rate of non-compliance
from	to			
[mm]		[pcs]	[pcs]	[%]
120	130	33732	1791	5,31
130	140	102378	4027	3,93
140	150	104042	14615	14,05
150	160	953965	27330	2,86
160	170	172722	7333	4,25
170	180	177486	2906	1,64
180	190	109357	7002	6,40
190	200	721600	60814	8,43
200	210	240003	3387	1,41
210	220	0	0	/
220	230	28672	356	1,24
Total		**2643957**	**129561**	**4,90**

Assembly line	Total production	Bent (NOK) modules	Rate of non-compliance
[-]	[pcs]	[pcs]	[%]
AL01	541269	19152	3,54
AL02	395620	6463	1,63
AL03	468293	14209	3,03
AL04	298152	25680	8,61
AL05	452050	14358	3,18
AL06	488573	49699	10,17
Total	**2643957**	**129561**	**4,90**

Floater design	Total production	Bent (NOK) modules	Rate of non-compliance
[-]	[pcs]	[pcs]	[%]
rotational	2146944	109322	5,09
fixed	497013	20239	4,07
Total	**2643957**	**129561**	**4,90**

FLS platform	Total production	Bent (NOK) modules	Rate of non-compliance
[-]	[pcs]	[pcs]	[%]
1.0	1294497	35185	2,72
1.3	506467	31811	6,28
1.3 L	842993	62565	7,42
Total	**2643957**	**129561**	**4,90**

Wire manufacturer	Total production	Bent (NOK) modules	Rate of non-compliance
[-]	[pcs]	[pcs]	[%]
Z	1552921	74798	4,82
K	852539	28842	3,38
B	238497	25921	10,87
Total	**2643957**	**129561**	**4,90**

In the collection above all 128 projects are included, that were produced in the evaluated period. In those data are thus included also projects which have rather low, acceptable rate of non-complying FLS or low, statistically insignificant volume of production, both of which bring in distortion and should not be considered.

In order to exclude such projects two filters have been applied:

- Projects which exhibit average rate of at least 100 of non-complying FLS per month (i.e. minimum 900 of total non-complying FLS in the analysed period of 9 months).
- Projects which exhibit long-termly at least 3% portion of non-complying FLS over the analysed period of 9 months.

Only projects which fulfil both filter criteria were further analysed.

Out of the total 128 projects only **23 fulfil** both filter criteria, which stands for as much as **18%** of all 128 projects.
However, these 23 projects exhibit number of **100 723** non-complying FLS which stands for as much as **78%** out of the total number of **129 561** non-complying FLS.

This finding corresponds to the Pareto distribution and it can be concluded that:
Approximately 80% of non-complying FLS come from approximately 20% of projects.

In order to identify any correlation between the evaluated criteria and the rate of non-complying FLS that have to be corrected by manual bending of the wire arm following matrix (table 7.2) is constructed.

The matrix shows correlation between all values of criteria which were used for the previous analysis and rate of non-complying FLS and it gives rating for particular combinations of the criteria values.

Tab. 7.2 Correlation matrix of analysed parameters.

Wire arm radius		130	140	150	160	170	180	190	200	210	220	230
from [mm]	to [mm]	120	130	140	150	160	170	180	190	200	210	220
120	130	X	X	X	X	X	X	X	X	X	X	X
130	140	X	X	X	X	X	X	X	X	X	X	X
140	150	X	X	X	X	X	X	X	X	X	X	X
150	160	X	X	X	X	X	X	X	X	X	X	X
160	170	X	X	X	X	X	X	X	X	X	X	X
170	180	X	X	X	X	X	X	X	X	X	X	X
180	190	X	X	X	X	X	X	X	X	X	X	X
190	200	X	X	X	X	X	X	X	X	X	X	X
200	210	X	X	X	X	X	X	X	X	X	X	X
210	220	X	X	X	X	X	X	X	X	X	X	X
220	230	X	X	X	X	X	X	X	X	X	X	X

Assembly line	AL01	AL02	AL03	AL04	AL05	AL06
AL01	X	X	X	X	X	X
AL02	X	X	X	X	X	X
AL03	X	X	X	X	X	X
AL04	X	X	X	X	X	X
AL05	X	X	X	X	X	X
AL06	X	X	X	X	X	X

Floater design	rotational	fixed
rotational	X	X
fixed	X	X

FLS platform	1.0	1.3	1.3 L
1.0	X	X	X
1.3	X	X	X
1.3 L	X	X	X

Wire manufacturer	Z	K	B
Z	X	X	X
K	X	X	X
B	X	X	X

below 5% of NOK rate (acceptable)
between 5 to 10 % of NOK rate
above 10 % of NOK rate
/ combination of values does not exist

7.4. Conclusions from data analysis

According to the evaluation applied following conclusions are drawn:

- The average rate of 4.9% of all produced fuel supply modules have FLS which does not comply with the acceptance criteria when checked at the output control. Therefore these have to be corrected by manual bending of the wire arm of FLS.
- Majority of FLS (approx. 78%) that do not meet the acceptance criteria come from minority (approx. 18%) of various projects (various FLS designs respectively).
- There is no proof of correlation between floater arm radius and rate of FLS that do not comply with the acceptance criteria.
- There is an increased rate of FLS not complying with the acceptance criteria at assembly lines AL04 (8.6 %) and AL06 (10.2 %).
- There is very low difference in the rate of FLS accuracy non-compliance between FLS with rotational floater and FLS with fixed floater design, therefore floater design is found to have negligible effect on meeting of the FLS acceptance criteria.
- Platform FLS 1.0 has considerably lower rate (2.7 %) of FLS non-complying with the acceptance criteria compared to the average value.
- Wire arm manufacturer B has considerably higher rate of FLS which do not comply with the acceptance criteria compared to other manufacturers.

8. MATERIALS ANALYSIS OF THE WIRE ARM OF FLS

Based on the tolerance analysis of dimensions of FLS components in the chapter 4 the dimensional accuracy of the wire arm has a major part in the tolerance chain.

Additionally, findings from the analysis of the data collected from assembly lines proved high variability of rate of NOK FLS among individual wire arm manufacturers.

8.1. Motivation

Materials analysis of wire arms is performed to proof or disproof influence of the wire arm material properties on dimensional instability of the wire arm in which case an increase of inaccuracy of FLS indication might occur. A comparison is done on samples from all individual wire manufacturers (Z, K and B).

Following tests are performed on which basis analysis is done:

- Tension test of the wire arm material
- Metallographic analysis of the structure of the wire arm material

8.2. Wire arm material specification

8.2.1. Basic description [13]

All manufacturers make the wire from chrome-nickel austenitic stainless steel:

- Material name: X10CrNi18-8 (previous: X12CrNi17-7)
- Material number: 1.4310 NS (AISI 302)

Chemical composition of the material is in the table 8.1.

Tab. 8.1 Chemical composition of the stainless steel X10CrNi18-8.

X10CrNi18-8 (1.4310 NS) chemical composition [%]								
C	Si	Mn	P	S	Cr	Mo	Ni	N
0.05 - 0.15	max 2.00	max 2.00	max 0.045	max 0.015	16.00 - 19.00	max 0.80	6.00 - 9.50	max 0.11

Stainless steel 1.4310 is essentially a leaner version of 1.4301, which as a result of its combination of high chromium and restricted nickel content, produces a metastable austenitic structure which will work harden, strengthen very rapidly when subjected to cold deformation.

Since this steel is used for the production of spring components, the final microstructure will contain a significant amount of shear induced martensite and as such will be relatively magnetic.

8.2.2. Effect of cold working [14], [15], [16]

The mechanical strength for spring applications is obtained by cold working the austenitic and ferritic steel types, as they are not hardenable by conventional heat treatments.

Deformation of the alloy X10CrNi18-8 at room or slightly elevated temperatures produces an increase in strength accompanied by a decrease in elongation value. A portion of this increase in strength is caused by partial transformation of austenite to martensite during deformation.

Tab. 8.2 Effect of cold-working on mechanical properties of stainless steel X10CrNi18-8. [16]

R	N/mm²	620	820	1000	1200	1320	1440	1620	1780
Rp 0.2	N/mm²	300	580	730	880	1020	1180	1300	1460
A	%	46	22	14	10	9	9	9	9
Reduction	%	**0**	**10**	**20**	**30**	**40**	**50**	**60**	**70**

8.2.3. Tensile strength

According to the norm EN 10270-3 tensile strength of a cold-worked wire depends on the nominal diameter of the wire.

For the wire diameter 2.5 mm from material X10CrNi18-8 the tensile strength limits are in the table 8.3.

Tab. 8.3 Tolerance of tensile strength.

X10CrNi18-8		
wire diameter	[mm]	2,5
R_m minimum	[MPa]	1600
R_m maximum	[MPa]	1900

8.2.4. Heat treatment [17], [18], [23]

Various processing operations during the manufacture of a component can generate internal stresses which can have a detrimental influence on the service life of the equipment in which it is employed. In order to eliminate or attenuate these residual stresses, stress relieving treatment can be employed.

Unlike martensitic steels, the austenitic stainless steels are not hardenable by heat treatment as no phase changes occur on heating or cooling.

There are two main reasons why stress relieving heat treatment is performed on cold rolled austenitic stainless steel:

- One reason is the stress corrosion cracking (SCC), which relies on tensile stresses as part of the failure mechanism. Stress relieving removes such residual tensile stresses and so improves the SCC resistance.
- The other main reason for stress relieving is to provide dimensional or shape stability. The risk of distortion can be reduced during forming or machining operations by stress relieving.

From the point of view of accuracy of FLS indication dimensional stability of the wire arm is the key factor. For that reason heat treatment is employed.

Heat treatment parameters

In the norm EN 10270-3 parameters recommended for heat treatment of cold worked springs made of wire are as follows:

- Temperature: 250 – 450 °C
- Duration: 30 minutes to 4 hours
- Means of cooling: air

It is also stated in the norm that if a moderate loss of the initial tension (induced by cold working) can be accepted, heat treatment temperatures of max. 200 °C for grade number 1.4310 are recommended. According to [17] holding for 10 to 20 minutes per millimetre of thickness is recommended at a temperature between 200 and 400 °C, followed by slow cooling. This treatment has the advantage that it does not cause any phase transformations.

8.3. Tensile test of the wire arm material

8.3.1. Specimen description

A straight long segment of the wire arm was cut off for the test (figure 8.1). In table 8.4 dimensions of the specimen are listed.

Five specimens of the wire arm were collected from each wire arm manufacturer, i.e. totally 15 specimens were tested.

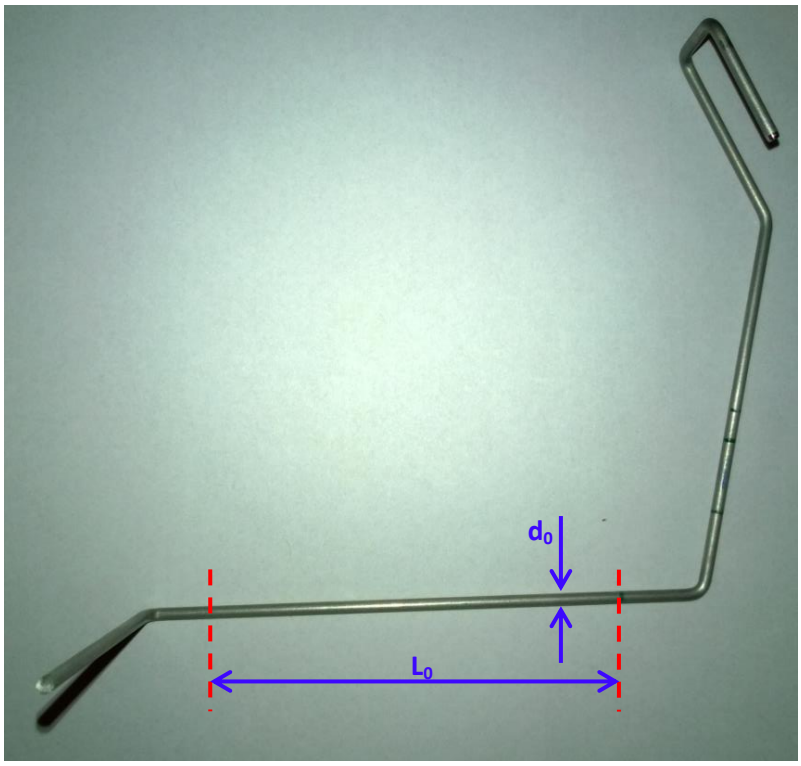

Fig. 8.1 Dimensions of the specimen cut off from the wire arm.

Tab. 8.4 Dimensions of specimen.

	d_0 [mm]	A_0 [mm2]	L_0 [mm]
K	2,50	4,91	75
Z	2,50	4,91	90
B	2,50	4,91	90

Material of the wire arm is supposed to be identical for all three manufacturers, i.e. X10CrNi18-8 NS. Nonetheless the heat treatment parameters are different at each manufacturer. In the table 8.5 parameters of the wire arm heat treatment are described.

Heat treatment of the wire arm is performed after the bending of the wire into designed shape of the wire arm.

Tab. 8.5 Heat treatment parameters (according to individual wire arm manufacturers).

	T [°C]	t [min]
K	180	30
Z	180	30
B	240	30

Both wire arm manufacturers K and Z set heat treatment temperature at 180 °C, i.e. below the temperature range 250 – 400 °C recommended in the norm. However temperature 180 °C complies with the temperature settings for cases if a moderate loss of the initial tension can be accepted, i.e. temperatures below 200 °C can be employed.

Material from manufacturer B is also annealed below the recommended interval; however the temperature is only 10 °C below the interval at 240 °C.

Based on the difference of annealing temperature settings a hypothesis is formulated:

8.3.2. Hypothesis:

The ultimate strength of the material from the wire arm manufacturer B (annealed at 240 °C) is expected to be lower compared to the ultimate strength of material from both manufacturers K and Z (annealed at 180 °C) due to the different settings of the temperature of annealing. All other material properties before annealing are considered identical for all three manufacturers K, Z and B.

8.3.3. Tensile test description [3], [21]

Tensile test was conducted according to the norm CSN EN ISO 6892-1 on the test machine Instron 5982. Tensile testing, also known as tension testing, is a fundamental materials science test in which a sample is subjected to a controlled tension until failure. Uniaxial tensile testing is the most commonly used for obtaining the mechanical characteristics of isotropic materials. The main product of a tensile test is a load versus elongation curve which is then converted into a stress versus strain curve. Basic mechanical properties such as yield strength, ultimate strength or ductility of the material can be specified from the stress-strain curve.

$$\sigma_y = \frac{F_y}{A_0} \tag{8.1}$$

$$\sigma_u = \frac{F_m}{A_0} \tag{8.2}$$

Ductility is evaluated from relative elongation:

$$\delta = \frac{L_m - L_0}{L_0} \cdot 100 \tag{8.3}$$

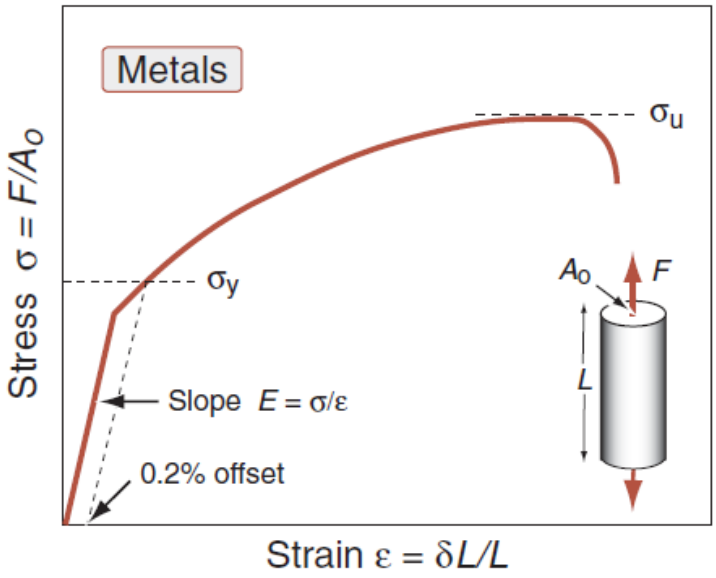

Fig. 8.2 Representative example of a stress–strain curve for a metal, showing the modulus, E, the 0.2 percent yield strength, σ_y, and the ultimate strength, σ_u. [3]

8.3.4. Test results

Tab. 8.6 Results of tension test of stainless steel wire.

sample Nr.	F_y [N]	σ_y0,2 [MPa]	F_m [N]	σ_u [MPa]	δ [%]
K01	7269,4	1480,9	8480,3	1727,6	3,2
K02	7612,0	1550,7	8564,8	1744,8	3,2
K03	7528,5	1533,7	8650,7	1762,3	3,3
K04	7378,8	1503,2	8359,1	1702,9	3,2
K05	7590,9	1546,4	8652,6	1762,7	3,2
avg	**7475,9**	**1523,0**	**8541,5**	**1740,1**	**3,2**
Z01	6820,2	1389,4	7855,9	1600,4	3,3
Z02	7132,9	1453,1	8427,8	1716,9	3,2
Z03	6967,0	1419,3	8094,0	1648,9	3,2
Z04	6817,7	1388,9	7877,5	1604,8	3,1
Z05	6832,5	1391,9	7927,1	1614,9	3,3
avg	**6914,1**	**1408,5**	**8036,5**	**1637,2**	**3,2**
B01	9013,9	1836,3	9482,2	1931,7	2,4
B02	8666,9	1765,6	9143,0	1862,6	2,4
B03	8550,5	1741,9	9026,2	1838,8	2,4
B04	8895,6	1812,2	9777,2	1991,8	2,5
B05	8731,7	1778,8	9708,5	1977,8	2,6
avg	**8771,7**	**1787,0**	**9427,4**	**1920,5**	**2,5**

Three samples from the manufacturer B (B01, B04, B05) have the ultimate strength above the upper limit 1900 MPa specified by the norm, also the average value of the ultimate strength of all specimens from the manufacturer B is above the specification (1920.5 MPa).

Yield strength of specimens from the manufacturer B even exceeds the ultimate strength of specimens from manufacturers Z and K.

Mechanical properties of samples from manufacturer B also show the highest variability.

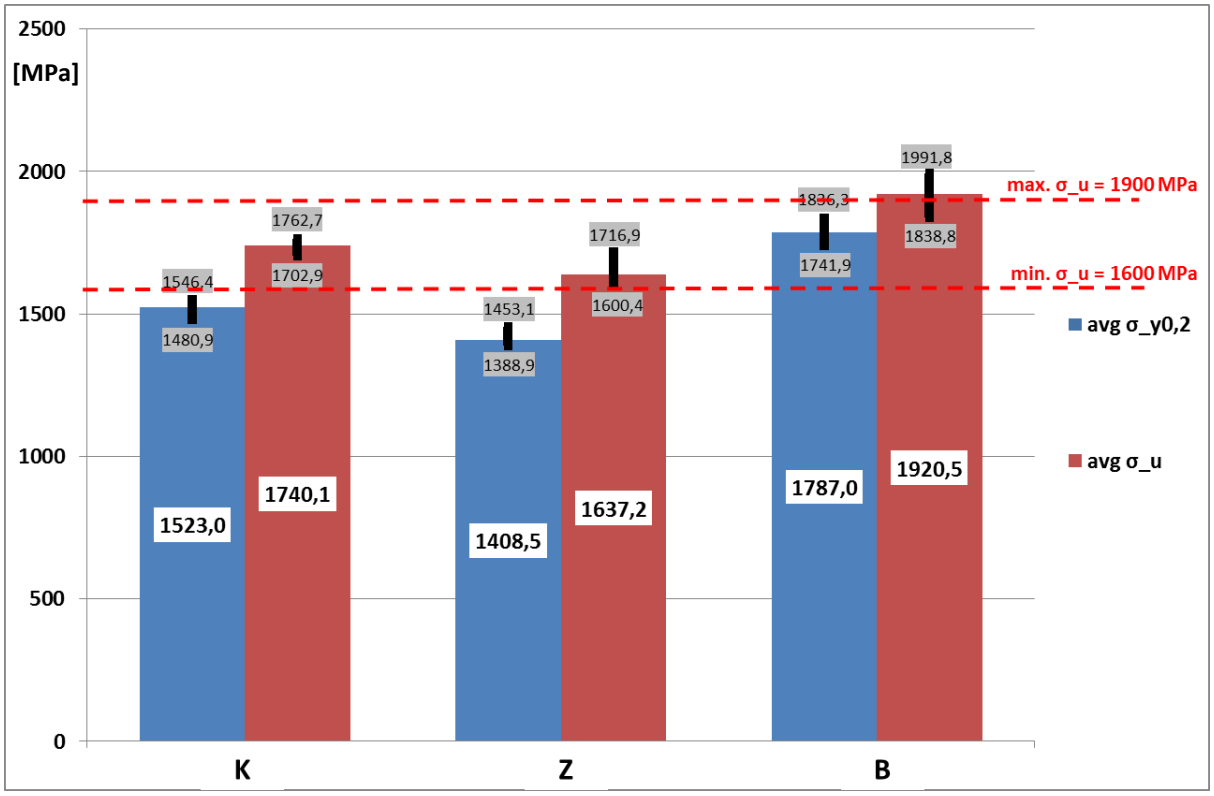

Fig. 8.3 Comparison of material properties (yield strength, σ_y and ultimate strength, σ_u) of the wire material from individual wire arm manufacturers K, Z and B. Average, lowest and highest values are compared to the minimum and maximum limits of the ultimate strength that are given in the norm.

8.4. Metallographic analysis of the wire arm material

Metallography is the study of the physical structure and components of metals, typically using microscopy.

8.4.1. Specimen preparation

Preparation of specimen for metallographic analysis is a sequence of steps (figure 8.4).

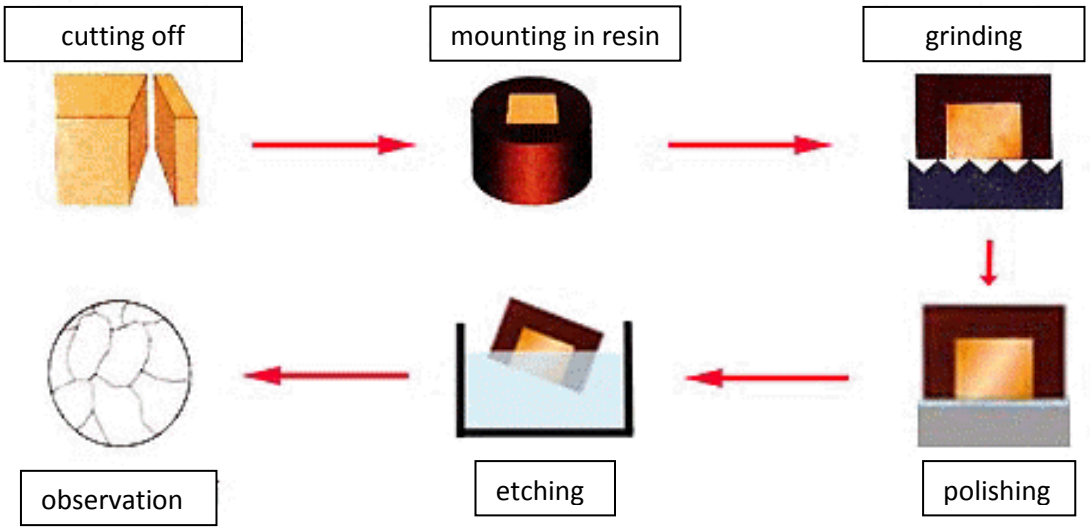

Fig. 8.4 Steps of preparation of specimen for the metallographic analysis. [22]

In order to ascertain and evaluate possible difference of the material structure of bends and the structure of straight wire segments, the bending of the wire arm was chosen for the examination. Hand pliers were used to cut the wire. Then the separated specimens were mounted into a castable acrylic cold mounting resin Varidur.

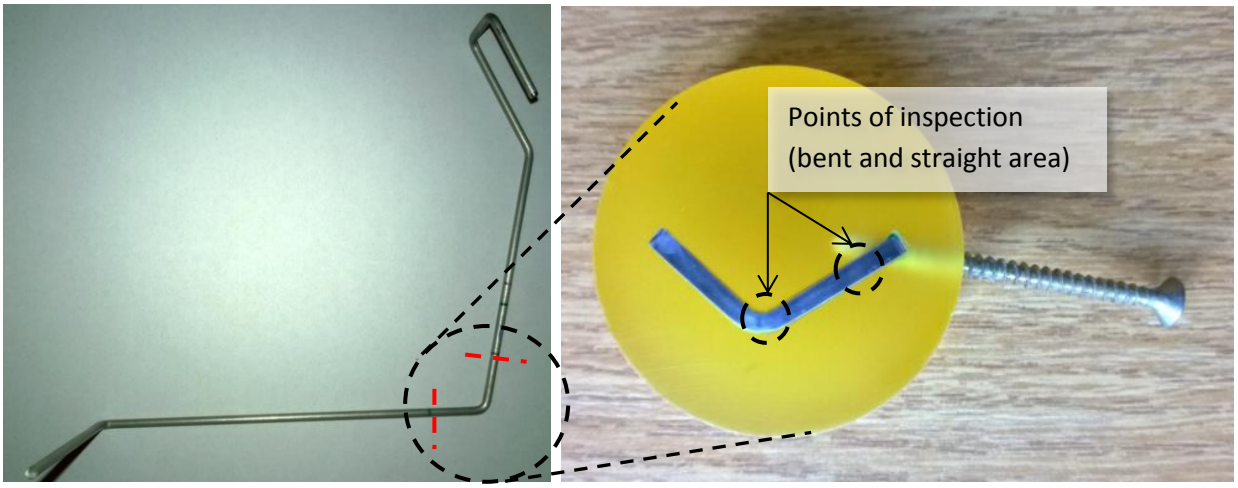

Fig. 8.5 Specimen for metallographic analysis.

When the resin cured specimens were manually grinded on the grinder MTH Kompakt 1031. Rotations of the grinder were set to approximately 200 rpm. For the initial grinding an abrasive paper

with grit number 80 was applied to achieve high material removal rate. The wire was grinded to the middle of its thickness (depth approximately 1.25 mm). After that the grinding series continued gradually with abrasive papers with grit numbers: 80, 180, 320, 600, 800, and 1000. In order to ensure that the previous rough grinding damage is removed, the specimen was rotated 90 degrees and continually ground until all the scratches from the previous grinding direction were removed. After grinding specimens were polished on the polisher Leco GPX 300 using Leco ultra lap diamond extender. Polishing was followed by the electrolytic etching for accentuating of the austenitic microstructure.

8.4.2. Test results

Microstructure was observed under the microscope Neophot 32, magnification was set to 250x. Images of the microstructure of samples from all manufacturers (K, Z, and B) are in the picture 8.6.

The austenitic structure is extremely deformed from the wire drawing process. The structure of the material is very difficult for etching. There is no observable difference in microstructure of the material among manufacturers Z, K and B. There is no observable difference in microstructure of the material in the bent wire zone compared to the straight wire zone.

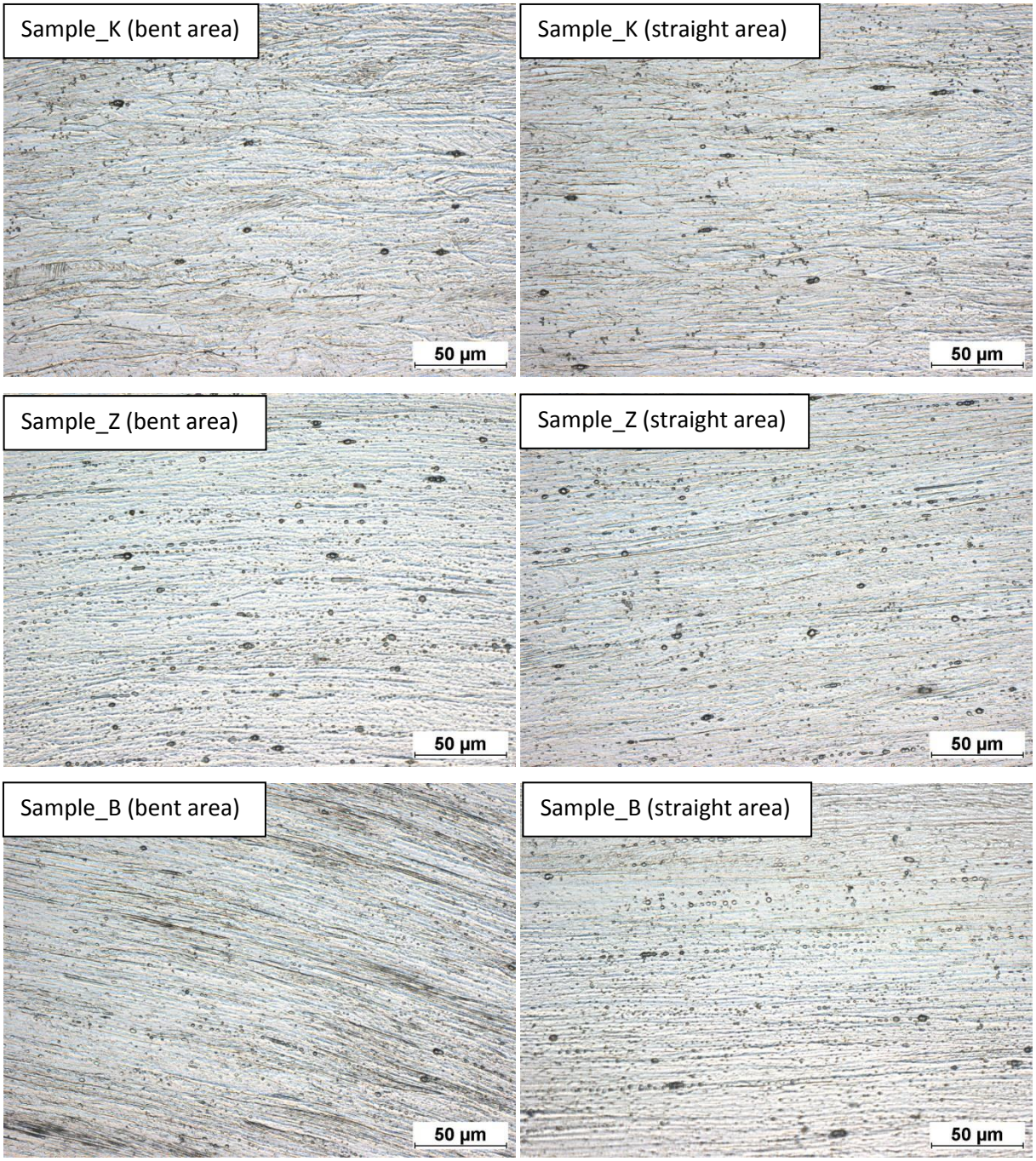

Fig. 8.6 Comparison of the austenitic structure of a cold-drawn wire from stainless steel X10CrNi18-8 NS; three wire arm manufacturers are compared (K, Z and B). Area in bending of wire and straight area are compared for each manufacturer.

9. CORRECTION OF DRY HEIGHT COORDINATE OF FLS CHECKPOINTS

As well as all other contemporary CAD software NX Unigraphics comprises an assembly mode which basically allows for creating assemblies out of individual 3D CAD parts. Mating of individual parts is determined by constrictions. These constrictions operate with fundamental geometrical shapes and curves into which every basic CAD part can be decomposed.

When it comes to mating of axial parts in NX Unigraphics, counterparts with designed free play are always mated using concentric constriction. Theoretical, concentric constriction however does not correspond to the situation in real assembly if there is a loose fit with free play.

In a real assembly parts are always in contact, i.e. in a real alignment there is a shift of position from the nominal. The actual difference between the ideal concentric parts position and the position of parts in a real situation poses an inaccuracy brought in by the TSG Wizard design software.

In this chapter the shift of FLS characteristic is analysed and a correction is suggested.

9.1. Calculation of the correction of the position shift in FLS construction

In case of the FLS assembly a shift of position in fits with free play should be considered and corrected. Two loose fits are analysed and a correction is suggested:

- Fit of floater on wire arm
- Fit of wiper on bearing pin

In the picture 9.1 FLS assembly is depicted with a scheme of forces acting on the assembly. There is the buoyant force from fuel F_{LIFT} acting on the floater and the gravitational force acting on the floater arm G_{FA}. In the detailed view both analysed fits are depicted. In the left part there is a comparison between the concentric (theoretical) fit as it is in the CAD model and the real fit in which the floater is lifted (shifted) vertically within the free play given by the loose fit of wire in the floater hole. The offset can be simply expressed:

$$\Delta H_1 = \frac{J - H}{2} \tag{9.1}$$

The sign is positive because the buoyant force shifts the floater upwards.

In the right part is a comparison between the concentric (theoretical) fit and the real fit in which the wiper body (and thus the whole floater arm) is dropped vertically due to the gravitational force. The size of the drop is equal to the free play given by the loose fit of wiper on the bearing pin:

$$\Delta H_2 = -\frac{M - L}{2} \tag{9.2}$$

The sign is negative because the gravitational force shifts the floater arm downwards.

The total value of the shift which should be corrected is then simple addition of both components:

$$\Delta H = \Delta H_1 + \Delta H_2 \quad (9.3)$$

$$\Delta H = \frac{J - H}{2} - \frac{M - L}{2} \quad (9.4)$$

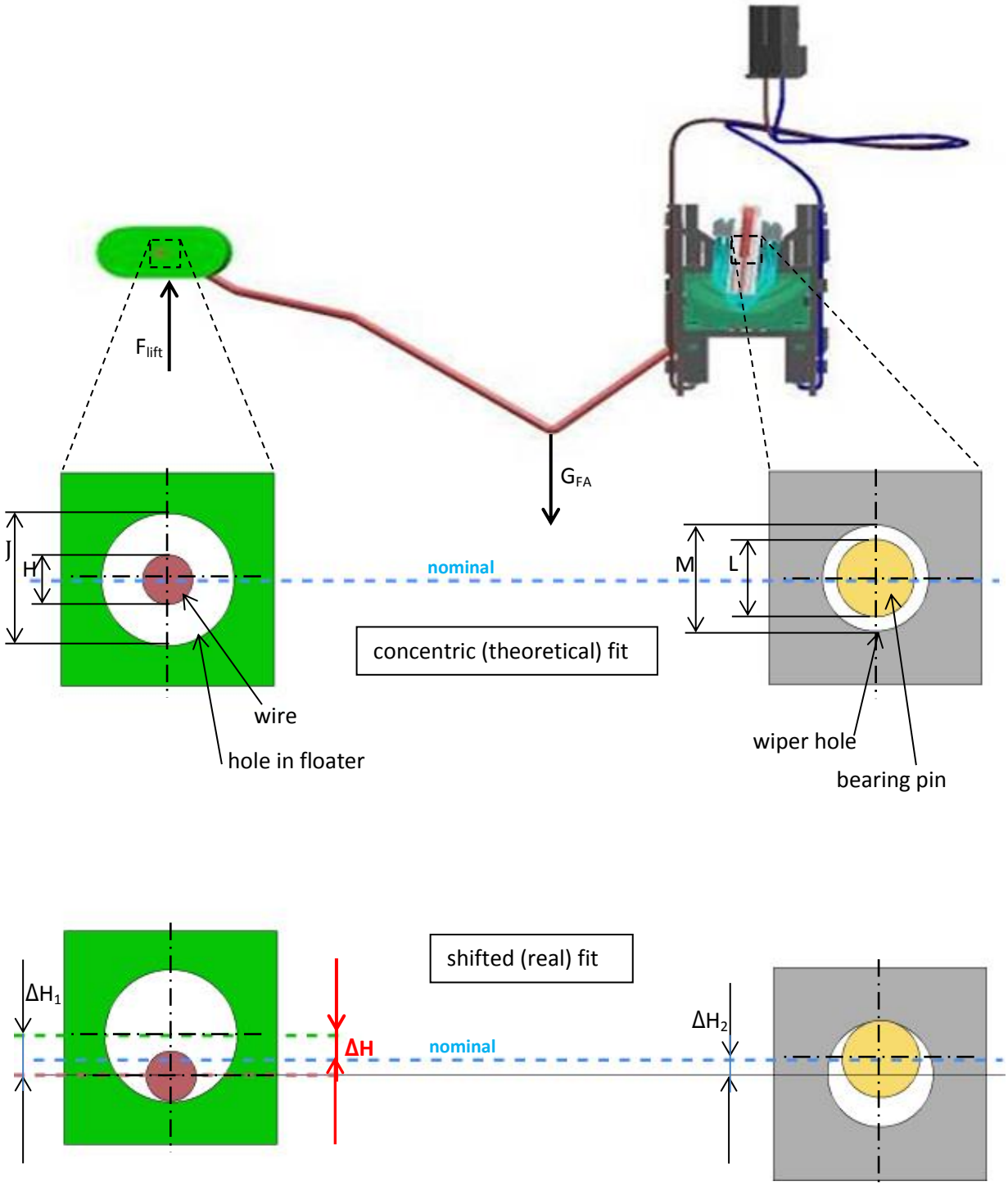

Fig. 9.1 Scheme of the vertical shift in loose fits of components of FLS (dimensions are only illustrative).

9.2. Application of the height correction values in the FLS design process

It is obvious from the figure 9.2 that the real FLS characteristic is shifted by the distance ΔH from the nominal (theoretical) characteristic position due to the shift of components in their loose fits.
This shift is thus a systematic error introduced into the measurement of FLS characteristic because all FLS drawings and also settings of the checkpoint measurement at assembly lines do not reflect this shift and consider only theoretical, concentric fits.

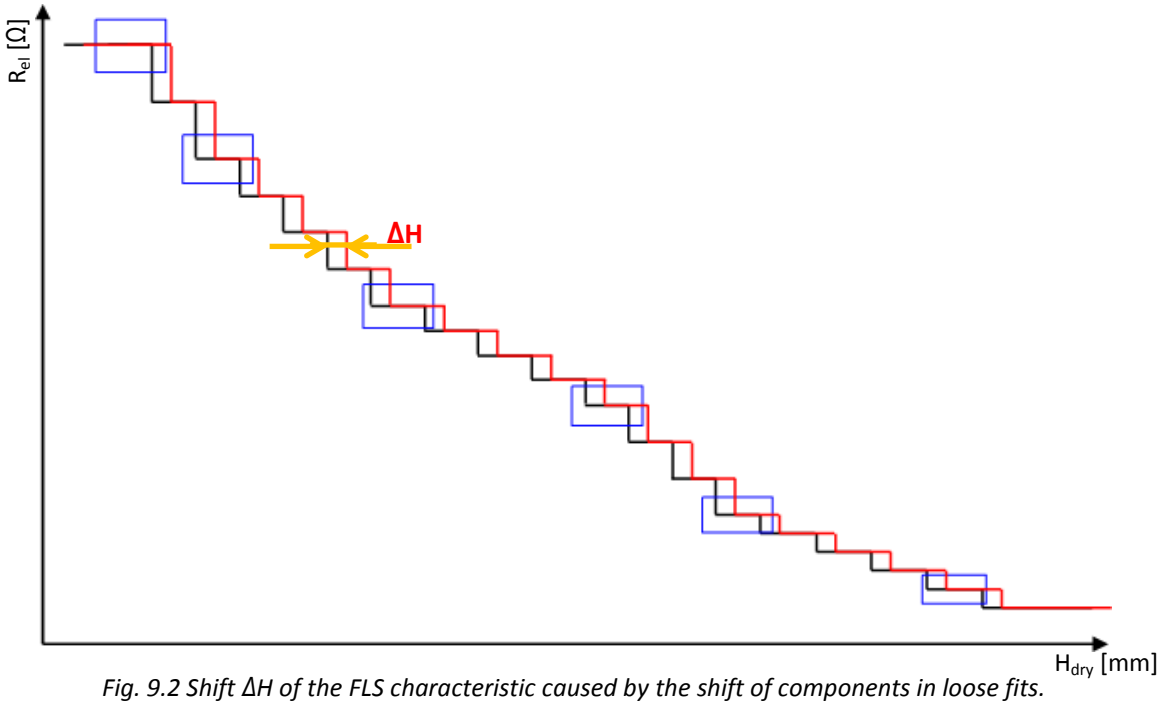

Fig. 9.2 Shift ΔH of the FLS characteristic caused by the shift of components in loose fits.

In order to eliminate this systematic error it is desirable to apply a correction of the theoretical dry height values H_{dry} that are calculated by TSG Wizard software in the process of a new FLS design.

In the FLS design when nominal H_{dry} checkpoint coordinates are calculated by TSG Wizard programme after that these values are transformed into corresponding angular coordinates of checkpoint pads on the resistor card layout. In order to eliminate the systematic error following measure is proposed:

Correction of the dry height coordinate of FLS checkpoints

Nominal H_{dry} checkpoint coordinates calculated by TSG Wizard should be corrected by the value ΔH. The corrected values should be then used as input for calculation of corresponding angular coordinates of checkpoint pads on the resistor card layout. Comparison of both current and proposed process is in the diagram 9.3.

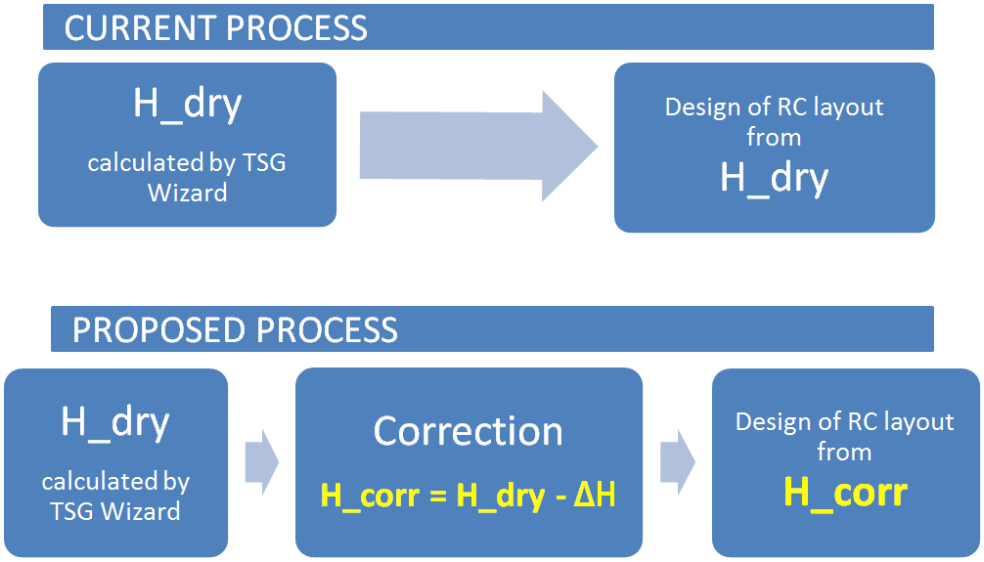

Fig. 9.3 Comparison of current design process and proposed design process in which correction of H_{dry} values is applied.

10. CHECKPOINT PAD WIDENING

As stated in the chapter 5 one of the parameters that directly affects the compliance with criteria for FLS indication accuracy is the width *w* of the step of the FLS height vs. resistance characteristic.

$$w = \frac{2\pi R}{360}(p + s) \cdot cos\gamma \qquad (10.1)$$

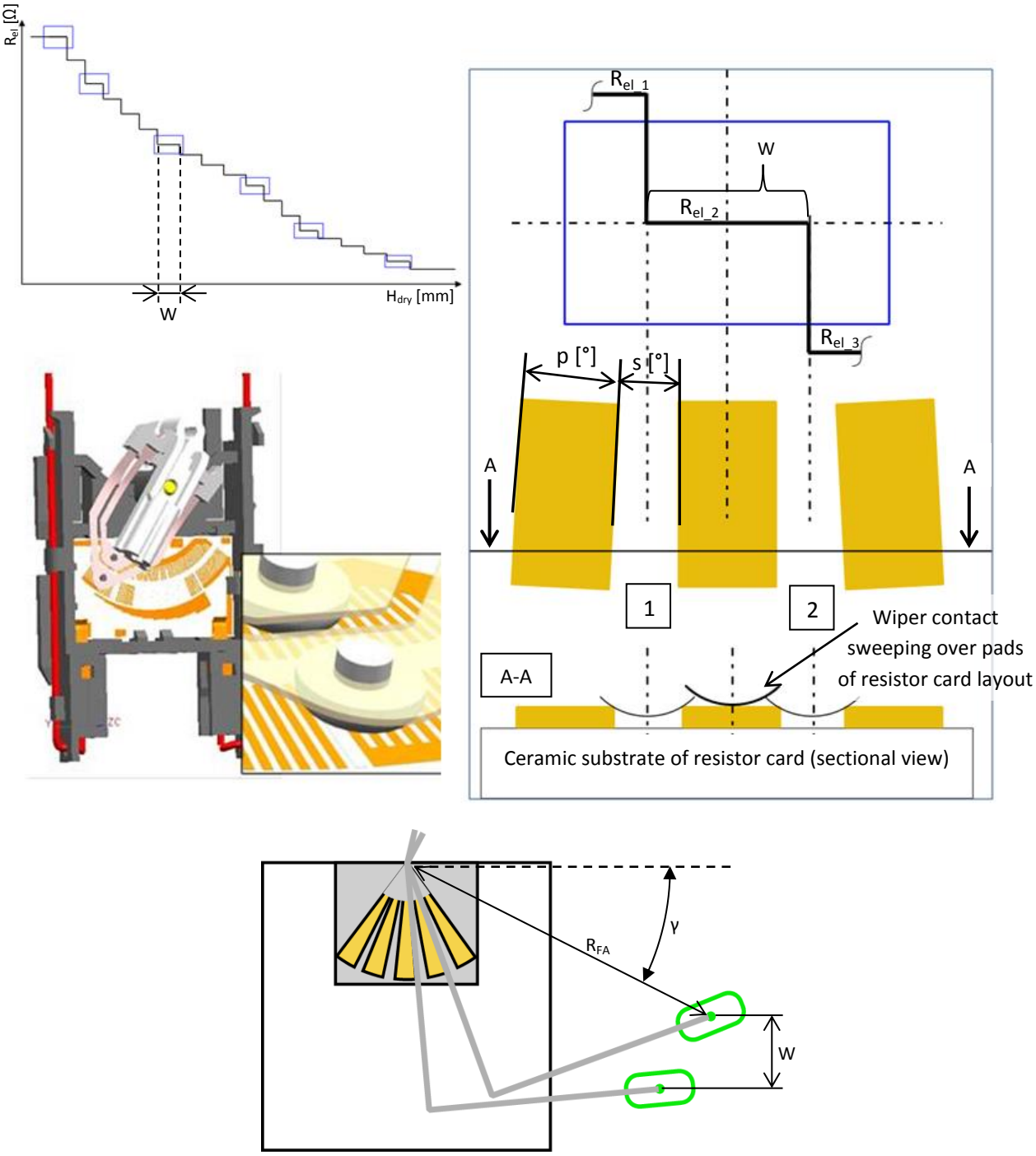

Fig. 10.1 Influence of the pad width (p) and the space width (s) of the resistor card layout and influence of the floater arm radius (R_{FA}) on the width (w) of step of the FLS characteristic.

In order to comply with the indication accuracy criteria checkpoint step of FLS height-resistance characteristic has to intersect the tolerance box in such way that at least 5% of the tolerance box width is overlapped by the characteristic.

In the picture 10.2 threshold characteristic positions can be seen and these are shifted by the distance *±y* from the nominal height value. The shift value corresponds to the actual tolerance of the height indication which means the higher is the permissible shift of characteristic *±y* the higher is the actual FLS height tolerance according to the Tolerance Box evaluation method.

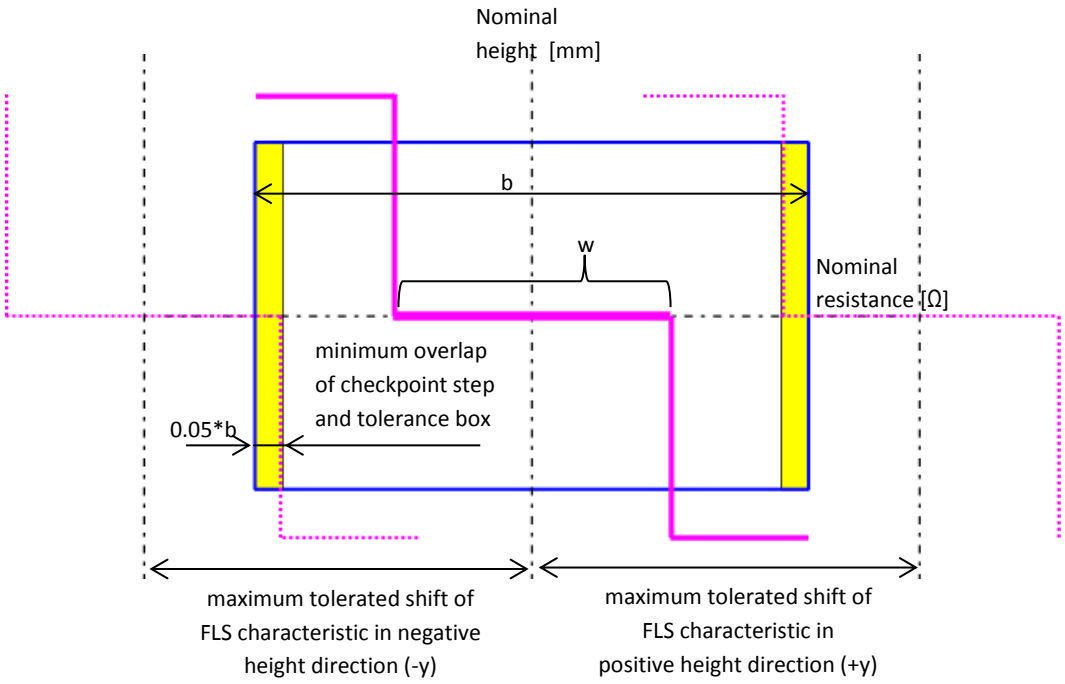

Fig. 10.2 Comparison of the FLS characteristic in the nominal position and characteristics shifted towards the tolerance borders given by the tolerance box width.

Tolerated shift of the characteristic in the height direction is calculated as:

$$\pm y_{tol\_box} = \frac{b}{2} - 0.05 \cdot b + \frac{w}{2} \tag{10.2}$$

i.e.

$$\pm y_{tol\_box} = \frac{b}{2} - 0.05 \cdot b + \frac{\frac{2\pi R}{360}(p+s) \cdot cos\gamma}{2} \tag{10.3}$$

Note:

In the following analysis value of the angle γ is neglected, i.e. simplified form of the equation (10.3) is considered:

$$\pm y_{tol\_box} = \pm \boldsymbol{y_0} = \frac{b}{2} - o + \frac{\frac{2\pi R}{360}(p+s)}{2} \tag{10.4}$$

10.1. Increase of tolerance by widening of the checkpoint pad

From the equation (10.4) it is apparent that with increasing pad width *p* also increases the tolerance of shift of the characteristic. In the picture 10.3 both characteristic with original and characteristic with increased pad width are compared. Original narrower pad and corresponding step of the characteristic are outlined with green hatched line. Width of space between pads is *s* for both cases. Wider pad p_w logically results in a wider step w_w in the height vs. resistance characteristic.

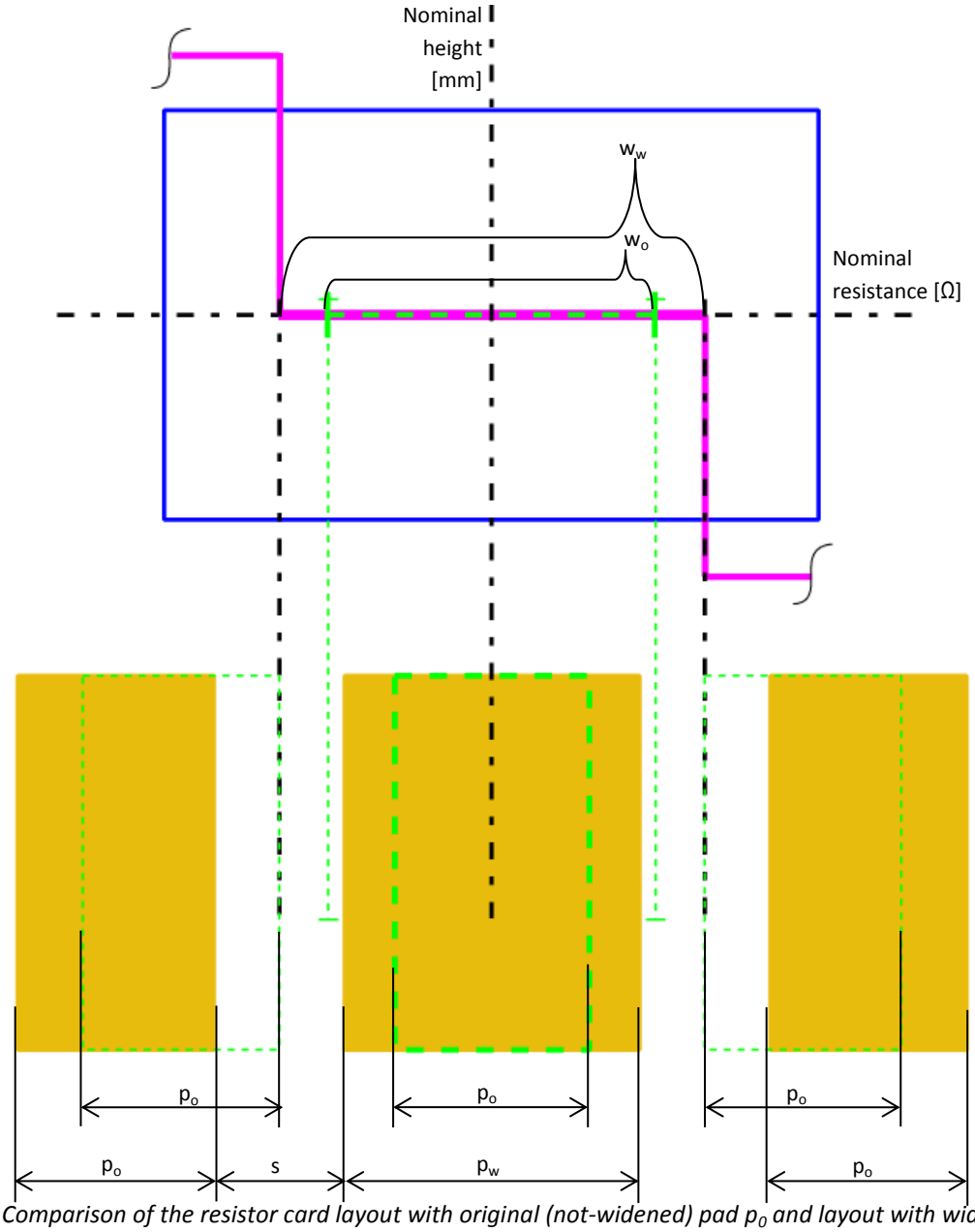

Fig. 10.3 Comparison of the resistor card layout with original (not-widened) pad p_0 and layout with widened pad p_w. Relevant width of step of characteristic is outlined for both cases.

The step width w_w of the characteristic with a wider pad is calculated:

$$w_w = \frac{2\pi R}{360}(p_w + s) \tag{10.5}$$

Where:

p_w is the width of a widened pad which is calculated:

$$p_w = K \cdot p_0 \tag{10.6}$$

Where:

K is a coefficient of the pad widening:

$$K = \frac{100 + k_w}{100} \tag{10.7}$$

Where:

k_w [%] – percentage of the pad widening (of the nominal dimension of the original pad width p_0)

The shift of the characteristic in the height direction is then calculated analogically as in the case of the original pad width:

$$\pm y_w = \frac{b}{2} - o + \frac{\frac{2\pi R}{360}(K \cdot p_0 + s)}{2} \tag{10.8}$$

In the picture 10.4 characteristics of both original and widened pad are compared. They are compared in the threshold positions when they fulfil the acceptance criteria of the minimal tolerance box overlap. It is obvious that the characteristic of the wider pad allows increased deviation from the nominal height position. The increment of tolerance of the height position deviation due to the wider pad design can be simply calculated as:

$$\Delta y = y_w - y_0 \tag{10.9}$$

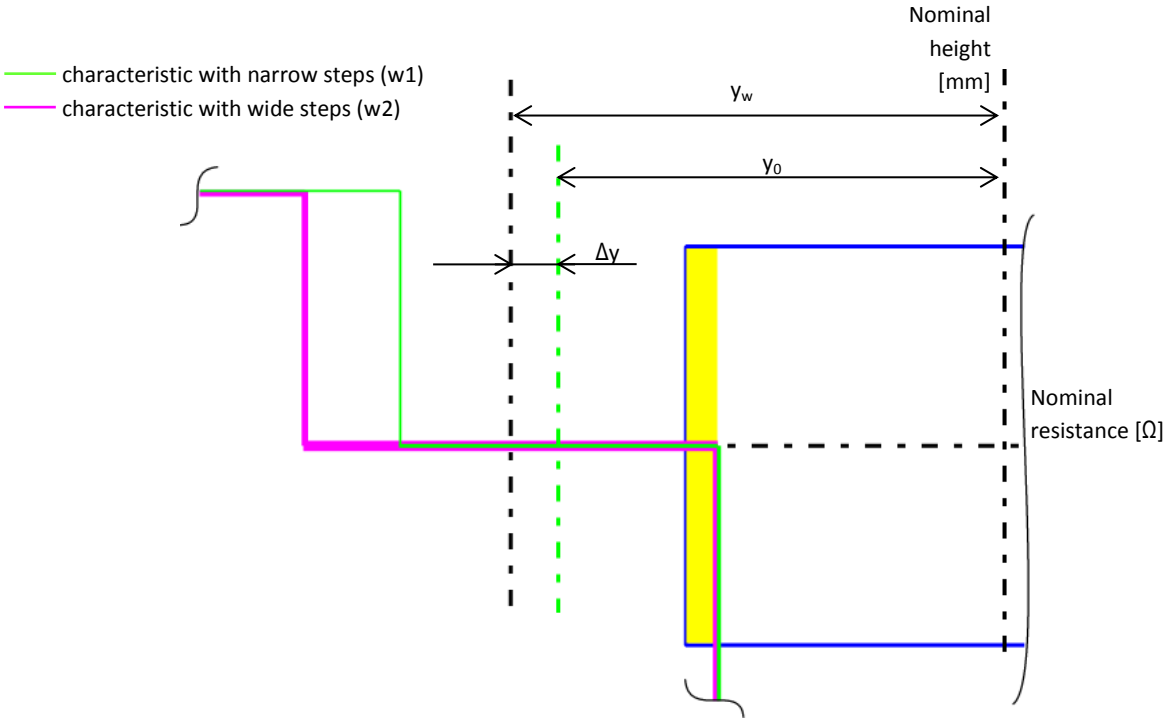

Fig. 10.4 Comparison of maximum tolerated shift of the FLS characteristic from the nominal position (characteristic with narrow steps is compared to the characteristic with wide steps).

Each FLS also exhibits certain degree of hysteresis *h* which limits the maximum tolerated height deviation and thus should be taken into account. Exact value of the hysteresis cannot be calculated, however it has been observed that value of hysteresis by majority ranges from 0.3° to 0.5°, both equations (10.4) and (10.8) thus should be modified:

$$y_0 = \frac{b}{2} - o + \frac{\frac{2\pi R}{360}(p_0 + s - \boldsymbol{h})}{2} \tag{10.10}$$

$$y_w = \frac{b}{2} - o + \frac{\frac{2\pi R}{360}(K \cdot p_0 + s - \boldsymbol{h})}{2} \tag{10.11}$$

In the table 10.1 the percentage is shown of an increase of tolerance of the height deviation *Δy*. It is shown for a representative set of floater arm radii (R_{FA} from 120 to 220 mm) and three various cases of actual pad widening (coefficient of the pad widening k_w is considered 20 %, 50 % and 100 %). For example if the pad was widened by 100% (i.e. double the original pad width), indication deviation greater by 20.2 % (for R_{FA} = 120 mm) would be tolerated by Tolerance Box method; even greater increase of deviation would be tolerated in case of a longer floater arm radius.

Tab. 10.1 Percentage of increase of tolerance of FLS indication deviation; various floater arm radii and various pad widening are considered.

Δy [%]	floater arm radius - R_{FA} [mm]					
k_w [%]	120	140	160	180	200	220
20	4,0	4,4	4,8	5,1	5,4	5,7
50	10,1	11,1	12,0	12,8	13,5	14,2
100	20,2	22,2	24,0	25,6	27,1	28,4

10.2. Pad widening for applications with limited pad to pad angle

In some customer projects there is an explicit specification of maximum angle m_{max} between two neighbouring pads of the resistance track. For such cases the checkpoint pad can be widened only to that extent given by the specification. Value of the angle m_+ between two regular pads which have original width is calculated:

$$m_+ = \frac{p_0 + p_+}{2} + s + s_+ + \frac{p_0 + p_+}{2} \tag{10.12}$$

Where: p_0 is the nominal width of a not widened pad

p_+ is the positive tolerance of the pad width

s is the nominal width of a space between pads

s_+ is the positive tolerance of the space width

m_+ is the maximum distance that can result between axes of symmetry of two neighbouring pads

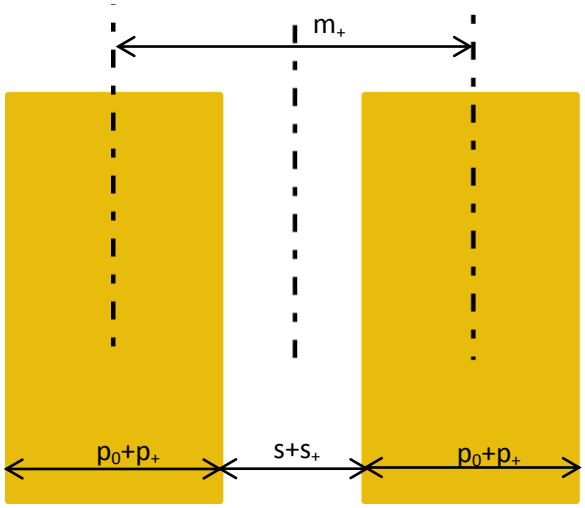

Fig. 10.5 Dependence of the distance between two pads on dimensions of pads and spaces.

In the table 10.2 representative numerical values of pad and space widths with tolerances are listed.

Tab. 10.2 Dimensions of pads and spaces of resistor card layout.

	nominal [deg]	+ tol [deg]	-tol [deg]
p	0.55	0.2	0
s	0.45	0.05	-0.05

If values from the table 10.2 are supplied in the equation (10.12) the maximum angle between two pads which can result from the current pad and space dimensions can be calculated:

$$m_+ = \frac{0.55 + 0.2}{2} + 0.45 + 0.05 + \frac{0.55 + 0.2}{2} \tag{10.13}$$

$$m_+ = 1.25 \tag{10.14}$$

However some customer specifications allow even wider pad to pad difference m_{w+} than value m_{+} calculated in the equation (10.14). This provides space for widening of the checkpoint pad.

Since a widened checkpoint pad is neighbouring a regular pad (width of which remains unchanged) the angle m_{w+} in that case is calculated:

$$m_{w+} = \frac{p_w + p_+}{2} + s + s_+ + \frac{p_o + p_+}{2} \tag{10.15}$$

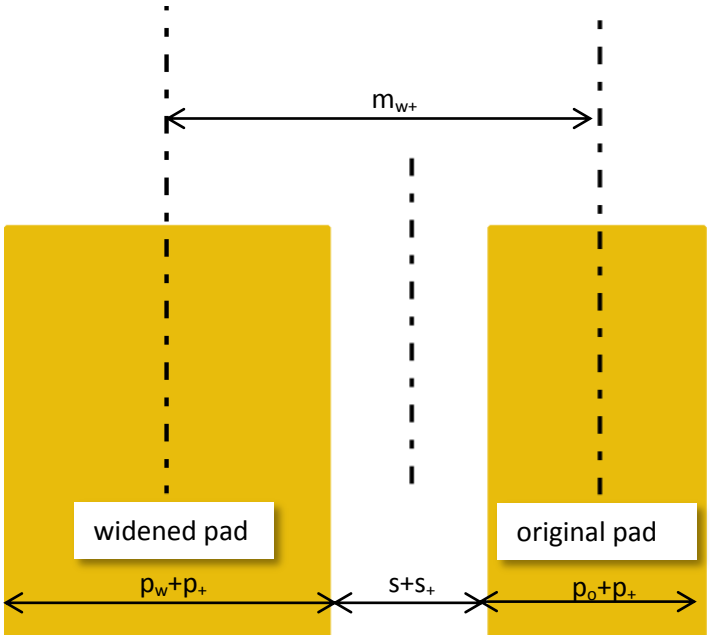

Fig. 10.6 Dependence of the distance between two pads on dimensions of pads and spaces (layout with a widened checkpoint pad).

In order to determine the maximum possible checkpoint pad width p_w with respect to the maximum allowed pad to pad angle m_{w+} given by the customer specification, the equation (10.15) is put in following form:

$$p_w = 2 \cdot \left(m_{w+} - \frac{p_0 + p_+}{2} - (s + s_+) - \frac{p_+}{2} \right) \tag{10.16}$$

Example

In some FLS applications the m_{w+} value is 1.4°, if this value and values from the table 10.2 are supplied in the equation (10.16); maximum nominal value of widened checkpoint pad p_w can be calculated:

$$p_w = 2 \cdot \left(1.4 - \frac{0.55 + 0.2}{2} - (0.45 + 0.05) - \frac{0.2}{2} \right) \tag{10.17}$$

$$p_w = 0.85° \tag{10.18}$$

Tab. 10.3 Dimensions of original pads and spaces and dimensions of widened pad (as a function of maximum distance between two neighbouring pads).

	nominal [deg]	+ tol [deg]	-tol [deg]
p_0	0.55	0.2	0
s	0.45	0.05	-0.05
m_{w_max}	1.4	0	
p_{w_max}	0.85	0.2	0

In order to quantify the increment in tolerance of the height deviation as a result of widened checkpoint pad, first the percentage of pad widening k_w should be calculated:

$$p_{w\_max} = K \cdot p_0 = \frac{100 + k_w}{100} \cdot p_0 \tag{10.19}$$

$$k_w = \frac{p_{w\_max}}{p_0} \cdot 100 - 100 \tag{10.20}$$

For the values from the example, k_w value is:

$$k_w = \frac{0.85}{0.55} \cdot 100 - 100 \tag{10.21}$$

$$k_w = 54{,}5\ \% \tag{10.22}$$

The original nominal pad width p_0 can be widened by up to 54.5% and still comply with the maximum angular difference m_{w+} = 1.4° between two neighbouring pads. The actual value of the increment of tolerance of the height deviation is then evaluated by supplying values into the equation (10.23):

$$\Delta y = y_w - y_0 \tag{10.23}$$

This can be modified:

$$\Delta y = \frac{\frac{2\pi R}{360} \cdot \frac{100+k_w}{100} \cdot p_0}{2} - \frac{\frac{2\pi R}{360} \cdot p_0}{2} \tag{10.24}$$

$$\Delta y = \frac{\frac{2\pi R}{360} \cdot p_0}{2} \cdot \left(\frac{100 + k_W}{100} - 1\right) \tag{10.25}$$

In the table 10.4 increment values Δy for various floater arm radii and values from the table 10.3 are listed:

Tab. 10.4 Increment Δy of the tolerance of deviation of the FLS characteristic due to pad widening.

k_w = 54.5 %	floater arm radius [mm]					
	120	140	160	180	200	220
y_0 [mm]	2,85	3,02	3,20	3,37	3,55	3,72
y_w [mm]	3,16	3,39	3,61	3,84	4,07	4,30
Δy [mm]	**0,31**	**0,37**	**0,42**	**0,47**	**0,52**	**0,58**
Δy [%]	**11,0**	**12,1**	**13,1**	**14,0**	**14,8**	**15,5**

10.3. Estimation of decrease of rate of NOK FLS as a result of pad widening

In the chapter 7 the average rate of FLS non-complying with the accuracy acceptance criteria was calculated as 4.9 % of total FLS production.

In order to estimate the decrease of rate of NOK FLS when design with widened checkpoint pad is applied a comparison is made of confidence intervals for both original and widened pad designs.

The estimation model is made with following assumptions and simplifications:

- The distribution of deviation of FLS indication $\pm y$ is assumed to be normal Gauss distribution.
- Mean value μ=0, i.e. distribution is assumed to be symmetrical around the nominal (exactly accurate) value.
- Standard deviation σ is estimated based on the average rate of FLS accuracy non-compliance from data analysis in the chapter 7.

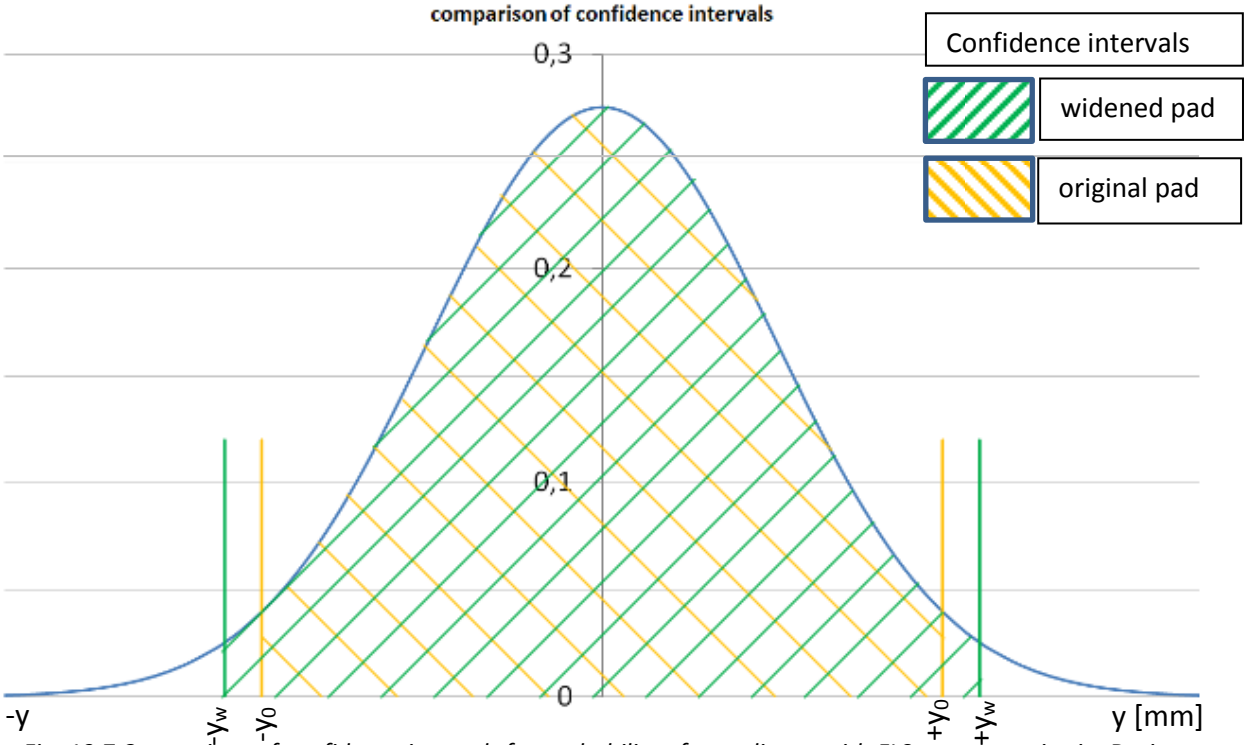

Fig. 10.7 Comparison of confidence intervals for probability of compliance with FLS accuracy criteria. Design with original (non-widened) pad is compared to the design with widened pad.

The confidence interval for the original checkpoint pad design is calculated as:

$$P_0(-y_0 \leq Y \leq +y_0) = 1 - \alpha_0 \qquad (10.26)$$

Where for α_0 value is supplied the average rate of NOK FLS 4.90% as it comes from data analysis in the chapter 7, i.e.:

$$\alpha_0 = 0.049 \qquad (10.27)$$

In order to estimate the decrease of rate of NOK FLS ΔP as an effect of the checkpoint pad widening the difference between confidence intervals of original (not widened) and widened pad are calculated:

$$\Delta P = P_w(-y_w \leq Y \leq +y_w) - P_0(-y_0 \leq Y \leq +y_0) \quad (10.28)$$

In order to calculate confidence interval for the widened pad P_w at first the standard deviation σ has to be evaluated.

Since there are no exact data on the actual value of parameter Y, standard deviation σ is evaluated from the confidence interval P_0 for the original checkpoint pad ($\alpha_0 = 0.049$).

$$P_0(-y_0 \leq Y \leq +y_0) = 1 - \alpha_0 = \int_{-y_0}^{+y_0} \frac{1}{\sigma\sqrt{2\pi}} \cdot e^{-\frac{(x-\mu)^2}{2\sigma^2}} dx \quad (10.29)$$

$$1 - 0.049 = \int_{-y_0}^{+y_0} \frac{1}{\sigma\sqrt{2\pi}} \cdot e^{-\frac{(x-\mu)^2}{2\sigma^2}} dx \;\rightarrow\; \sigma \; is\; calculated \quad (10.30)$$

The standard deviation σ expressed from the equation (10.30) is then supplied in the calculation of the confidence interval P_w for the widened checkpoint pad:

$$P_w(-y_w \leq Y \leq +y_w) = 1 - \alpha_w = \int_{-y_w}^{+y_w} \frac{1}{\sigma\sqrt{2\pi}} \cdot e^{-\frac{(x-\mu)^2}{2\sigma^2}} dx \quad (10.31)$$

From which parameter α_w describing probability of FLS not complying with the confidence interval (in case of design with widened checkpoint pad p_w) can be simply expressed:

$$\alpha_w = 1 - \int_{-y_w}^{+y_w} \frac{1}{\sigma\sqrt{2\pi}} \cdot e^{-\frac{(x-\mu)^2}{2\sigma^2}} dx \quad (10.32)$$

The equation for the estimate of the decrease of rate of NOK FLS ΔP can then be simplified:

$$\Delta P = P_w(-y_w \leq Y \leq +y_w) - P_0(-y_0 \leq Y \leq +y_0) = 1 - \alpha_w - (1 - \alpha_0) \quad (10.33)$$

$$\Delta P = 1 - \alpha_w - (1 - \alpha_0) \quad (10.34)$$

$$\Delta P = \alpha_0 - \alpha_w \quad (10.35)$$

Example

Since the tolerance range provided by the Tolerance Box method varies significantly with increasing floater arm radius three different representative designs are analysed (short, medium and long floater arm).

Tab. 10.5 Values of tolerance of deviation from nominal H_{dry} for both original (not widened) pad and widened pad (y_0 vs. y_w). Values are calculated from relevant input parameters (R, b, s, p); three representative floater arm radii are considered.

floater arm radius	**R**	**[mm]**	**120**	**170**	**220**
tolerance box width	b	[mm]	4	4	4
nominal space width of RC layout	s	[deg]	0,45	0,45	0,45
nominal pad width of RC layout (original)	p_0	[deg]	0,55	0,55	0,55
nominal pad width of RC layout (widened)	**p_w**	**[deg]**	**0,85**	**0,85**	**0,85**
± height tolerance (original pad)	±y_0	[mm]	±2,85	±3,28	±3,72
± height tolerance (widened pad)	**±y_w**	**[mm]**	**±3,16**	**±3,73**	**±4,30**

Equal value of probability of FLS accuracy non-compliance $\alpha_0 = 0.049$ is assumed for all floater arm radii (based on the average rate 4.9% of FLS accuracy non-compliance from the data collection in the chapter 7).

Tab. 10.6 Probability α_0 of non-compliance with accuracy criteria (original, not widened checkpoint pad p_0).

floater arm radius	R	[mm]	120	170	220
probability of non-compliance with confidence interval of indication accuracy (original pad p_0)	α_0	/	0,049	0,049	0,049

When values from the tables 10.5 and 10.6 are supplied in the equation (10.30), the standard deviation σ is estimated (for the mean value μ=0):

Tab. 10.7 Standard deviation σ of FLS indication deviation y (according to various floater arm radii).

floater arm radius	R	[mm]	120	170	220
standard deviation	σ	/	1,45	1,67	1,89

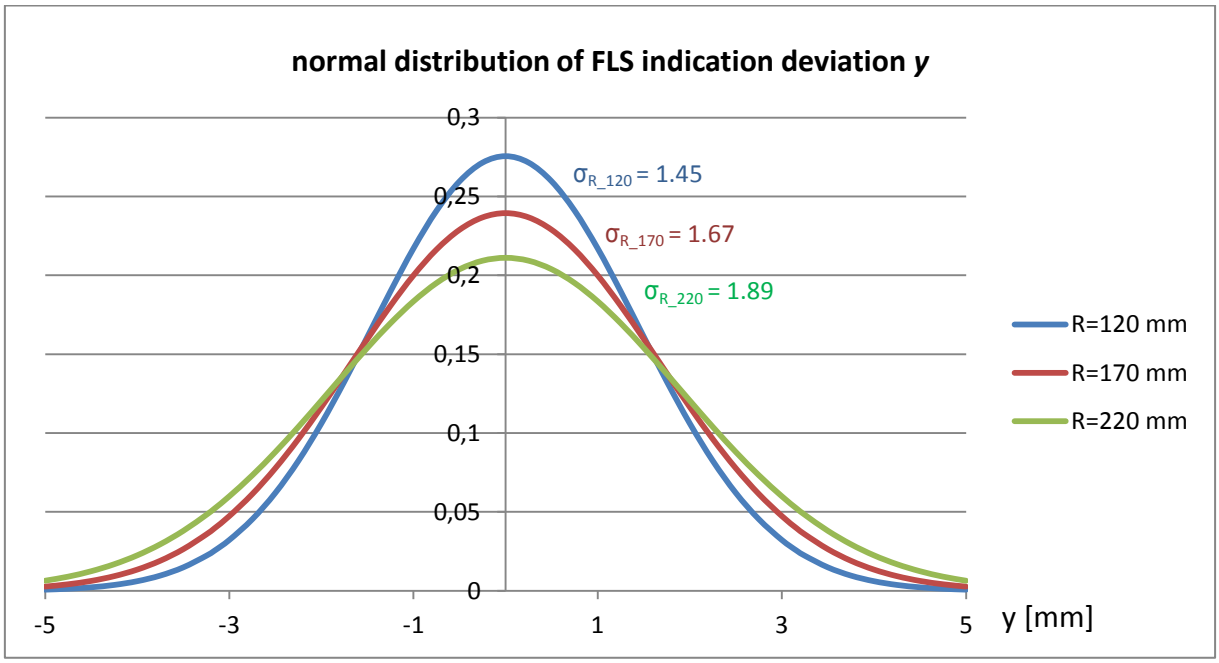

Fig. 10.8 Normal distribution of the FLS indication deviation y; three different floater arm radii are compared.

When values of the standard deviation from the table 10.7 and values of the height tolerance provided by the widened checkpoint pad $\pm y_w$ from the table 10.5 are supplied into the equation (10.32), value α_w of the probability of FLS accuracy non-compliance (for FLS design with widened checkpoint pad p_w) is calculated:

Tab. 10.8 Probability α_w of non-compliance with accuracy criteria (widened checkpoint pad p_w).

floater arm radius	R	[mm]	120	170	220
probability of non-compliance with confidence interval of indication accuracy (widened pad)	α_w	/	0,0291	0,0252	0,0229

In the table 10.9 decrease of the probability ΔP of FLS not complying with the accuracy criteria is evaluated when the nominal pad width is widened. In this representative example equal NOK probability 4.9% before widening was considered for all floater arm radii. The decrease of probability of FLS not complying with the accuracy criteria according to the floater arm radius ranges from 1.99 percentage points for short floater arms to 2.61 percentage points for long floater arms.

Tab. 10.9 Decrease of probability of FLS accuracy non-compliance ΔP as a result of widening of checkpoint pad.

floater arm radius	[mm]	120	170	220
original (not widened) checkpoint pad p_0				
NOK probability	[%]	4,90	4,90	4,90
OK probability	[%]	95,10	95,10	95,10
widened checkpoint pad p_w				
NOK probability	[%]	2,91	2,52	2,29
OK probability	[%]	97,09	97,48	97,71
Decrease of probability of FLS accuracy non-compliance				
ΔP	**Δ[%]**	**1,99**	**2,38**	**2,61**

DISCUSSION OF RESULTS

Discussion of results from data analysis (chapter 7)

Data from assembly lines were collected in order to identify any correlation between FLS design parameters and rate of inaccuracy of FLS indication.

Following conclusions are drawn:

- The average rate of 4.9% of all produced fuel supply modules have FLS which does not comply with the acceptance criteria when checked at the output control. Therefore these have to be corrected by manual bending of the wire arm of FLS.
- Majority of FLS (approx. 78%) that do not meet the acceptance criteria come from minority (approx. 18%) of various projects (various FLS designs respectively).
- There is no proof of any correlation between the floater arm radius and the rate of FLS that do not comply with the acceptance criteria.
- There is an increased rate of FLS not complying with the acceptance criteria at assembly lines AL04 (8.6 %) and AL06 (10.2 %).
- There is a very low difference in the rate of FLS accuracy non-compliance between FLS with a rotational floater and FLS with a fixed floater design, therefore the floater design is found to have negligible effect on the meeting of FLS acceptance criteria.
- Platform FLS 1.0 has considerably lower rate (2.7 %) of FLS non-complying with the acceptance criteria compared to the average value.
- **Wire manufacturer B has considerably higher rate (10.9 %) of FLS which do not comply with the acceptance criteria compared to other manufacturers (K – 3.4 % and Z – 4.8 %).**

Discussion of results from materials analysis (chapter 8)

Materials analysis of wire arms was performed to proof or disproof influence of the wire arm material properties on the dimensional instability of the wire arm among all three manufacturers K, Z and B. Therefore a hypothesis was formulated that the wire arm material from the manufacturer B is expected to have lower ultimate strength compared to K and Z due to different heat treatment parameters.

Following conclusions are drawn from the tensile test and from the metallographic analysis of the wire arm material:

- **Hypothesis was invalidated.** The ultimate strength of the material from the manufacturer B (annealed at 240 °C) **is not** lower compared to the ultimate strength of the material from both manufacturers K and Z (annealed at 180 °C).

- On the contrary the ultimate strength of the material from the manufacturer B was proved to be higher by 180 MPa compared to the manufacturer K (approx. 10% higher) and by 283 MPa compared to the manufacturer Z (approx. 17% higher)
- Ductility of the material from the manufacturer B is lower compared to both manufacturers K and Z by 0.7 percentage point (2.5% vs. 3.2%)
- Thus it can be assumed that the criterion formulated in the hypothesis was not met, i.e. **not all** other material properties before annealing are identical for all three manufacturers K, Z and B.
- It can be assumed that material properties are different among manufacturers K, Z and B already before the heat treatment of the material is performed, this difference could be caused by:
    - Different parameters of the cold working process by the manufacturer B compared to the manufacturers K and Z
    - Different material properties of the input semi-product material purchased by the manufacturer B compared to the manufacturers K and Z

  which could be the root cause for substantially higher tensile strength of the material from the manufacturer B before annealing.
- Due to this possible difference in the tensile strength before annealing, even despite higher annealing temperature applied by the manufacturer B (240 °C vs. 180 °C by manufacturers K and Z) the tensile strength of material B after annealing (1920 MPa) exceeds the tensile strength of the material K (1740 MPa) and Z (1637 MPa) and also the upper limit of the tensile strength given by the norm 10270-3 for the wire diameter 2.5 mm (1900 MPa).
- The austenitic structure is extremely deformed from the wire drawing process.
- The structure of the material is very difficult for etching.
- There is no observable difference in the microstructure of the material among manufacturers Z, K and B.
- There is no observable difference in the microstructure of the material in the bent wire zone compared to the straight wire zone.

Conclusion from design change proposals

Two design change proposals were elaborated, application of which would result in an increase of compliance with the FLS accuracy criteria:

Correction of the dry height coordinate of FLS checkpoints (chapter 9)

- Correction of dry the height coordinate of FLS checkpoints calculated by TSG Wizard is proposed.

- Correction is proposed to eliminate systematic error from shifts in loose fits of FLS assembly that are not considered in the current TSG Wizard design model.
- By application of the corrected checkpoint dry height coordinates for the design of the layout of resistor card, the shift ΔH of the FLS characteristic would be eliminated.

Checkpoint pad widening (chapter 10)

- Widening of the checkpoint pads of resistor card layout is proposed. According to the Tolerance Box evaluation method the width of the checkpoint pad directly affects size of tolerated shift of the characteristic in the height direction.
- Relation between the extent of pad widening k_w and the actual increase of the tolerance Δy is derived.
- Particular analysis is given to the FLS applications in which explicit maximum angular difference is defined between two neighbouring steps of the resistor card layout. In a representative example values of the increase of tolerance Δy are calculated for various floater arm radii.
- Estimation is carried out of a decrease of probability ΔP of FLS not complying with the accuracy criteria at the output control if the design with widened pad p_w is applied.

CONCLUSION

This thesis determined an objective to analyse root causes of an increased frequency of indication inaccuracy which was encountered in the series production of potentiometric fuel level sensors (FLS) in Robert Bosch Ceske Budejovice GmbH. This issue significantly obstructs fluency of production and results in increased production costs. Therefore an additional objective was formulated to propose measures application of which would lead to a significant reduction of the number of FLS non-complying with the indication accuracy criteria.

In the theoretical part working principle of a potentiometric FLS was described and compared with other currently utilized fuel measure systems. Thorough description of stages of FLS design process was detailed with a particular focus on forces acting on the floater arm of FLS. Furthermore a worst case tolerance chain of dimensions of FLS components was calculated in order to gain information on the maximum theoretical indication inaccuracy of FLS. This was followed by a detailed description of tolerance methods applied for the evaluation of the FLS indication accuracy, the deviation of indication respectively. Finally the theoretical part was finished with the specification of arrangement of FLS characteristics measurement at the output control of FLS assembly.

The practical part was opened with an analysis of data collected from FLS assembly lines. The total FLS production between November 2013 and July 2014 was assorted and the rate of beyond specification FLS that do not comply with the tolerance of indication accuracy was then analysed according to various FLS parameters. The overall average rate of FLS accuracy non-compliance was 4.9 % and 78 % of all non-complying FLS that did not meet the acceptance criteria came from only 18% of various FLS designs which corresponds to the Pareto distribution. Considerably higher occurrence of non-complying FLS are identified on the assembly lines AL04 (8.6 %) and AL06 (10.2 %). These lines thus should be further inspected, with particular focus on the calibration of the FLS measuring bench. Among other it was discovered that FLS, in which wire arm delivered by the manufacturer B is assembled, show a substantially more frequent occurrence of the accuracy non-compliance in comparison to other manufacturers K and Z (10.9 % vs. 3.4 % and 4.8 %).

Based on that finding an analysis of material properties of the wire arm was performed for all three wire arm manufacturers K, Z and B. Two material tests were performed, namely tension test and metallographic analysis. Based on the fact that wire arms undergo a heat treatment after they are cold-worked and the temperature set by the manufacturer B is higher (240 °C) compared to the manufacturers Z and K (180 °C) a hypothesis was formulated. The hypothesis expected lower

ultimate strength of the wire arm material from the manufacturer B (compared to K and Z) as a result of a more intense stress relief at elevated heat treatment temperature. This hypothesis was invalidated; conversely the ultimate strength of the material from the manufacturer B exceeded both K and Z.

Therefore a conclusion was assumed that material properties are substantially variable among manufacturers K, Z and B already before the heat treatment of the material is performed. That is assumed to be caused either by different parameters of the cold working process at the manufacturer B compared to the manufacturers K and Z or by comparatively different material properties of the input semi-product material purchased by the manufacturer B compared to the manufacturers K and Z.

The metallographic analysis showed extremely deformed austenitic structure, which is a result of the intense cold drawing. There was not found any observable difference in the microstructure of the material among manufacturers Z, K and B when observed under a light microscope.

Two design change proposals were elaborated, application of which would result in an increased frequency of compliance with the FLS accuracy criteria.

Firstly, in order to reach an accuracy enhancement of FLS checkpoints a correction of the dry height coordinate of the FLS checkpoints was proposed. This correction is proposed to eliminate the systematic error caused by shifts in loose fits of the FLS assembly that are not considered in the current TSG Wizard design model.

Secondly, widening of checkpoint pads of the resistor card layout is proposed in order to increase probability that FLS will comply with the indication accuracy criteria. Relation was described between the extent of the checkpoint pad widening and the actual increase of tolerance of the FLS indication deviation. Checkpoint pad widening was also detailed for applications with an explicitly specified maximum distance between two neighbouring pads. Estimation was made of a decrease of probability of the FLS accuracy non-compliance as a result of widening of the checkpoint pad. In a representative example the rate of FLS accuracy non-compliance is estimated to decrease from current 4.9 % to 2.0 % for short floater arm radii and from 4.9 % to 2.6 % for long floater arm radii if checkpoint pads are widened from 0.55° to 0.85°.

FLS indication accuracy and its verification at the output control of final assembly can be affected by wide range of causes. This thesis provided a complex analysis and pointed out those parameters which have a detrimental effect on the FLS indication accuracy. Moreover, design changes undemanding for implementation were proposed and their positive effect on decrease of the rate of FLS accuracy non-compliance was described.

REFERENCES

[1] ĎAĎO, S. a kol. *Měření průtoku a výšky hladiny*. Prague: BEN – technická literatura, 2005. ISBN 80-7300-156-X.

[2] TURNER, John. *Automotive Sensors.* New Jersey: Momentum Press, 2009. ISBN-13: 978-1-60650-009-5.

[3] ASHBY, Michael F. *Material Selection in Mechanical Design.* Oxford: Butterworth-Heinemann, 2005. ISBN 0 7506 6168 2.

[4] BEVER, Michael B. et al. *Encyclopaedia of Materials Science and Engineering.* Pergamon Press, 1986. ISBN 0-08-022158-0.

[5] BUSCHOW, K. H. Jürgen et al. *Encyclopaedia of Materials: Science and Technology.* Elsevier Science, 2001. ISBN 0-08-043152-6.

[6] DOSTAL, Cyril et al. *Engineered Materials Handbook: Engineering Plastics, Vol. 2.* ASM International, 1988. ISBN 0-87170-279-7.

[7] FLEMING, William J., Overview of Automotive Sensors. *IEEE Sensors Journal*, Vol. 1, No. 4, 2001, ISSN 1530-437X.

[8] Fuel level measurement for commercial and special-purpose vehicles. *VDO* [online]. 2008 [cit. 2014-12-24]. Available from: http://www.vdo.com/generator/www/com/en/vdo/main/hidden/downloads/commerical_vehicles/flc_61200_vdo_sensor_eng_en.pdf?redirect=false

[9] Liquid Level Sensing. *Infineon* [online]. 2009 [cit. 2014-12-24]. Available from: http://www.infineon.com/dgdl/AppNote_Liquid_Level_Sensing_Rev.1.0.pdf?folderId=db3a30431ce5fb52011d4cae1f582dad&fileId=db3a30432313ff5e0123a385f3b2262d

[10] TERZIC, Jenny. *Ultrasonic Fuel Level Sensor Development in Automotive Applications*. Swinburne, 2011. Doctoral Dissertation. Swinburne University of Technology.

[11] NITROPHYL® Design Guide. *Rogers* [online]. © 2014 [cit. 2014-12-24]. Available from: http://www.rogerscorp.com/ec/nitrophyl_design.aspx

[12] MACEK, Karel et al. *Kovové materiály*. Prague: CTU Publishing house, 2006. ISBN 80-01-03513-1.

[13] Chromium-nickel austenitic stainless steel 1.4310. *Deutsche Edelstahlwerke* [online]. 2007 [cit. 2014-12-24]. Available from: http://www.dew-stahl.com/fileadmin/files/dew-stahl.com/documents/Publikationen/Werkstoffdatenblaetter/RSH/1.4310_en.pdf

[14] Heat treatment of stainless steels for spring applications. *British Stainless Steel Association* [online]. © 2014 [cit. 2014-12-24].
Available from: http://www.bssa.org.uk/topics.php?article=137

[15] Stainless steel Type 302: Effect of Cold Work. *Shanghai STAL Precision Stainless Steel* [online]. © 2013 [cit. 2014-12-24].
Available from: http://www.stal.com.cn/pdffile/302304304l305.pdf

[16] Technical card: X10CrNi18-8. *Lucefin* [online]. 2012 [cit. 2014-12-24].
Available from: http://www.lucefin.com/wp-content/files_mf/1.4310a301en.pdf

[17] CUNAT, Pierre-Jean. *Working with stainless steel.* Euro Inox, 2008. ISBN 978-2-87997-181-0.

[18] Stress relieving heat treatments for austenitic stainless steels. *British Stainless Steel Association* [online]. © 2014 [cit. 2014-12-24].
Available from: http://www.bssa.org.uk/topics.php?article=76

[19] Level sensor. In: Wikipedia: the free encyclopaedia [online]. San Francisco (CA): Wikimedia Foundation, 2001- [cit. 2015-01-03]. Available from: http://en.wikipedia.org/wiki/Level_sensor

[20] CIES. Magneto Resistive Fuel Level Senders [online]. © 2014 [cit. 2015-01-03].
Available from: https://www.ciescorp.net/

[21] Tensile testing. In: Wikipedia: the free encyclopaedia [online]. San Francisco (CA): Wikimedia Foundation, 2001- [cit. 2015-01-03].
Available from: http://en.wikipedia.org/wiki/Tensile_testing

[22] Metalografie I. - příprava vzorku pro pozorování mikroskopem. *Laboratorní práce VŠCHT* [online]. 2008 [cit. 2015-01-04].
Available from:
http://old.vscht.cz/met/stranky/vyuka/labcv/labor/fm_metalografie_1/index.htm

[23] EN 10270-3:2011. Steel wire for mechanical springs. Stainless spring steel wire. BSI, 2011.

ÚMI, Fakulta strojní
ČVUT Praha

Zkušební dávka: DP-Royt.is_tens

Zkouška tahem ČSN EN ISO 6892-1

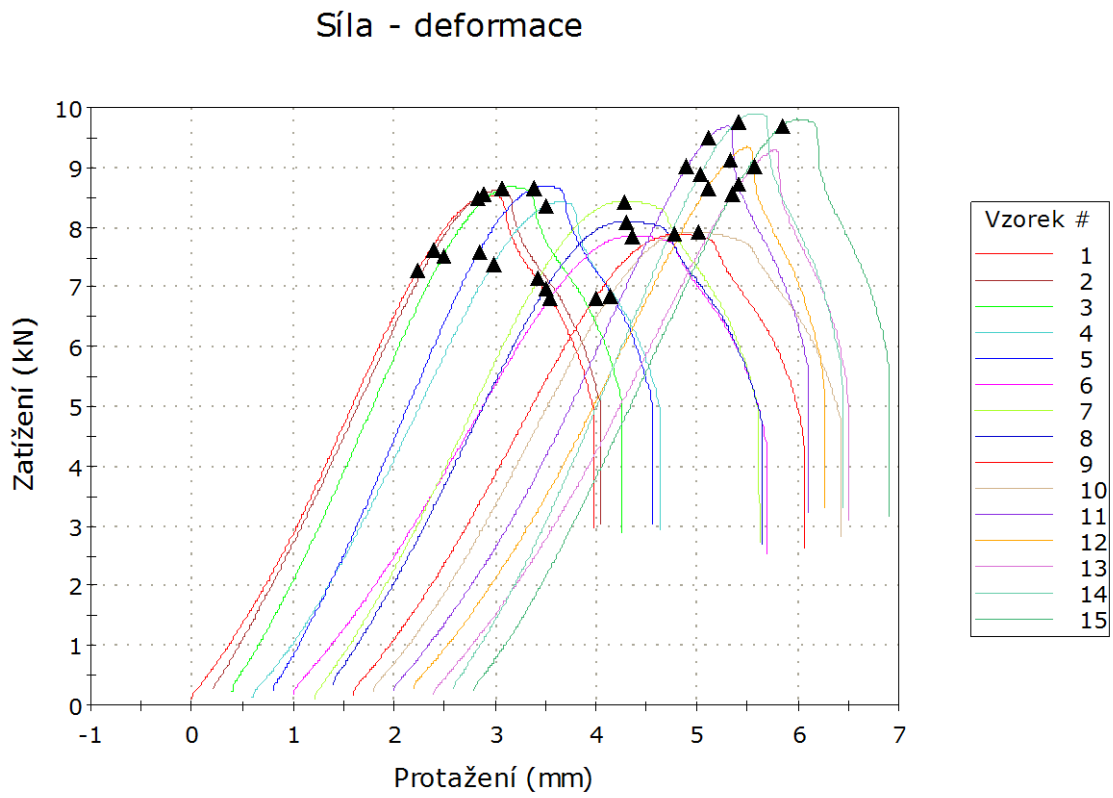

	Jmenovka vzorku	Mez kluzu (Posun 0,2 %) (MPa)	Mez pevnosti Rm (MPa)
1	KO1	1480,9	1727,6
2	KO2	1550,7	1744,8
3	KO3	1533,7	1762,3

ÚMI, Fakulta strojní
ČVUT Praha

	Jmenovka vzorku	Mez kluzu (Posun 0,2 %) (MPa)	Mez pevnosti Rm (MPa)
4	KO4	1503,2	1702,9
5	KO5	1546,4	1762,7
6	ZO1	1389,4	1600,4
7	ZO2	1453,1	1716,9
8	ZO3	1419,3	1648,9
9	ZO4	1388,9	1604,8
10	ZO5	1391,9	1614,9
11	BO1	1836,3	1931,7
12	BO2	1765,6	1862,6
13	BO3	1741,9	1838,8
14	BO4	1812,2	1991,8
15	BO5	1778,8	1977,8